ISTANBUL TECHNICAL UNIVERSITY ★ EARTHQUAKE ENGINEERING AND DISASTER MANAGEMENT INSTITUTE

ANALYSIS OF DYNAMIC RESPONSE AND INSTABILITY OF A CAISSON TYPE GRAVITY QUAY WALL – SEABED SYSTEM UNDER WAVES

M.Sc. THESIS

Hasan Giray BAKSI

Earthquake Engineering and Disaster Management Institute

Earthquake Engineering Program

MAY 2017

ISTANBUL TECHNICAL UNIVERSITY ★ EARTHQUAKE ENGINEERING AND DISASTER MANAGEMENT INSTITUTE

ANALYSIS OF DYNAMIC RESPONSE AND INSTABILITY OF A CAISSON TYPE GRAVITY QUAY WALL – SEABED SYSTEM UNDER WAVES

M.Sc. THESIS

Hasan Giray BAKSI
(802121017)

Earthquake Engineering and Disaster Management Institute

Earthquake Engineering Program

Thesis Advisor: Assoc. Prof. Dr. Mehmet Barış Can ÜLKER

MAY 2017

İSTANBUL TEKNİK ÜNİVERSİTESİ ★ DEPREM MÜHENDİSLİĞİ VE AFET YÖNETİMİ ENSTİTÜSÜ

KESON TİPİ RIHTIM DUVARI – DENİZ TABANI SİSTEMİNİN DALGA ETKİLERİ ALTINDAKİ DİNAMİK TEPKİSİ VE DURAYSIZLIĞININ İNCELENMESİ

YÜKSEK LİSANS TEZİ

Hasan Giray BAKSI
(802121017)

Deprem Mühendisliği Anabilim Dalı

Deprem Mühendisliği Programı

Tez Danışmanı: Doç. Dr. Mehmet Barış Can ÜLKER

MAYIS 2017

Hasan Giray BAKSI, a M.Sc. student of ITU Earthquake Engineering and Disaster Management Institute student ID 802121017, successfully defended the thesis entitled “ANALYSIS OF DYNAMIC RESPONSE AND INSTABILITY OF A CAISSON TYPE GRAVITY QUAY WALL – SEABED SOIL SYSTEM UNDER WAVES”, which he prepared after fulfilling the requirements specified in the associated legislations, before the jury whose signatures are below.

Thesis Advisor : **Assoc. Prof. Dr. Mehmet Barış Can ÜLKER** ....
Istanbul Technical University

Jury Members : **Assoc. Prof. Dr. Mehmet Barış Can ÜLKER** ....
Istanbul Technical University

Assoc. Prof. Dr. Veysel Şadan Özgür KIRCA ....
Istanbul Technical University

Asst. Prof. Dr. Gökçe TÖNÜK ....
MEF University

Date of Submission : 04 May 2017
Date of Defense : 17 May 2017

To my family,

FOREWORD

First of all, I would like to express my deep gratitude to Dr. Ulker, my research advisor, for his patience, guidance and useful critiques during this research work. His labor was not less than mine to make a high-quality thesis, certainly. I would also like to thank Dr. Kirca for their critical recommendation and support that made this research possible.

Especially to Belgin, my wife, thanks for giving me your patience, encouragement and love even in hard times during this period.

May 2017

Hasan Giray BAKSI
(Civil Engineer)

TABLE OF CONTENTS

Page

ABBREVIATIONS

ASTM	**:** American Society for Testing and Materials International
CTQ	**:** Caisson Type Quay Wall
DOF	**:** Degree of Freedom
FD	**:** Fully Dynamic
FE	**:** Finite Elements
FEM	**:** Finite Element Method
GM	**:** Silty Gravel
GW	**:** Well Graded Gravel
MPC	**:** Multi Point Constraint
SP	**:** Poorly Graded Sand
PD	**:** Partly Dynamic
QS	**:** Quasi Static
Q4	**:** Quadrilateral 4-noded
Q8	**:** Quadrilateral 8-noded
USCS	**:** Unified Soil Classification System
1-D	**:** One Dimensional
2-D	**:** Two Dimensional
3-D	**:** Three Dimensional

SYMBOL LIST

$\mathbf{B}$	: Strain-nodal displacement matrix
c_i	: Coefficient of convergence
c_v	: Consolidation coefficient
$\boldsymbol{C}$	: Damping matrix
$\boldsymbol{C_f}$	: Damping matrix of fluid
C_{ww}	: Damping matrices
D_{ijkl}	: Tangent material rigidity
d	: Water depth
$\boldsymbol{d}$	: Nodal displacement vector
E	: Elasticity modulus
$\mathbf{E}$	: Elasticity modulus matrix
E_C	: Elasticity modulus of clay
E_R	: Elasticity modulus of rubble
E_S	: Elasticity modulus of seabed
E_W	: Elasticity modulus of caisson wall
f	: Force vector
$\mathbf{f_m}$	: Master force vector
$\mathbf{f_s}$	: Slave force vector
$\mathbf{f_u}$	: Uncommited force vector
$\hat{\mathbf{f}}$	: Modified force vector
$\mathbf{F_f}$	: Force matrix of fluid
$\mathbf{F_s}$	: Force matrix of solid
F_u, F_w	: Force vectors
g	: Gravitational acceleration
G	: Elastic Lame parameter; shear modulus
h	: Depth of soil / porous medium
H	: Wave height
H_d	: Drainage distance of the layer
k_R	: Permeability of rubble
k_C	: Permeability of clay
k_z	: Vertical permeability
k_x	: Horizontal permeability
k_S	: Permeability of seabed
K	: Stiffness
$\mathbf{K}$	: Stiffness matrix
K_f	: Bulk modulus of fluid
$\mathbf{K_s}$	: Stiffness matrix of solid
K_u, K_w	: Stiffness matrices
$\hat{\mathbf{K}}$	: Modified stiffness matrix
L	: Wavelength
m	: Mass; Kronecker delta vector
m_v	: Volumetric compressibility

$\boldsymbol{M_s}$	: Mass matrix of solid
$\boldsymbol{M_{sf}}$	: Relative mass matrix of fluid
M_{uu}, M_{ww}	: Mass matrices
n	: Porosity
n_S	: Porosity of seabed
n_C	: Porosity of clay
n_R	: Porosity of rubble
N_u, N_w	: Shape function matrices
p	: Pressure
S_C	: Saturation of clay
S_R	: Saturation of rubble
S_S	: Saturation of seabed
T	: Wave period
$\boldsymbol{T}$	: Transformation matrix
T_v	: Time factor
u	: Displacement of solid part
$\mathbf{u}$	: Displacement vector
$u_{i,j}$, $u_{j,i}$	: Solid displacement
$\mathbf{u_m}$	: Master displacement vector
$\mathbf{u_s}$	: Slave displacement vector
$\mathbf{u_u}$	: Uncommited displacement vector
$\hat{\mathbf{u}}$	: Modified displacement vector
v	: Poisson's ratio
v_W	: Poisson's ratio of caisson wall
p	: Pore pressure
q	: Load amplitude
S	: Degree of saturation
S_m	: Effective mean stress
S_{xz}	: Shear stress
S_{xx}, S_{zz}	: Normal stresses
w	: Relative fluid displacement
v	: Poisson's ratio
v_C	: Poisson's ratio of clay
v_S	: Poisson's ratio of seabed
x_i	: Approximate value of point
γ_C	: Unit weight of clay
γ_S	: Unit weight of seabed
γ_W	: Unit weight of water
γ_R	: Unit weight of rubble
δ_{ij}	: Kronecker delta
ε_{ij}	: Total strain
ε_{kk}	: Volumetric strain
ε_{kl}	: Total strain
$\varepsilon_{kl}{}^{0}$	: Initial strain
ε_x	: Strain in x direction
ε_y	: Strain in y direction
ρ	: Unit weight
ρ_f	: Unit weight of pore fluid
λ	: Elastic Lame parameter lambda
σ_x	: Normal stress in x direction

σ_y	: Normal stress in y direction
σ_{ij}	: Total stress
σ'_{ij}	: Effective stress
σ'_m	: Effective mean stress
τ_{xy}	: Shear stress in x-y directions
ω	: Wave angular frequency

LIST OF TABLES

Page

LIST OF FIGURES

Page

ANALYSIS OF DYNAMIC RESPONSE AND INSTABILITY OF A CAISSON TYPE GRAVITY QUAY WALL – SEABED SYSTEM UNDER WAVES

SUMMARY

The investigation of the mechanics of saturated porous media is an important subject matter studied in geomechanics and geo-engineering. The mechanical changes in a soil-structure system under external loads can be examined depending on the movement of both solid and liquid phases in relation to each other in the saturated seabed soil. That is called the problem of "coupled flow and deformation" and the related governing equations are the "poroelasticity" equations developed first by M. Biot in 1941 who later included the dynamic terms. Such terms subsequently are used in developing simplified mathematical formulations in terms of the inertial forces associated with motions of individual phases in the differential equations. These different formulations are obtained in order to provide solutions to the flow and deformation problem for the degrees of freedom of the system as well as internal forces and reactions. In the problems that involve saturated porous media, dynamic response is analyzed based upon key loading characteristics and physical properties of the media which are used to decide whether the simplified formulations are feasible or not for that particular soil-structure interaction problem. In this study, dynamic response of a caisson type quay wall (CTQ) – seabed – backfill soil system exposed to harmonic standing wave loads as well as the instantaneous liquefaction potential of seabed and backfill soil are evaluated. The focus is mainly on the characteristics of the dynamic response of saturated porous seabed and backfill soil around the caisson and their contribution to the CTQ instability under wave loading. In this study, the mathematical model is first developed considering a CTQ structure-seabed-backfill system which is located in the Kobe port of Japan that experienced damage during the Hyogo-Ken Nanbu earthquake in 1995. The classical finite element method is utilized in discretizing the governing poroelasticity equations of the mathematical model. Numerical results are then obtained for each formulation in terms of the variations of vertical and horizontal solid displacements, pore water pressure and shear stress variations in temporal and spatial domains. In addition, the CTQ-seabed system is also analyzed in terms of its instability under standing waves considering instantaneous liquefaction of the soil. By assuming some air voids present in the nearly saturated seabed and the backfill, such phenomenon is analyzed numerically and the regions of instantaneous liquefaction are identified inside the domain in terms of zero or positive contours of mean effective stress. Subsequently, a number of parametric studies is conducted to determine the effects of permeability, soil type and standing wave period on the dynamic response and instability of the system. As a result some interesting results are obtained as far as the dynamic response of the CTQ - seabed system and instantaneous liquefaction potential of seabed and backfill soil are concerned which are thought to be useful for coastal and geotechnical design engineers and researchers working in this field.

KESON TİPİ RIHTIM DUVARI – DENİZ TABANI SİSTEMİNİN DALGA ETKİLERİ ALTINDAKİ DİNAMİK TEPKİSİNİN VE DURAYSIZLIĞININ İNCELENMESİ

ÖZET

Suya doygun gözenekli ortamların mekanik özelliklerinin araştırılması, jeomekanik ve jeo-mühendislik disiplinlerinde incelenen önemli konulardan biridir. Özellikle dış yüklerin etkisi altındaki bir zemin sisteminde meydana gelebilecek mekanik değişiklikler, suya doygun deniz tabanı katmanlarındaki gerek katı gerekse sıvı fazların birbirlerine göre hareketine bağlı olarak incelenebilmektedir. Buna "*birleşik akış ve deformasyon*" problemi adı verilir ve ilişkili denklemleri 1941 senesinde M. Biot tarafından geliştirilmiştir. Daha sonra bu denklemlere, dinamik terimler de ilave edilerek "poroelastisite" denklemine ulaşılmıştır. Bu terimler de daha sonra, diferansiyel denklemlerde tekil fazların hareketleriyle ilişkili atalet kuvvetleri açısından basitleştirilmiş matematik formülasyonların geliştirilmesinde kullanılmıştır. Bu farklı formülasyonlar sistemin serbestlik derecelerinin yanı sıra; iç kuvvetler ve reaksiyonlar için akış ve deformasyon problemine çözüm getirmek amacıyla elde edilmiştir.

Suya doygun gözenekli ortamı içeren problemlerde sistemde oluşan dinamik tepki, basitleştirilmiş formülasyonların söz konusu zemin - yapı etkileşimi problemi için uygun olup olmadığını kararlaştırmak adına kullanılan esas yükleme çeşitleri ve söz konusu ortamın fiziksel özellikleri temel alınarak analiz edilmektedir. Poroelastisite denklemlerinde genel olarak kullanılan ve gerek katı gerekse sıvı fazın atalet terimlerini de içeren durum tam dinamik (FD) formülasyon olarak tarif edilmektedir. Sıvı fazın ataletinden kaynaklanan etkilerin ihmal edildiği durumlar için kısmi dinamik formülasyon (PD) ve hem katı hem de sıvı faza ait atalet terimlerinin ihmal edildiği durumlar için yarı statik formülasyon (QS) elde edilerek bu çalışmadaki tüm tüm analizler bu iki formülasyon (PD ve QS) cinsinden çalışılmıştır.

Öncelikle belirli bir harmonik yük etkisi altında çalışmakta olan bir boyutlu zemin kolonunun davranışı nümerik hesap yapılarak elde edilmiş, böylece düşey yer değiştirmeler ve dalga genliğine göre normalize edilmiş boşluk suyu basınçlarının yüksekliğe bağlı değişim grafikleri elde edilmiştir. Söz konusu sonuçlar analitik çözümlerle karşılaştırılarak kabul edilebilir hassasiyette doğrulama gerçekleştirilmiştir. Bu doğrulama işleminde kabul kriteri olarak %3'ün altında bir yakınsama seviyesine ulaşılmış olması belirlenmiştir. Ardından bir sonraki aşamaya geçilerek, sadece tek bir dalga boyu için ilerleyen dalga yükleri etkisi altında serbest sahada çalışan ve sadece tek bir zemin katmanından meydana gelen gözenekli ve suya doygun bir zemin yapısının iki boyutlu matematiksel modeli oluşturulmuştur. Bu model, sistemin serbest sahada çalışması ve dalganın zemin katmanı yüzeyinde sürekli ilerleyen bir hareket sürdürmesi sebebiyle matematiksel modelin sol ve sağ

tarafındaki sınır koşulları birbirine doğrusal bir fonksiyonla bağlı olacak şekilde tarif edilerek sadece tek bir dalga boyu için hazırlanmıştır. Genel olarak bu çalışma içerisindeki tüm matematiksel modellerde tanımlanan poroelastisite denklemlerinin ayrıklaştırılması için klasik sonlu elemanlar yöntemi (FEM) kullanılması sebebiyle, sonlu eleman parçalarının boyutlarında küçülmeye gidilerek bir kaç defa çözüm gerçekleştirilmiş ve alınan sonuçların %3'lük kabul edilebilir yakınsama derecesine ulaşmasının ardından matematiksel modelleme kıstası belirlenmiştir. Bu işlemler yapılırken de yine bir boyut için gerçekleştirilen çözümde de olduğu gibi nümerik sonuçlar ile analitik sonuçlar; yakınsama kontrolleri, katı faz için elde edilen düşey yer değiştirmeler, ilerleyen dalga genliğine göre normalize edilmiş boşluk suyu basınçları ve efektif normal gerilmelerin derinliğe göre değişimi cinsinden karşılaştırılmıştır. Sonuçlarda görülen kabul edilebilir yakınsama kriterinin yakalanmasıyla birlikte harmonik duran dalga yüklerine maruz kalan bir keson tipi rıhtım duvarı (CTQ) - deniz tabanı - dolgu zemin sisteminin dinamik tepkisi değerlendirme işlemine geçilmiştir. Açık denizde ilerleyen dalganın rıhtım duvarı yüzeyinden yansımasıyla birlikte ardındaki dalgalar ile girişimde bulunarak duran dalga formuna dönüşmesi nedeniyle bu aşamada duran dalga etkisi dikkate alınmıştır. Bu sistemin matematiksel modelinin temsil ettiği alanın genişliği, farklı malzeme özelliklerine sahip çok sayıda katmanın bir arada kullanılması ve su derinliğinin model içerisinde değişkenlik göstermesi sebebiyle elde edilen sonuçların doğruluğunu kontrol edebilmek adına önceki bölümlerde de olduğu gibi sonlu eleman parçalarının model alanı içerisindeki boyutu küçültülerek ve dolayısıyla sayısı da kademeli olarak arttırılarak rıhtım duvarının ön topuk bölgesinden geçen düşey doğrultudaki bir kesit üzerinden elde edilen sonuçlar karşılaştırılmış ve sistemi en doğru şekilde temsil edecek sonlu eleman boyutları belirlenmiştir. Bununla beraber, açık deniz etkisini de sisteme doğru bir şekilde tanımlayabilmek için de matematiksel modelin açık denizi temsil eden düşey kenarının rıhtım duvarı ile arasındaki mesafe kademeli olarak arttırılmış ve benzer şekilde en uygun açık deniz mesafesi, duran dalga boyu cinsinden belirlenerek matematiksel modele aktarılmıştır. Bu çalışmadaki temel odak noktası ağırlıklı olarak suya doygun gözenekli deniz tabanının ve dolgunun etrafındaki toprağın dinamik tepkisinin özelliklerine ve bunların duran dalga yükleri altındaki rıhtım duvarı duraysızlığına olan katkısıdır. Çalışmada, Japonya'nın Kobe limanında bulunan ve 1995 yılındaki Hyogo-Ken Nanbu depreminde önemli derecede hasar gören bir rıhtım duvarı - deniz tabanı - dolgu sistemi dikkate alınmıştır. Bu analizler sırasında, hem PD hem de QS formülasyonlarında, katı faz için zamansal ve mekansal alanlardaki düşey ve yatay yer değiştirmeler, duran dalga genliğine göre normalize edilmiş boşluk suyu basınçları ve kayma gerilmelerinin derinlikle değişim varyasyonları açısından sayısal sonuçlar elde edilmiş ve karşılaştırılmalı olarak sunulmuştur.

CTQ – deniz tabanı sistemi ayrıca, zemindeki ani sıvılaşma potansiyeli göz önüne alınarak duran dalga etkisi altında rıhtım duvarı duraysızlığı açısından da değerlendirilmiştir. Bu analizler sırasında, sistemin dinamik tepkisinin araştırıldığı bir önceki bölümden farklı olarak mevcut rıhtım duvarının, zemin katmanlarının ve deniz suyunun kendi ağırlıklarından ötürü oluşan kuvvetler de matematiksel modele aktarılmıştır. Neredeyse suya doygun deniz tabanı katmanında ve dolgu alanında küçük hava boşlukları bulunduğunu varsayarak suya doygunluk derecesi deniz tabanı için S=0.999 olacak şekilde tarif edilmiş, bu olgu sayısal olarak analiz edilmiş ve ani sıvılaşma bölgeleri hesaplanan ortalama efektif gerilmenin sıfır veya pozitif konturları cinsinden hesap alanı içerisinde tanımlanmıştır. Daha sonra duran dalga yüksekliği sabit tutularak söz konusu sistem içerisinde sadece deniz tabanındaki farklı geçirgenlik, zemin tipi ve açık denizde meydana gelen duran dalga periyodu süresindeki (lineer dalga teorisine göre aynı zamanda dalga boyundaki) değişikliklere göre sistemde oluşan dinamik tepkileri ve rıhtım duvarı duraysızlığı üzerindeki etkileri belirlemek amacıyla bir takım parametrik çalışmalar yürütülmesinin ardından her iki formülasyon (PD ve QS) için elde edilen sonuçlara ilişkin karşılaştırma grafikleri sunulmuştur. Bununla beraber, bu çalışmanın geliştirilmesi için ileriki zamanlarda yapılması düşünülen ve malzemenin doğrusal olmayan davranışlarının da hesaba katılması ile birlikte sistemin gerçek tepkisine en yakın sonuçların elde edilebilmesi adına ön bilgi oluşturabilecek şekilde kritik bölgelerin gösterilebildiği kayma gerilmesi diyagramları da ayrıca gösterilmiştir. Sonuç olarak, deniz tabanı ve dolgu toprağının ani sıvılaşma potansiyeline bakıldığında, söz konusu CTQ - deniz tabanı sisteminin duran dalga etkisi altındaki dinamik tepkisi ve duraysızlığı üzerinde, bu alanda çalışan kıyı ve jeoteknik tasarım mühendisleri ile diğer araştırmacılar için yararlı olabileceği düşünülen sonuçlar elde edilmiştir.

1. INTRODUCTION

Today, the use of sea lanes has become very common both in terms of tourism as well as in passenger transport and shipping for commerce. In this respect, a significant budget is being spent to build ports worldwide. Therefore, coastal protection measures are taken for all kinds of hazards that may arise from the sea and constitute a physical threat to the port. Particularly, these measures are constructing breakwaters along the coasts of communities and building quay walls along the coastlines by harbor regions. The main task of these structures is to maintain stability of coasts against severe wave actions. The idea here is to provide resistance to both oscillatory and impact loads and other external disastrous effects such as ship strikes. At the same time, they also provide security for structures on and around the ports.

Quay walls are marine structures that are built as a part of a port to sustain port's integrity and provide protection. They are the most common types of construction for docks because of their durability, ease of construction and capacity to reach deep seabed levels. The design of gravity quay walls requires sufficient capacity for three design criteria; sliding, overturning and allowable bearing capacity under the base of the wall.

Until today, plenty of studies done by a large number of researchers is at a satisfactory level to calculate the reaction they have given under static loads. Unfortunately, since it is not possible to say the same thing under seismic loads, therefore research studies on this subject are still conducted. In addition, because these structures are directly connected to the sea, they have to be resistant not only to structural loads, but also to wave loads. In the ocean, not only the impact of gigantic waves called *tsunamis* generated mostly as a result of an an earthquake but waves caused by large ship transits can also be quite challenging to incorporate their effects on such protecting systems in these marine structures. In addition, the effects of these waves on the soil layers lying under or at the back of the structures can also bring about secondary problems.

There are several different ways to build these marine structures. Prefabricated and L-shaped reinforced concrete structures on rubble fill, the caisson walls formed by filling the reinforced concrete caisson with soil filling material, facing panels used reinforcement bars to the walls of the anchorage technique and block walls which are constructed by stacking reinforced concrete blocks are some of the current construction techniques. The correct design of these marine structures is vital. As a consequence of erroneous designs, for example, there may be problems such as wall experiencing rocking motion that may cause collapse, excessive displacement, breakage, cracking and insufficient resistance to wave loads to prevent the water passage to seaport. However, the liquefaction that may occur in other soil layers in the system to which the wall is attached is a serious hazard for structures located on or near the shore. Unfortunately, it is not uncommon to see such failures among the ports of the world coasts in this way.

While breakwaters are mainly used to protect the majority of a port against wave action, it is safe to say that quay walls act as a secondary measure against coastal hazards. Thus, it is also not a common practice to evaluate the dynamic response of quay walls under severe wave conditions as more often than not it is breakwaters' job to protect such systems. However, sometimes that is not the case (i.e. the Ambarli Port or the Asya Port in Turkey) and either there is no breakwater placed at all or that quay wall acts as a protector while the breakwater is being built. Hence, conducting such analyses for evaluating the quay wall response becomes a requirement for us, researchers.

In the former, quay wall needs to be analyzed against severe wave action which is the primary cause of instability while in the latter; the primary cause of instability becomes the earthquake excitation. Today, it is possible to see that many researchers focus on damages experienced by such systems that can occur under earthquake loads. However, it is not correct to just ascertain such dynamic effects exclusively through earthquake loads. A coastal structure that has not been damaged by earthquakes or has not been subjected to any previous seismic shaking can suffer severe damage under the influence of progressive or standing waves. Surprisingly, just few studies that consider waves as the major cause of failure are made by the researchers. In these studies, a gravity type quay wall containing several layers of concrete blocks with a special cross section is generally analyzed under standing wave effects. On the other hand, in the coastal areas prone to earthquakes, it is absolutely necessary to examine the dynamic response of the CTQ. For this purpose, various researchers have worked on such coastal structures which are mentioned below in the brief literature survey.

It has been common to examine the response of coastal structures under various types of waves using numerical models frequently used in the solution of geo-engineering problems. With the increased use of computers and the help of advanced softwares, finite element (FE) models are created and thus, more accurate results are achieved.

In this study, following the development of the FE model which models the system in question, parametric studies are carried out using different soil types, wave periods and permeability coefficients. The time required for the system to reach steady state during loading is taken into account. Then, standing wave-induced pore water pressures, solid soil displacements, shear stresses are evaluated and the instantaneous liquefaction potential of a real CTQ-rubble-seabed system damaged in the 1995 Hyogoken-Nanbu earthquake in Port Island is computed through classical finite element analyses.

2. LITERATURE REVIEW

2.1 Quay Walls as Marine Structures

Among the few studies that consider waves as the major cause of failure, Shireishi et al. (1976) takes a gravity type quay wall comprising several layers of concrete blocks with a special shape under standing wave effects. Much later, George (2007) investigates some of the old ports with scour problems in their quays that are exposed to standing waves. Standing wave effects are also investigated for other caisson type structures (Tsai and Lee, 1995; Kudella et al., 2006; Ulker et al., 2010). In the coastal regions that are prone to earthquakes, it is necessary to study the dynamic response of caisson type quay walls (CTQ). For example Sugano et al. (1996) investigate the effect of Hyogoken- Nanbu earthquake on caisson type coastal structures (such as the one in the Kobe Port). Alyami et al. (2007) use generalized plasticity model to generate simulations of seismic performance of the caisson in the same port. Furthermore, El-Sharnouby et al. (2004) study the importance of design parameters and focus on the analysis of gravity quay walls. Design steps are presented in terms of a computer program that takes into account all factors affecting their analysis. Then, Iai (2011) focuses on seismic performance criteria of gravity coastal structures. More recently, Tasiopoulou et al. (2014) studies the CTQ at the Piraeus Port under seismic loading using the finite difference method.

2.2 Poroelasticity in the Analysis of Coastal and Marine Structures

The earlier form of the *theory of poro-elasticity* was developed as *the theory of consolidation* by Terzaghi (1925) for a one-dimensional situation. In his original theory, Terzaghi accepts that the deformation of the soil is essentially caused by the rearrangement of the particle distribution. It also assumes that the compressiblity of pore fluid and that of solid particles can be practically neglected. In subsequent presentations of the theory, these effects are also considered in detail. Rendulic

(1936) develop these studies and perform analyzes in three dimensions. Biot (1941) was the one who generalized the consolidation theory to three spatial dimensions and later included the dynamic terms (Biot 1955, 1962). We now call the theory "coupled flow and deformation theory".

In recent years, the poroelasticity formulation is applied to coastal structures, such as quay walls and breakwaters by various researchers. These structures are responsible for preventing the risks of structural and soil instability in terms of instantaneous liquefaction, progressive build-up of pore pressure, excessive deformation of marine structures and shear failure (Zen et al., 1987; Maeno and Nago, 1988). Moreover, the research studies in the following years have shown that a significant amount of pores in the seabed layer and remarkable magnitudes of stresses in the rubble mound occur (Lundgren et al, 1989; Silvester and Hsu, 1989). Then, the constitutive equations presented to combine and relate the various approaches proposed in the literature are evaluated (Detournay and Cheng, 1993). This is followed by studies of pore pressures and effective stress in coastal structures (Mase et al, 1994). In addition to analytical models, numerical models have also been developed specifically for estimating liquefaction, in particular the book of computational geomechanics (Zienkiewicz et al., 1999). In these studies, the poro-elastic model is the simplest constructor relation and is used in most analytical models. The elasto-plastic model is more popular in computational geomechanics and gives more accurate results to the experiments in both sites and laboratories. The stability of seabed underneath marine gravity structures subjected to wave loads is studied by De Groot et al. (2006). Kudella et al. (2006) conducted large-scale model experiments and investigated the effect of instantaneous and residual pore pressure generation underneath a caisson breakwater in relation to the stability of seabed. Following the development of the technology and the use of computers, the introduction of advanced software that enables the preparation of mathematical models of the above mentioned problems using classical FE models has been introduced (Verruijt, 2013).

2.3 Liquefaction Studies

In the analysis of the liquefaction potential in the field, "Simplified Liquefaction Analysis" is widely used at earlier times (Seed and Idriss, 1971). The liquefaction resistance of soil layers is often correlated with the results of field trials. Although seabed liquefaction under progressive waves has been extensively investigated, only a few works have been done on the liquefaction of seabed under standing waves. Sekiguchi et al. (1995) used a centrifugal wave test to obtain some useful experimental data. The test set-up by Sassa and Sekiguchi (1999) was designed to measure pore pressures that indicated that the antinodal section was where the liquefaction was observed, although the soil did not encounter any shear stresses in the section. Other study results show that the residual liquefaction causes that blocks on marine structures sink in such a liquefied soil as a result of their own weight (Suzuki et al., 1998; Sumer et al., 1999). The latter study examines the damage caused on coastal structures as a result of wave-induced liquefaction and associated drifting movement (Kirca, 2013).

In addition, instantaneous liquefaction studies have been the center of attention for researchers, in the last couple of decades. This mechanism occurs in a seabed having some air in the voids. Therefore; the major cause of sinking of breakwaters is investigated in terms of instantansoue liquefaction (Sakai et al., 1995; Sumer and Fredsøe, 2002; Ulker et al., 2010; Ulker et al., 2012; Ulker 2012). Moreover, studies on tsunami scour and sedimentation have been carried out with the potential for instantaneous liquefaction (Yeh and Li, 2008). Then, in a comprehensive study on instantaneous liquefaction, analytical solutions and numerical models are developed for the response of plane strain saturated porous media, and wave-induced response of seabed in free field and around a breakwater under pulsating/breaking waves are investigated (Ulker, 2009). Recently, the effect of degree of saturation on instantaneous liquefaction of seabed around a rubble mound breakwater is presented by (Ulker and Massah Fard, 2016).

3. MATHEMATICAL FORMULATION OF POROELASTICITY: DYNAMICS OF SATURATED POROUS SEABED

It is generally undesirable to describe soils as solid materials in geomechanics. Soils are composed of varying size and shape of solid particles, and often the pore space between these particles is filled with a fluid (generally water). This multi-phase structure is called "saturated or partially saturated porous media" in soil mechanics. The deformation of this porous medium depends on the rigidity of the porous material and the flow of the fluid in the pores. If the permeability of the material is negligibly small, rate of deformations decrease due to partly the viscous actions of the fluid in the pores but mostly due to reduction of the ability for flow to take place through the small size pores. The simultaneous deformation of a porous medium and the flow of pore fluid is the main subject matter in geomechanics. Therefore, it is necessary to analyze the soil response under external loads by using the equations governing the actual behavior as observed in nature. These equations are derived considering three basic physical laws namely;

1. Constitutive law
2. Law of conservation of momentum
3. Law of conservation of mass

These laws result in;

- The stress-strain relationship
- The momentum balance (i.e. equilibrium equations)
- The mass balance equation, (i.e. continuity equation)

respectively.

3.1 Governing Equations

Saturated poromechanics is described as the 'theory of coupled flow and deformation' developed first by Biot (1941, 1955 and 1962) which is also known as *the theory of dynamic consolidation* as indicated before. Principle of effective stress, as introduced by Terzaghi (1925), is defined as the stress developed as the average of contact stresses along a cross section in the soil skeleton. In developing a general mathematical formulation governing the behavior of this two-phase soil field, the following assumptions are made:

(1) The water and the gas phases within the porous medium are considered as a single compressible fluid.

(2) The effect of gas diffusing through water and movement of water vapor is neglected.

In addition, it is assumed that the total stresses can be decomposed into the sum of the effective stresses and pore pressure by writing:

$$\sigma_{ij} = \sigma_{ij}' - \delta_{ij} p \tag{3.1}$$

where σ_{ij}' is effective stress, σ_{ij} is total stress, δ_{ij} is Kronecker delta and p is pore pressure. Tension is taken as positive in this equation. Strain, ε_{ij} is defined as,

$$\varepsilon_{ij} = \frac{1}{2}\left(u_{i,j} + u_{j,i}\right) \tag{3.2}$$

where $u_{i,j}$ and $u_{j,i}$ are the derivatives of soil displacement. The effective stress-strain relation can be written as,

$$\sigma_{ij}' = D_{ijkl}(\varepsilon_{kl} - \varepsilon_{kl}{}^{0}) \tag{3.3}$$

where D_{ijkl} is the tangent material rigidity matrix and $\varepsilon_{kl}{}^{0}$ is the initial strain. By using the Lame's parameters of elasticity (λ and G), stress-strain relationship becomes:

$$\sigma_{ij}' = \lambda \varepsilon_{kk} \delta_{ij} + 2G\varepsilon_{ij} \tag{3.4}$$

where ε_{kk} is volumetric strain and ε_{ij} is shear strain in indicial notation. Considering the inertial forces associated with both the soil skeleton and the pore water, governing equations in "Fully Dynamic Formulation (FD)" form are obtained as:

$$\sigma_{ij,j} + \rho g_i = \rho \ddot{u}_i + \rho_f \ddot{\bar{w}}_i \tag{3.5}$$

$$-p_{,i} + \rho_f g_i = \rho_f \ddot{u}_i + \frac{\rho_f \dot{\bar{w}}_i}{n} + \frac{\rho_f g}{k_i} \dot{\bar{w}}_i \tag{3.6}$$

$$\dot{u}_{i,i} + \dot{\bar{w}}_{i,i} = -\frac{n}{K_f} \dot{p} \tag{3.7}$$

where g is the gravitational acceleration, ρ and ρ_f are the unit weights of soil and fluid, K_f is the bulk modulus of the pore fluid, n is porosity, w is the relative fluid displacement and u is the displacement of the solid part. By omitting the acceleration terms in these equations one by one, we can obtain the Partly Dynamic (PD) formulation first and then the Quasi Static (QS) formulation. Throughout this thesis, the focus will be entirely on these simplified forms; hence, the numerical formulations are developed accordingly. Nonetheless, by using the tensorial forms, we can write the FD as:

$$-\nabla^T \sigma + \rho_f \ddot{\bar{w}} + \rho \ddot{u} = \rho g \tag{3.8}$$

$$\nabla^T p + \frac{\rho_f}{n} \ddot{\bar{w}} + \rho_f \ddot{u} + \frac{\rho_f g}{k} \dot{\bar{w}} = \rho_f g \tag{3.9}$$

$$\nabla^T u + \nabla^T w + \frac{n}{K_f} p = 0 \tag{3.10}$$

3.2 Simplified Forms

As mentioned, it is possible to have different idealizations in the governing equations of the coupled flow and deformation problem depending on the motion of fluid in the pores and the soil skeleton in addition to permeability of the porous medium. These are called the partially dynamic (PD) form and the quasi-static (QS) form.

Neglecting the inertial terms associated with the relative pore fluid displacement, we obtain the equation system for PD as:

$$\sigma_{ij,j} + \rho g_i = \rho \ddot{u}_i \tag{3.11}$$

$$-p_{,i} + \rho_f g_i = \rho_f \ddot{u}_i + \frac{\rho_f g_i}{k_i} \dot{\bar{w}}_i \tag{3.12}$$

$$\dot{u}_{i,i} + \dot{\bar{w}}_{i,i} = -\frac{n}{K_f} \dot{p} \tag{3.13}$$

We can write the equation below by combining (3.1), (3.2) and (3.3),

$$\sigma_{ij} = D_{ijkl} u_{k,l} - \delta_{ij} p \tag{3.14}$$

Equations (3.11) and (3.14) are combined to give;

$$D_{ijkl} u_{k,lm} - \delta_{ij} p_{,j} = \rho \ddot{u}_i \tag{3.15}$$

and (3.12) and together with (3.13) result in:

$$\dot{u}_{i,j} + \left(\frac{-k_i}{\rho_f g_i} p_{,j} - \frac{k_i}{g_i} \ddot{u}_i \right)_{,i} = -\frac{n}{K_f} \dot{p} \tag{3.16}$$

Equations (3.15) and (3.16) is the final form of the simplified PD formulation. If we omit all inertial terms in the system above we get the QS formulationsand the governing equations become:

$$D_{ijkl}u_{k,lm} - \delta_{ij} p_{,j} = 0 \tag{3.17}$$

$$\dot{u}_{i,j} + \left(\frac{-k_i}{\rho_f g_i} p_{,j} \right)_{,i} = -\frac{n}{K_f} \dot{p} \tag{3.18}$$

4. NUMERICAL FORMULATION

As in many engineering branches, it is difficult to describe a problem in geo-engineering as close to the actual behavior observed in real life as possible and to determine the natural behavior of engineering systems under dynamic loads. Solving these difficult problems with the available scientific methods is possible exclusively through numerical methods implemented in computers that can do many operations simultaneously in a short amount of time. For that, we need numerical methods to solve a series of algebraic linear (or nonlinear) system of equations gathered from actual governing partial differential equations of the physical system. In this thesis, the classical finite element method (FEM) is used to discretize the governing equations of poroelasticity as was presented in the previous chapter. Below presents a summary of the FE formulations in Ulker (2009) and used here.

4.1 Finite Element Formulations

The necessary FE formulation is derived based on the “principal of virtual work” written in terms of weak formulation of the governing equations followed by the FE approximation of field variables and their time derivatives within the domain of interest.

The FE formulation of the PD formulation is presented first in this section. If we neglect the inertial terms associated with the relative fluid acceleration ($\ddot{w}$), we obtain the matrix form equation of motion below:

$$\begin{bmatrix} \mathbf{M_s} & 0 \\ \mathbf{M_{sf}} & 0 \end{bmatrix} \begin{Bmatrix} \ddot{\boldsymbol{U}} \\ \ddot{\boldsymbol{P}} \end{Bmatrix} + \begin{bmatrix} 0 & 0 \\ \mathbf{C^T} & \mathbf{C_f} \end{bmatrix} \begin{Bmatrix} \dot{\boldsymbol{U}} \\ \dot{\boldsymbol{P}} \end{Bmatrix} + \begin{bmatrix} \mathbf{K_s} & \mathbf{-C} \\ 0 & \mathbf{K_f} \end{bmatrix} \begin{Bmatrix} \boldsymbol{U} \\ \boldsymbol{P} \end{Bmatrix} = \begin{Bmatrix} \boldsymbol{F_s} \\ \boldsymbol{F_f} \end{Bmatrix} \tag{4.1}$$

The sub-matrices here are:

$$\mathbf{K_s} = \int_\Omega [B_u]^T \underset{\approx}{D} [B_u] d\Omega \tag{4.2}$$

$$\mathbf{K_f} = \int_\Omega \left[B_p\right]^T \frac{[k]}{\rho_f g} \left[B_p\right] d\Omega \tag{4.3}$$

$$\mathbf{C} = \int_\Omega [B_u]^T \{m\} \left[N_p\right] d\Omega \tag{4.4}$$

$$\mathbf{C_f} = \int_\Omega \left[N_p\right]^T \frac{n}{K_f} \left[N_p\right] d\Omega \tag{4.5}$$

$$\mathbf{M_s} = \int_\Omega [N_u]^T \rho [N_u] d\Omega \tag{4.6}$$

$$\mathbf{M_{sf}} = \int_\Omega \left[B_p\right]^T \frac{[k]}{g} [N_u] d\Omega \tag{4.7}$$

where m is the Kronecker delta vector, $\mathbf{K_s}$ and $\mathbf{K_f}$ are the stiffness matrices of solid, $\mathbf{C}$ and $\mathbf{C_f}$ are the damping matrices of system and fluid, $\mathbf{M_s}$ and $\mathbf{M_{sf}}$ are the mass matrices of solid and fluid, B_p and B_u are the strain – displacement matrices for pressure and displacement, N_p and N_u are the shape function vectors for pressure and displacement, respectively. More information related to these shape functions is given in the next section.

The FE formulation of the QS forms of governing equations is the one where all the inertial terms are neglected. The obtained equations are approximated by the same shape functions which are specified in spatial dimensions. Consequently we can have,

$$\begin{bmatrix} 0 & 0 \\ \mathbf{C^T} & \mathbf{C_f} \end{bmatrix} \begin{Bmatrix} \dot{\boldsymbol{U}} \\ \dot{\boldsymbol{P}} \end{Bmatrix} + \begin{bmatrix} \mathbf{K_s} & \mathbf{-C} \\ 0 & \mathbf{K_f} \end{bmatrix} \begin{Bmatrix} \boldsymbol{U} \\ \boldsymbol{P} \end{Bmatrix} = \begin{Bmatrix} \boldsymbol{F_s} \\ \boldsymbol{F_f} \end{Bmatrix} \tag{4.8}$$

5. FINITE ELEMENT ANALYSES: DETAILS

5.1 Spatial Integration

5.1.1 Gauss quadrature

In this thesis, the Gauss-Quadrature numerical integration method is used with the idea of defining a number of specific locations in the domain of interest where variables converge at a maximum rate with the use of some integral parameters eliminating the obligation of using the function values at certain equally spaced points. In this method, an 'n' number of parameter evaluations of the integral corresponds to a $2n-1$ degree polynomial approximation or such an order approach. Families of methods based on this principle are known as the "Gauss quadrature method". This method can be used if $f(x)$ is known explicitly. Gauss integral formulations are the most accurate in the interval of integration of [-1, 1]. The general form is given as:

$$\int_{-1}^{1} f(x)dx \cong \sum_{i=1}^{n} c_i f(x_i) \tag{5.1}$$

where x_i is the approximate value of the point, n is the number of terms used, c_i is the coefficient of convergence. This is the real integration formula for a polynomial at the degree of $2n-1$. The parameters for Gauss quadrature is given below in Table 5.1.

Table 5.1: Parameters for Gauss quadrature.

n	x_i	c_i
2	≅±0.57735	1
3	0	8/9
	≅±0.77459	5/9
4	≅±0.861136	0.34785
	≅±0.339981	0.652145

5.1.2 Shape functions

The element types are called as Constant Strain Triangle (CST), Linear Strain Triangle (LST), Linear Quadrilateral (Q4), and Quadratic Quadrilateral (Q8). CST and Q4 are usually used together in a mesh with linear elements. LST and Q8 are generally applied in a mesh composed of quadratic elements. Quadratic elements are preferred for stress analysis because of their high accuracy and the flexibility in modeling complex geometry such as curved boundaries. Figures 5.1 and 5.2 show the Q8 and Q4 elements into $\xi - \eta$ space respectively.

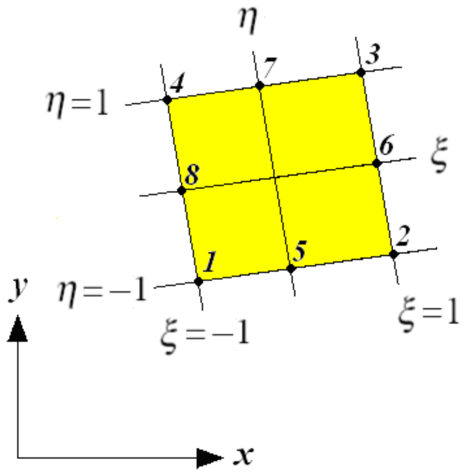

Figure 5.1: Quadratic 8-noded element (Q8).

There are eight nodes for this element, four corners nodes and four mid-side nodes. In the natural coordinate system (ξ, η) the eight shape functions are shown below as:

$$N_1 = \frac{1}{4}(1-\xi)(\eta-1)(\xi+\eta+1) \tag{5.2}$$

$$N_2 = \frac{1}{4}(1+\xi)(\eta-1)(\xi-\eta+1) \tag{5.3}$$

$$N_3 = \frac{1}{4}(1+\xi)(\eta+1)(\xi+\eta-1) \tag{5.4}$$

$$N_4 = \frac{1}{4}(1-\xi)(\eta+1)(\xi-\eta+1) \tag{5.5}$$

$$N_5 = \frac{1}{2}(1-\eta)(1-\xi^2) \tag{5.6}$$

$$N_6 = \frac{1}{2}\ (1+\xi)(1-\eta^2) \tag{5.7}$$

$$N_7 = \frac{1}{2}\ (1+\eta)(1-\xi^2) \tag{5.8}$$

$$N_8 = \frac{1}{2}\ (1-\xi)(1-\eta^2) \tag{5.9}$$

We have $\sum_{i=1}^{8} N_i = 1$ at any point inside the element. The displacement field is given by

$$u = [\sum_{i=1}^{8} N_i u_i] \tag{5.10}$$

$$v = [\sum_{i=1}^{8} N_i v_i] \tag{5.11}$$

which are quadratic functions over the element. Strains and stresses over a quadratic quadrilateral element are quadratic functions, which are better representations.

The Q8 elements for the u-field integration are generally preferred because of more accurate modeling of shear and volumetric deformations of the soil and due to spatial convergence.

The shape functions used for the pressure are preferred as having one order of polynomial degree less than they are for the displacement DOF, since the rate of convergence of the pressure is greater than the rate of convergence of the displacement. Thus, Q8 shape functions for the u-field and Q4 shape functions for the p-field are used in the finite element analyses. The shape functions for Q4 are shown below:

$$N_1 = \frac{1}{4}\ (1-\xi)(1-\eta) \tag{5.12}$$

$$N_2 = \frac{1}{4}(1+\xi)(1-\eta) \tag{5.13}$$

$$N_3 = \frac{1}{4}(1+\xi)(1+\eta) \tag{5.14}$$

$$N_4 = \frac{1}{4}(1-\xi)(1+\eta) \tag{5.15}$$

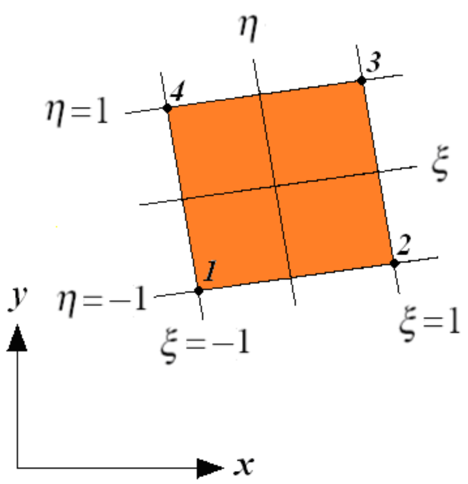

Figure 5.2: Quadrilateral 4-noded element (Q4).

Figure 5.3 shows the basic FEM features used in the analyses. In this figure; DOF1, DOF2 and DOF3 represent the horizontal displacements, vertical displacements and pore water pressures, respectively.

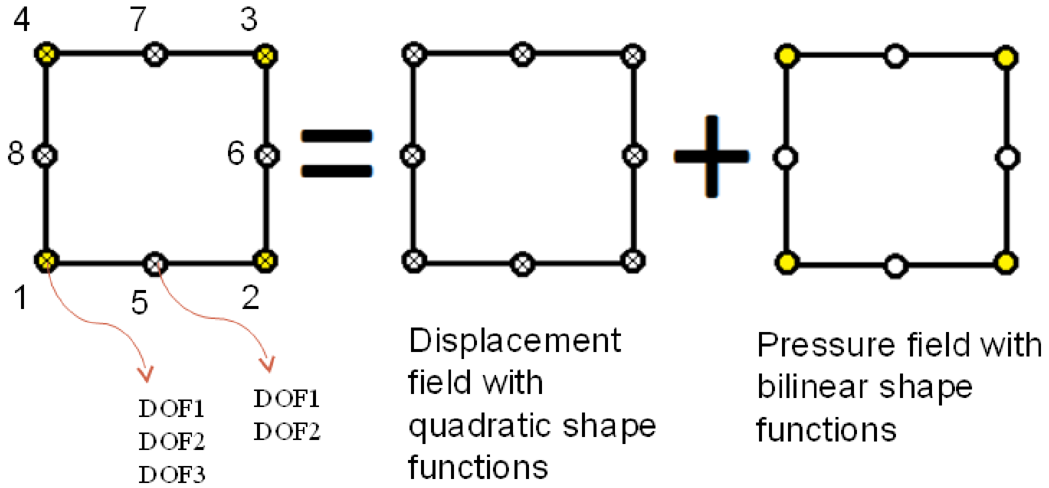

Figure 5.3: Basic FEM features used in analyses.

5.2 Temporal Integration

5.2.1 Implicit Newmark-β method

Time integration for obtaining the numerical results is carried out by using the *Implicit Newmark-β Method*. So, at time step *n+1*, we have,

$$\underset{\approx}{M}\ddot{\underset{\sim}{X}}_{n+1}+\underset{\approx}{C}\dot{\underset{\sim}{X}}_{n+1}+\underset{\approx}{K}\underset{\sim}{X}_{n+1}=\underset{\sim}{R}_{n+1} \tag{5.16}$$

For the X vector, the relations for the acceleration, velocity and the displacement are,

$$\ddot{X}_{n+1}=\ddot{X}_n+\delta\ddot{X}_{n+1} \tag{5.17}$$

$$\dot{X}_{n+1}=\dot{X}_n+\Delta t\left[\left(1-\gamma\right)\ddot{X}_n+\gamma\ddot{X}_{n+1}\right] \tag{5.18}$$

$$X_{n+1}=X_n+\Delta t\dot{X}_n+\frac{\Delta t^2}{2}\left[\left(1-2\beta\right)\ddot{X}_n+2\beta\ddot{X}_{n+1}\right] \tag{5.19}$$

Here, γ and β are the Newmark parameters controlling the stability and convergence of the numerical solution that have a certain range of values to be able to obtain unconditional stability with certain accuracy. The second order accuracy is attained for numerically undamped scheme if γ=0.5 and β=0.25. Conversely, if numerical damping is desired, then the accuracy declines to first order. By solving (5.15) for $\ddot{X}_{n+1}$, then substituting it into (5.14), we get

$$\ddot{X}_{n+1}=\frac{1}{\beta\Delta t^2}\left(X_{n+1}-X_n-\Delta t\dot{X}_n\right)-\left(\frac{1}{2\beta}-1\right)\ddot{X}_n \tag{5.20}$$

$$\dot{X}_{n+1}=\frac{\gamma}{\beta\Delta t}\left(X_{n+1}-X_n\right)-\left(\frac{\gamma}{\beta}-1\right)\dot{X}_n-\Delta t\left(\frac{\gamma}{2\beta}-1\right)\ddot{X}_n \tag{5.21}$$

These equations are substituted into (5.12) and then are solved for X_{n+1}. It becomes,

$$\left(\frac{1}{\beta\Delta t^2}M+\frac{\gamma}{\beta\Delta t}C+K\right)X_{n+1}=M\left(\frac{1}{\beta\Delta t^2}X_n+\frac{1}{\beta\Delta t}\dot{X}_n+\left(\frac{1}{2\beta}-1\right)\ddot{X}_n\right)$$
$$+C\left(\frac{\gamma}{\beta\Delta t}X_n+\left(\frac{\gamma}{\beta}-1\right)\dot{X}_n+\Delta t\left(\frac{\gamma}{2\beta}-1\right)\ddot{X}_n\right)+R_{n+1} \tag{5.22}$$

The above statement leads to a procedure that solves for the displacement first at step n+1. Then using (5.16) and (5.17), velocity and accelerations are calculated. It can be shown that Newmark method has unconditional stability when

$$2\beta \geq \gamma \geq 0.5 \tag{5.23}$$

If $\gamma > 0.5$, Newmark method displays numerical damping which is highest for 0.6. To obtain the highest possible dissipation while retaining unconditional stability, the following choice of β would be appropriate, (Cook et al. 2001),

$$\beta=\frac{1}{4}\left(\gamma+\frac{1}{2}\right)^2 \tag{5.24}$$

6. VERIFICATION ANALYSES

The main purpose of this chapter is that the mathematical formulations presented in Chapter 4 are implemented in a computer program developed by (Guddati et al., 2009) and requires verification by solving a number of basic problems in the free field where there is no coastal structure in the vicinity, which have their analytical solutions readily available. So, two problems with soil layers in 1-D and 2-D are picked along with their analytical solutions developed by Ulker (2009). The idea behind this is that possible FE results matching with their analytical counterparts provide confidence in both the mathematics of the formulation and their implementation into a computer as a code.

6.1 Problem 1: One-Dimensional Soil Column Response under Cyclic Wave

6.1.1 Problem definition

In this section the general analytical solutions for 1-D response are presented. The solution is developed for a soil column that refers a porous media under cyclic wave loading for PD formulations. The input data for soil material and the numerical values of the other parameters used in 1-D analysis are presented in Table 6.1. Figure 6.1 presents the 1-D seabed soil under cyclic wave loading. The cyclic wave induced pressures and forces are applied in terms of time histories evaluated from the equation below:

$$q_{i,j} = q_0 \cos(\omega . t_i) \tag{6.1}$$

where $q_{i,j}$ is the pressure, q_0 is the wave amplitude and ω is the wave angular frequency.

Table 6.1: Numerical values of the parameters used in 1-D analysis.

Parameter	Symbol	Unit	Value
Depth of soil	h	m	20
Elasticity modulus of soil	E	kN/m^2	13500
Poisson's ratio	v	-	0.3
Vertical permeability	k_z	m/s	0.001
Horizontal permeability	k_x	m/s	0.001
Bulk modulus of pore water	K_f	kN/m^2	2.3x10^6
Saturation	S	-	1
Porosity	n	-	0.3
Unit weight of soil	γ_s	t/m^3	2
Unit weight of water	γ_w	t/m^3	1
Gravitational acceleration	g	m/s^2	9.81
Period	T	s	1

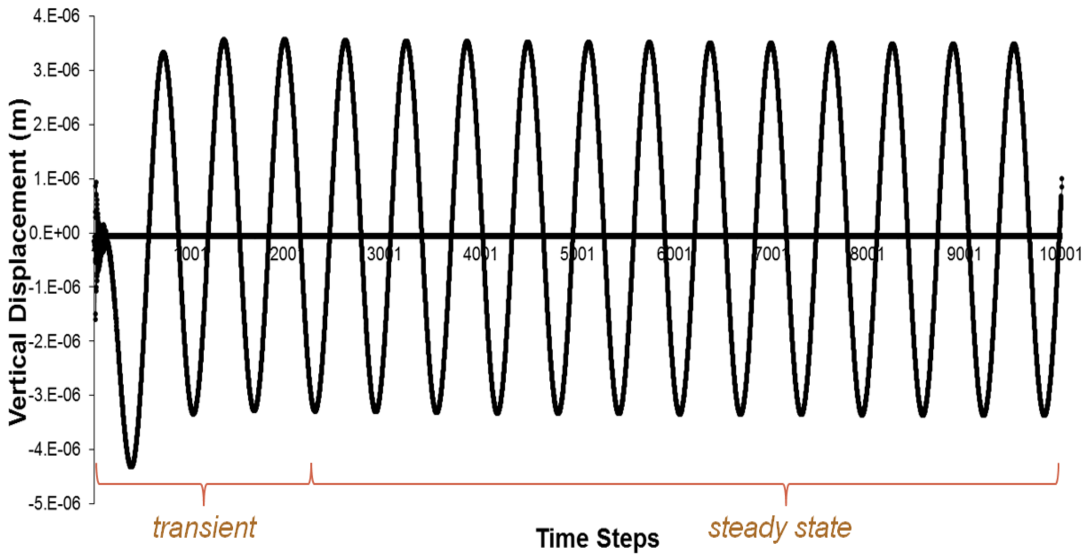

Figure 6.1 : Reaching steady state for any point on soil column.

During the analysis, the time steps are taken into account so that the effect of the loading on the soil column reaches the stationary state. Figure 6.1 shows the time-dependent distribution of the movement at any point in the soil column, where it can be seen that the movement has reached the steady state after initial forcing.

6.1.2 Boundary conditions

In this section, the necessary boundary conditions are defined in the solution of an FE analysis for 1-D soil column which is presented in its original 2-D fashion including the horizontal displacement, u_x. However, it should be noted here that, this dimension and its displacement are not considered in the analyses. For both left and right boundary conditions, the rollers are used in terms of permitting the displacement just vertically. For bottom, the all nodes fixed, so they cannot move in any direction. Pore pressures values are zero for all edges. The boundary conditions are also presented in Figure 6.2.

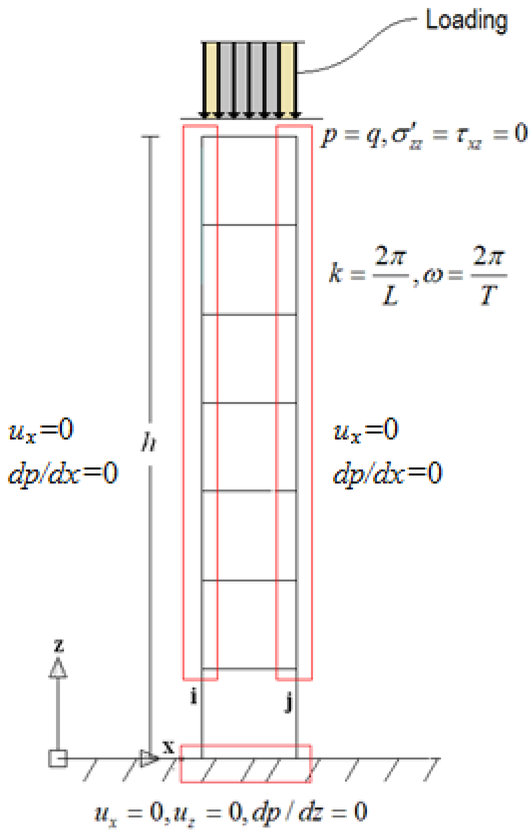

Figure 6.2 : Boundary conditions for 1-D soil column.

6.1.3 Results of the analyses for 1-D soil column

When we evaluate the behavior of vertical displacements and void pressures in the column for analytical and FE solutions, we see that the results we obtain are at acceptable levels, because very close values are calculated (Figure 6.3 and 6.4).

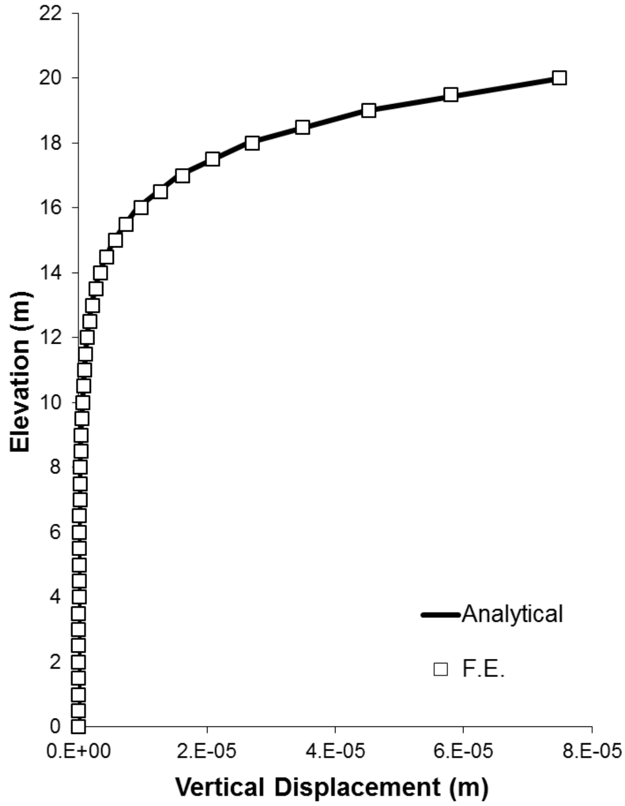

Figure 6.3 : Vertical displacements by elevation for 1-D soil column.

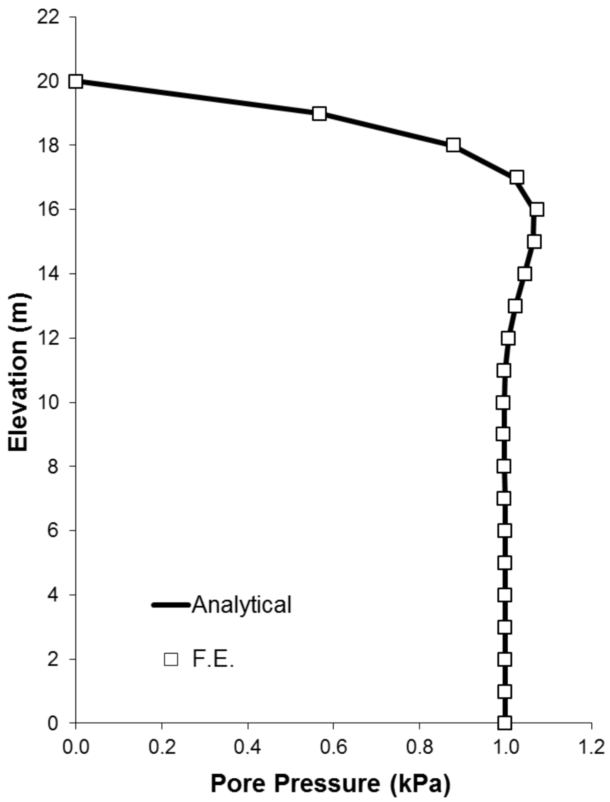

Figure 6.4 : Pore pressure by elevation for 1-D soil column.

6.2 Problem 2: Two-Dimensional Seabed Layer Response under Progressive Wave Loading

6.2.1 Problem definition

In this section, dynamic response for a 2-D plane strain layer of a saturated porous seabed layer under progressive wave loads in free field is investigated to obtain the vertical and horizontal solid displacements as well as the pore pressures and stress distributions in the seabed layer. The input data for seabed material can be seen in Table 6.1. Figure 6.1 presents the 2-D seabed soil under progressive wave loading.

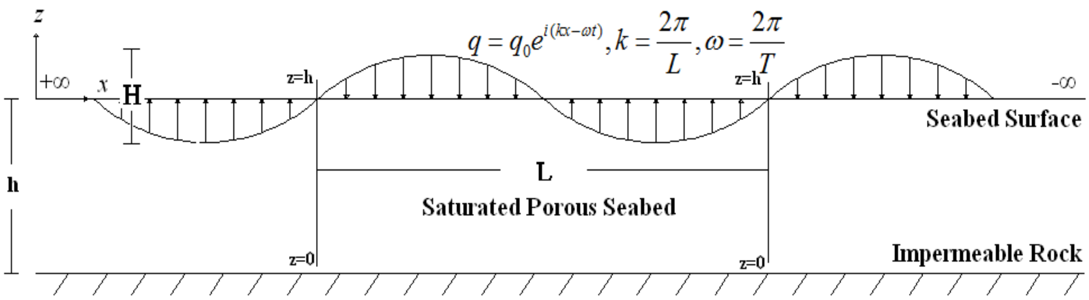

Figure 6.5 : A layer of saturated porous seabed under progressive wave loading.

6.2.2 Stress calculation

The stress state in an element is evaluated in classical finite element analyses by the following relation,

$$\begin{Bmatrix} \sigma_x \\ \sigma_y \\ \sigma_{xy} \end{Bmatrix} = \mathbf{E} \begin{Bmatrix} \varepsilon_x \\ \varepsilon_y \\ \gamma_{xy} \end{Bmatrix} = \mathbf{EBd} \tag{6.2}$$

where **B** is the strain-nodal displacement matrix, **E** is elasticity modulus matrix and **d** is the nodal displacement vector which is known for each element once the global FE equation has been solved. Stresses can be evaluated at integration points inside the element. Contour plots are usually used in FEA software packages (at post-processing) for users to visually inspect the stress results.

Table 6.2: Numerical values of the parameters used in 2-D free field analysis.

Parameter	Symbol	Unit	Value
Depth of seabed	h	m	7
Elasticity modulus of soil	E	kN/m^2	13500
Poisson's ratio	v	-	0.3
Vertical permeability	k_z	m/s	0.001
Horizontal permeability	k_x	m/s	0.001
Bulk modulus of pore water	K_f	kN/m^2	$2.3x10^6$
Saturation	S	-	1
Porosity	n	-	0.35
Unit weight of soil	γ_s	t/m^3	2
Unit weight of water	γ_w	t/m^3	1
Gravitational acceleration	g	m/s^2	9.81
Wave height	H	m	2.5
Wave length	L	m	7
Water depth	d	m	7
Period	T	s	1

6.2.3 Boundary conditions

In this section, the necessary boundary conditions are defined in the solution of an FE analysis for 2-D. Multi-point constraints (MPCs) are an advanced feature that enable the user mathematically connect different nodes in terms of theirs DOFs in the analysis. The actual use of MPCs is a "master and slave" situation: the displacement at the slave node (node i) is desired to be a linear function of the master node (node j). Figure 6.2 shows the model of a portion of a long seabed layer. The left edge of seabed layer uses symmetry boundary conditions; this restrains the model in terms of displacements and pore pressures. Therefore, it simulates the right edge of the model ofseabed layer. For a long soil layer, the typical portion of the soil to the right side of the model forces those nodes to remain in pre-specified values. Herewith, these MPCs are used to indicate that the DOFs of all the nodes, which are located on the vertical edges of the seabed, model shown in Figure 6.2 are equal in space at each time step. In addition, with this feature, it is possible to calculate the wave effect of the whole seabed system by modeling for only a single wavelength of the progressive wave.

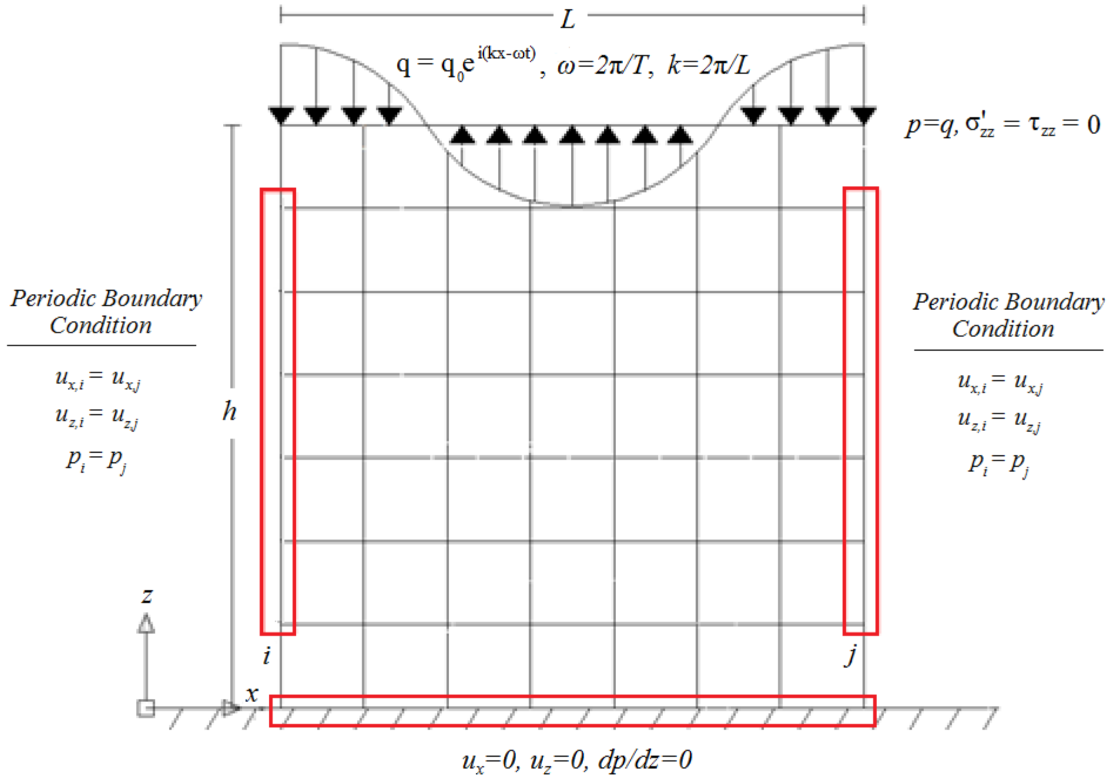

Figure 6.6: Progressive wave seabed system with boundary conditions.

In relation to this, we can write the following FE equations for the unconstrained master stiffness equation:

$$\mathbf{K.u} = \mathbf{f} \tag{6.3}$$

The master – slave transformation is then:

$$\mathbf{u} = \mathbf{T\hat{u}} \tag{6.4}$$

Following modified stiffness and force relations become:

$$\hat{\mathbf{K}} = \mathbf{T}^{\mathrm{T}}\mathbf{KT} \tag{6.5}$$

$$\hat{\mathbf{f}} = \mathbf{T}^{\mathrm{T}}\mathbf{f} \tag{6.6}$$

where $\mathbf{K}$ is stiffness matrix, $\mathbf{u}$ is displacement matrix, $\mathbf{f}$ is force matrix, $\mathbf{T}$ is transformation matrix, $\hat{\mathbf{K}}$ is modified stiffness matrix, $\hat{\mathbf{f}}$ is modified force matrix, $\hat{\mathbf{u}}$ is modified displacement matrix. As a final point the modified stiffness equation is obtained as:

$$\hat{\mathbf{K}}\hat{\mathbf{u}} = \mathbf{f} \tag{6.7}$$

The DOFs are classified into three types: independent or uncommitted, masters and slaves. Including these DOFs, equation (5.6) can be rewritten as:

$$\begin{bmatrix} K_{uu} & K_{um} & K_{us} \\ K_{um} & K_{mm} & K_{ms} \\ K_{us} & K_{ms} & K_{ss} \end{bmatrix} \begin{bmatrix} u_u \\ u_m \\ u_s \end{bmatrix} = \begin{bmatrix} f_u \\ f_m \\ f_s \end{bmatrix} \tag{6.8}$$

6.2.4 Finite element model

The FE model is set by using the Q8 elements (Figure 6.7). Each Q8 element is “1m x 1m” and X and Y values are equal to 7 m. For progressive wave, the wavelength is 7 m also. Multipoint constraints are assigned to all the nodes located along the left and right edges in order to transfer all boundary values in one side to the other side. Because of having an impermeable rock layer at the bottom of this FE mesh, fixed constraints are assigned to those nodes. There is no vertical or horizontal displacement value at fixed boundaries. The pore water pressure values are calculated at all corner nodes and the displacements are obtained at all nodes which in other words means a Q8 approximation is made for the solid displacements (*u*) nevertheless Q4 shape functions are used to interpolate pore water pressure (*p*) variation among the nodes. For the sake of brevity only the absolute value, variations of solid displacements, pore water pressures and vertical effective stresses are presented in the Figures 6.9,6.10 and 6.11 below, respectively. It can be seen clearly that the all results seem to match well with the corresponding analytical solutions obtained from (Ulker and Rahman, 2009).

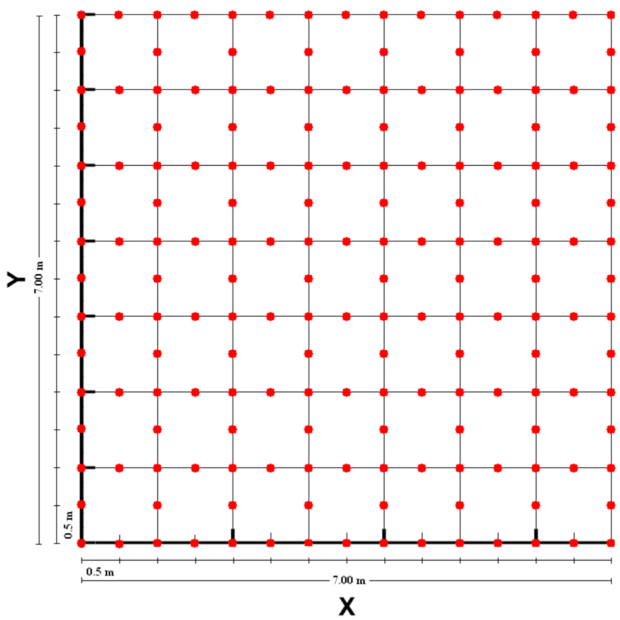

Figure 6.7 : FE mesh.

The first analysis is run for a 7x7 element FE mesh. After the first analysis, convergence check is made for the finite element model results. In this context, two finer meshes of 14x14 and 28x28 elements are prepared to solve the problems using the finite elements again. QS pore pressure response is calculated for each mesh and results are compared with the analytical counterparts obtained from (Ulker, 2009). Consequently, the results of the 14x14 mesh are considered as the optimum ones and such mesh is taken in the rest of the analyses. Convergence check results are presented in Figure 6.8.

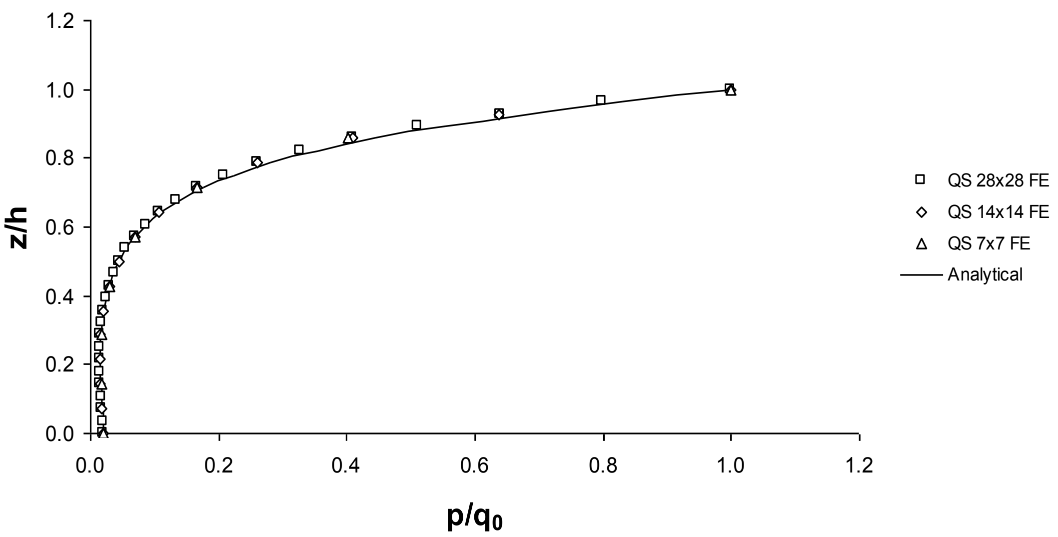

Figure 6.8 : Convergence check by pore pressure variations in depth.

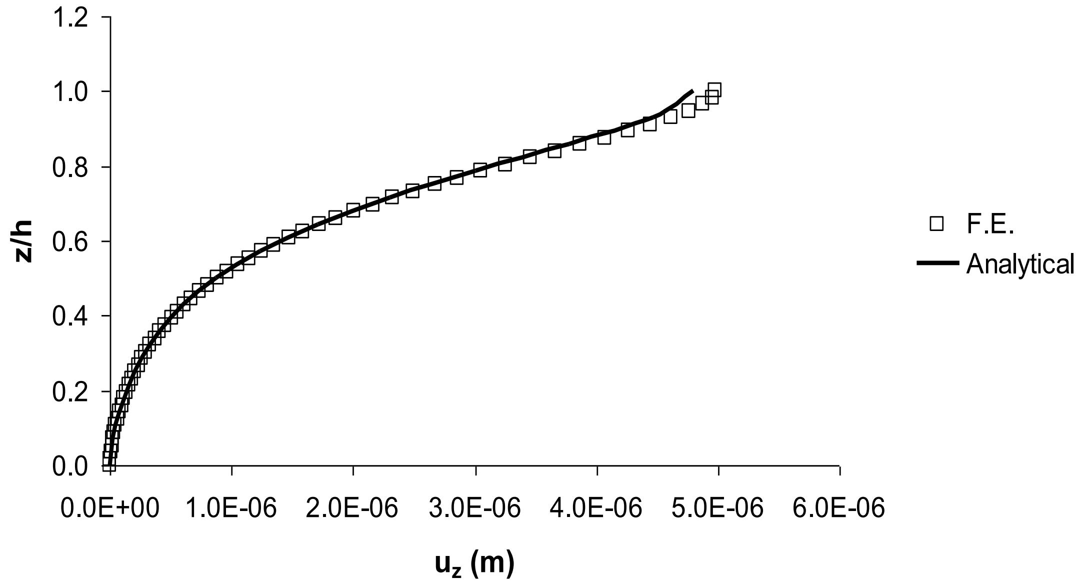

Figure 6.9 : Vertical displacement variation with depth in PD solution.

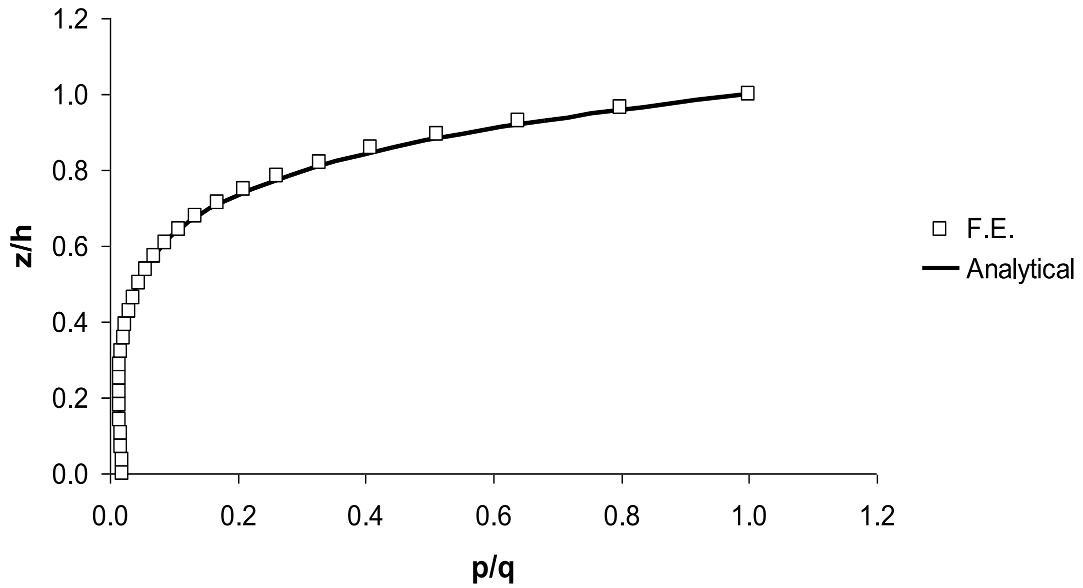

Figure 6.10 : Pore pressure variation with depth in PD solution.

It is possible to say that our comparison results are at a satisfactory level. Therefore, we know that there is no drawback to using the numerical formulations presented earlier in our subsequent analyses of the actual wave-quay-wall-seabed interaction problem (Figures 6.9-6.10-6.11).

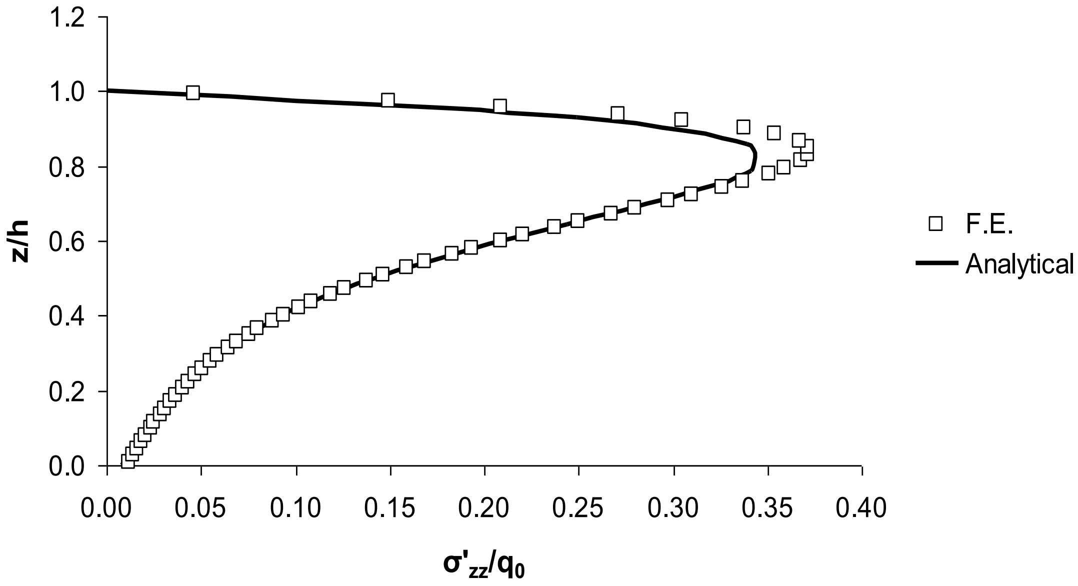

Figure 6.11 : Effective vertical stress by depth in PD solution.

7. DYNAMIC RESPONSE ANALYSIS OF CAISSON TYPE QUAY WALL (CTQ) – SEABED SYSTEM UNDER STANDING WAVES

7.1 Introduction

In coastal engineering, though atypical, it is possible that quay-walls are subjected to considerable wave forces. The reason for that to be atypical is that most of the time they serve the purpose of protecting coastal regions against severe wave action as a secondary measure while it is breakwaters' job to provide such protection. However, sometimes during the construction of breakwaters it becomes necessary to maintain a certain level of coastal integrity particularly against ocean waves. This is made possible by gravity quay walls and thus, it is not uncommon to analyze gravity quay-walls against standing wave motion as opposed to seismic excitations, which is a more common hazard as far as analysis considerations are concerned. In this study, the dynamic response of a caisson type gravity quay wall (CTQ) under standing waves is analyzed. FE solutions of the quay wall-seabed system are obtained by using the poroelasticity formulation. Standing wave form is integrated into the FE model as a natural boundary condition in terms of force – time and pressure – time histories using the linear wave theory. The dynamic response of the system is obtained in terms of pore pressure, solid displacements and stress distributions in the seabed around the quay wall and in the foundation and backfill soil.

7.2 Finite Element Analyses

In this chapter, a plane strain FE model is built using the actual structural and material properties based on the cross sections of the CTQ at the Kobe Port (Figure 7.1). The material zones are as follows: 1- Saturated back fill material, 2-Seabed soil, 3- Backfill, 4 and 5- Rubble mound fill, 6 and 7- Clay layer and 8- Caisson type quay wall. The 2-D cross-section considered in the analyses is seen in Figure 7.1 and the actual zone numbering in Figure 7.2 where the FE mesh is also presented. In making the model, boundary conditions play a key role. That is, on the left seabed lateral boundary, time – dependent variations of DOF of the analytical solutions obtained for a single layer in free field are prescribed. The sole reason for that is, as we move further away from the caisson, a free-field seabed behavior will dominate the response under progressive waves and the effect of the structure will recede. Thus, we can comfortably locate the left lateral boundary at such a place and not really worry about its physical effect in terms of numerical values on the dynamic response of the CTQ. Therefore, the minimum distance required to have such an effect without a significant effect around the CTQ has been determined to be about four times the incoming wavelength (4L) in this study considering a maximum absolute error between the two consecutive pore pressure response results to be 3% which is, for all engineering purposes, sufficient. As for other boundary conditions, constrained boundary conditions at the impermeable rock bottom are applied for vertical and horizontal displacements. The properties of boundary conditions are presented in Table 6.1. In addition, horizontal displacement and pore pressure DOF are assumed to vanish on the right lateral boundary. Lastly, along the surfaces of clay layer, seabed, rubble mound fill and at the front face of the caisson, standing wave induced pressures and forces are applied in terms of time histories evaluated from the linear wave theory as:

$$q_{i,j} = q_0 \cosh(k.z_{i,j}) \cos(k.x_{i,j}) \cos(\omega.t_i) \tag{7.1}$$

where $q_{i,j}$ is the pressure, q_0 is the wave amplitude, k is the wave number and ω is the wave frequency. Dynamic response of this CTQ – seabed system is analyzed in terms of displacements, pore pressures as well as effective and shear stress distributions around and under the CTQ assuming plane strain stress state for the respective elements. These distributions are obtained for sections 1-1, 2-2 and 3-3 as shown in Figure 7.1. In the below, results of a number of necessary parametric studies considering key wave and soil parameters such as permeability and wave period are presented. Table 7.1 shows the numerical values of the parameters used in analyses.

Table 7.1 : Numerical values of the parameters used in CTQ-Seabed analyses.

Properties	**Symbol**	**Value (Unit)**
Seabed Density	γ_S	1.72 – 2.07 (t/m^3)
Seabed Young's Modulus	E_S	16000-260000 (kPa)
Seabed Poisson's Ratio	v_S	0.3–0.33
Seabed Permeability	k_S	10^{-6} – 10^{-4} – 10^{-2} (m/s)
Seabed Porosity	n_S	0.28
Seabed Saturation	S_S	1
Clay Density	γ_C	1.7 (t/m^3)
Clay Young's Modulus	E_C	10330 (kPa)
Clay Poisson's Ratio	v_C	0.4
Clay Permeability	k_C	10^{-8} (m/s)
Clay Porosity	n_C	0.5
Clay Saturation	S_C	1
Rubble Density	γ_R	2.00 (t/m^3)
Rubble Young's Modulus	E_R	160000 (kPa)
Rubble Poisson's Ratio	v_R	0.33
Rubble Permeability	k_R	0.1 (m/s)
Rubble Porosity	n_R	0.25
Rubble Saturation	S_R	1
Caisson Density	γ_W	2.5 (t/m^3)
Caisson Young's Modulus	E_W	2x10^7 (kPa)
Caisson Poisson's Ratio	v_W	0.18

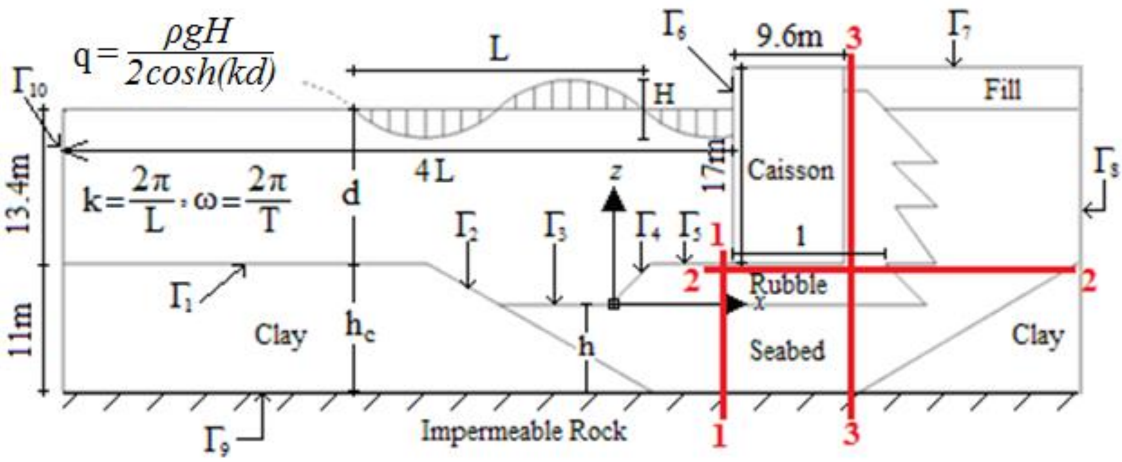

Figure 7.1: Physical model of CTQ at the Kobe Port and relevant sections.

Table 7.2: Boundary conditions of CTQ-Seabed system.

Boundary Name	Condition
Γ_1 , Γ_2 , Γ_3 , Γ_4 , Γ_5 , Γ_6	$p=[\rho gH/2\cosh(kd)]\cosh(kz)\cos(kx)\cos(\omega t)$
Γ_7	$p=0$
Γ_8	$u_x=u_z=p=0$
Γ_9	$u_x=u_z=dp/dn=0$
Γ_{10}	Obtained from the free field analytical solution.

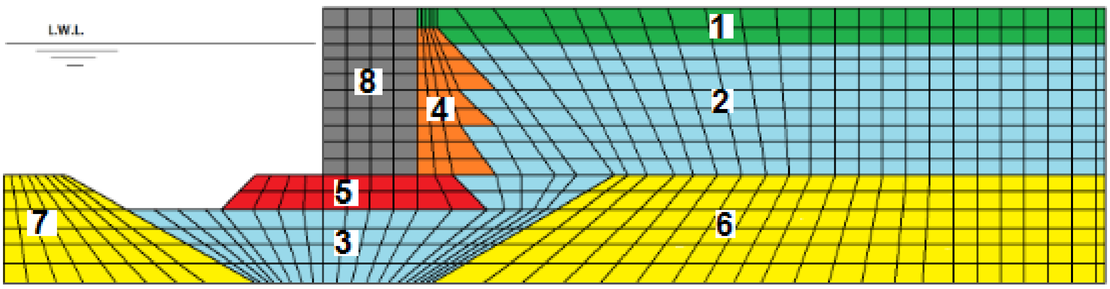

Figure 7.2: CTQ – Kobe Port F.E. mesh and material zone numbers.

7.3 Results of Analyses

In this section, under the effect of the standing wave, the response results obtained from the parametric studies are presented. All of the work is performed for a time duration of 300 seconds, which is determined based on the principle that the response of the entire system must reach steady state since the load is harmonic in time. Firstly, the effect of changes in the permeability of the seabed (isotropic permeability is assumed) on the dynamic response of the system is investigated. Secondly, various soil types are considered for the seabed. Here, different results are obtained by assigning different values of elasticity modulus, unit weight and poisson's ratio for each seabed soil. Finally, the response of CTQ system under various standing wave periods is studied parametrically. It is also taken into account that the variation in wave period values changes the wavelengths according to the dispersion formulation for intermediate depth in the linear wave theory that is:

$$\left(\frac{2\pi}{T}\right)^2 = \frac{2\pi g}{L}\tanh\left(\frac{2\pi d}{L}\right) \tag{7.2}$$

where T is standing wave period, g is gravitational acceleration, L is wavelength and d is water depth (Dean and Dalrymple, 1991).

Table 7.3 : Wave properties taken in the CTQ-Seabed analyses.

Wave Parameters	**Symbol**	**Value (Unit)**
Water Depth	d	13.4 (m)
Wave Length	L	38-104-165 (m)
Wave Height	H	4 (m)
Wave Period	T	5-10-15 (s)

7.3.1 Effect of seabed permeability

When we examine the response results of section 1-1, we see that dynamic response in general, is function seabed permeability. For example, when we compare the QS formulation solutions with that of the PD, we see that there is a negligible difference between the results of all three parametric studies. However, as for the seabed permeability, when it decreases, there is an increase in the displacements in both horizontal and vertical directions. The system gives the same response in PD solutions as well; however, the result is that the increase in displacements is more obvious (Figure 7.3, 7.4)

As the permeability differences between the seabed and the rubble mound fill zone decrease, the pore pressure response gets closer to each other for section 1–1. Especially, for the seabed with permeability value k=10^{-2} m/s, the distribution of the pore pressures is rather uniform. Regarding this, the effect of the small difference in the permeability values between the rubble mound and the seabed cannot be disregarded. In addition, it should benoted that inertial terms are at negligible levels. With the decrease in permeability values, the effect of inertial terms becomes more, as well as the pressure differences between the seabed and the rubble mound fill increase. There is little effect of permeability of seabed on pore pressures in the rubble (Figure 7.5).

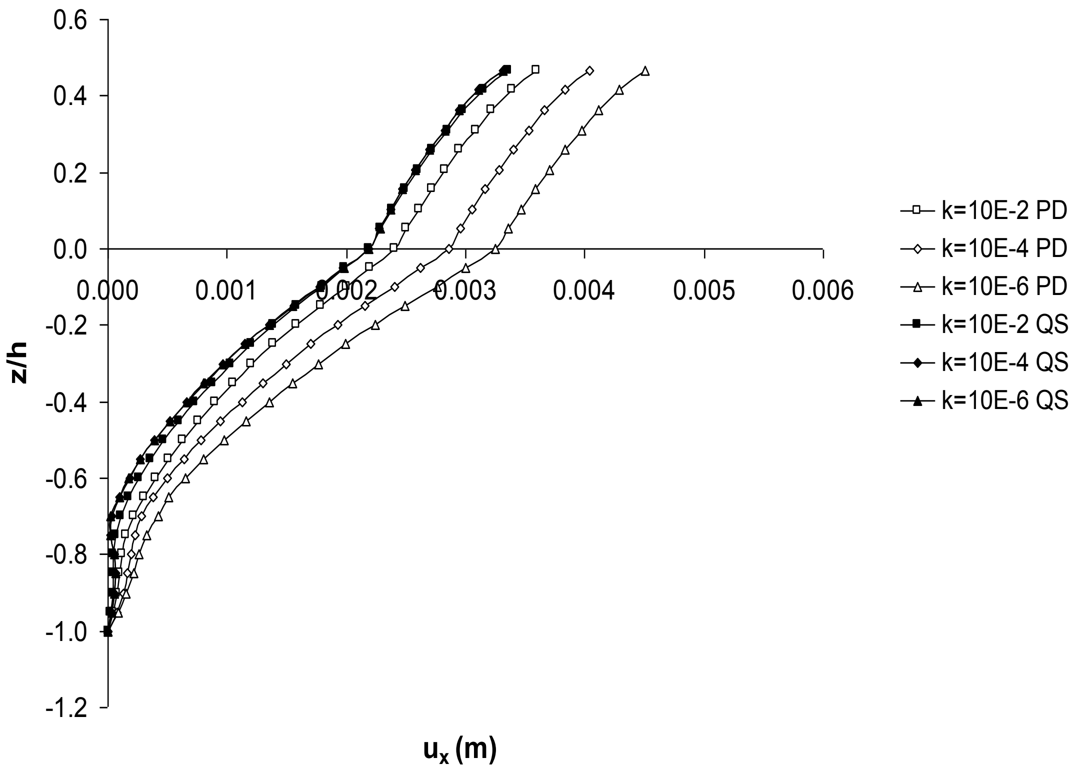

Figure 7.3: Effect of permeability on horizontal displacement in section 1-1.

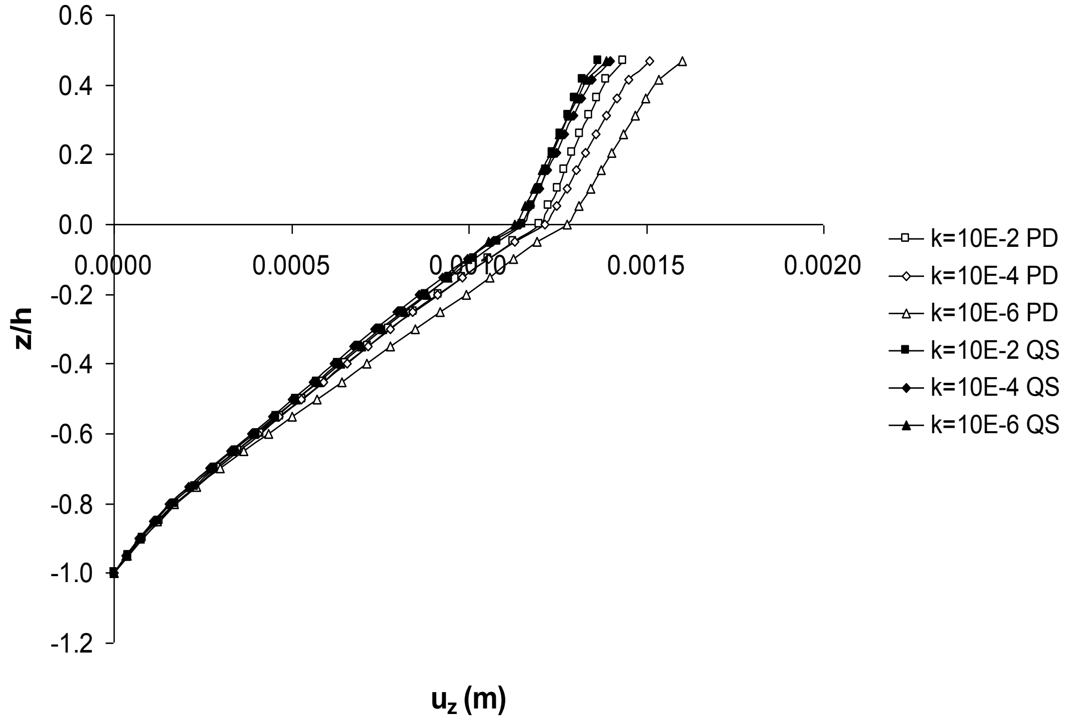

Figure 7.4: Effect of permeability on vertical displacement in section 1-1.

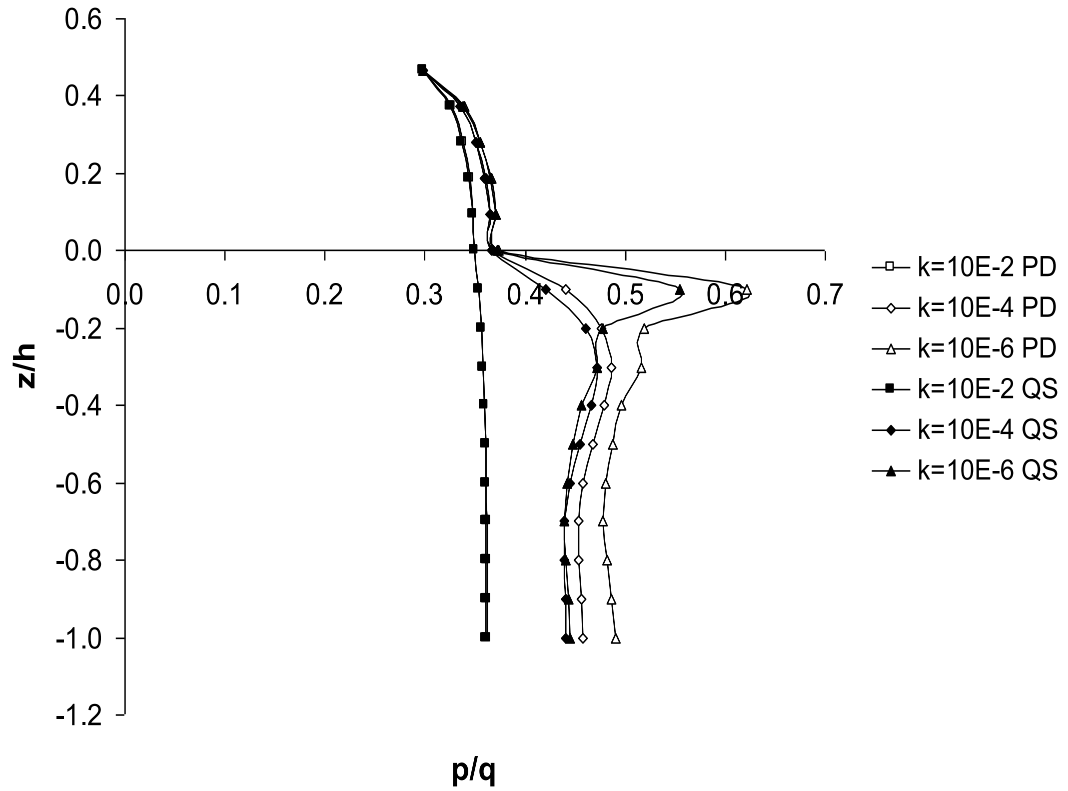

Figure 7.5: Effect of permeability on pore pressure in section 1-1.

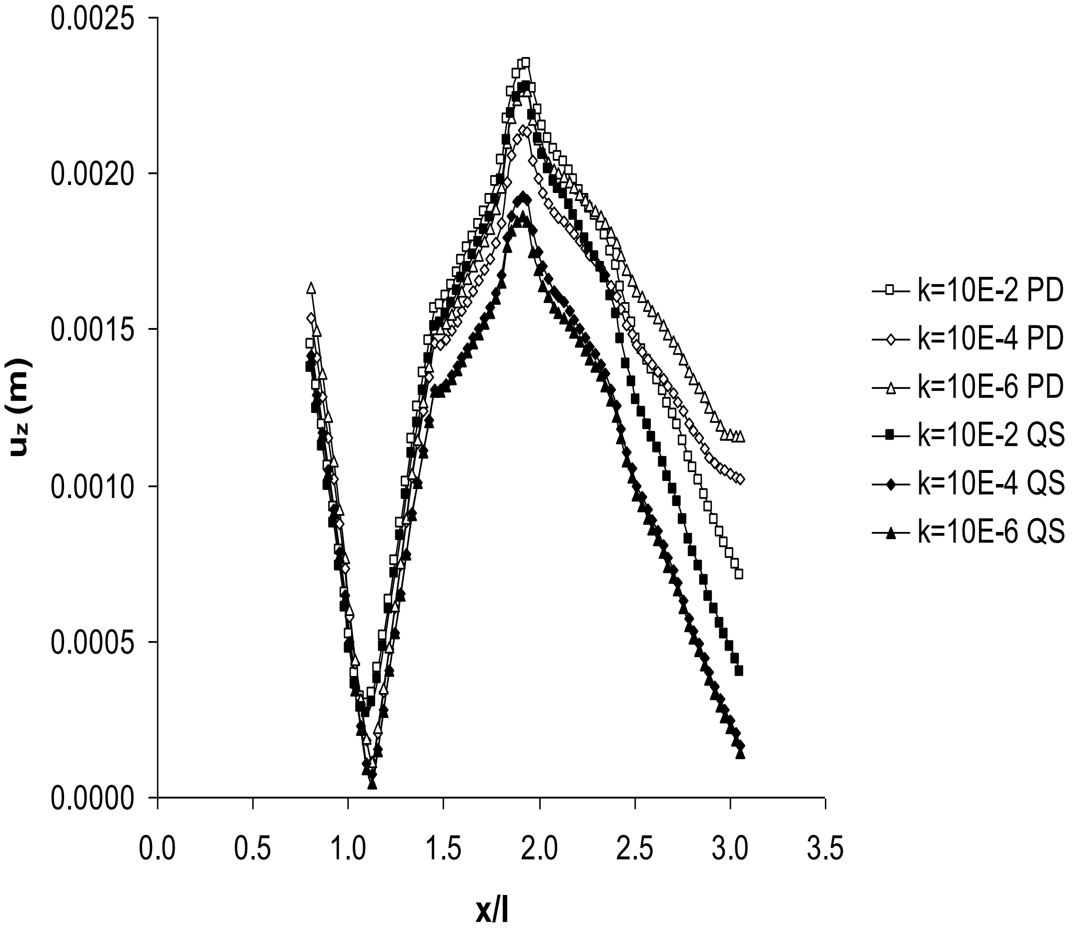

Figure 7.6: Effect of permeability on vertical displacement in section 2-2.

If we look at Figure 7.6 showing the results along section 2 – 2, we can see that the vertical displacements are particularly large in the toe sections of the caisson wall due to the rocking effect. The displacement values in the middle region of the caisson wall base are, therefore, less than those at the ends. According to Figure 7.6, the increase continues in the lower parts of the rubble mound fill backfill, while it tends to decrease with the passage to the seabed zone. Moreover, as we move away from the wall, the effects of the change in permeability values on the vertical displacements become more apparent. This effect continues until the end of such section. The effect of inertial terms increases in the same way. It is possible to say that the greatest vertical displacement value is at the intersection of "rubble backfill - seabed".

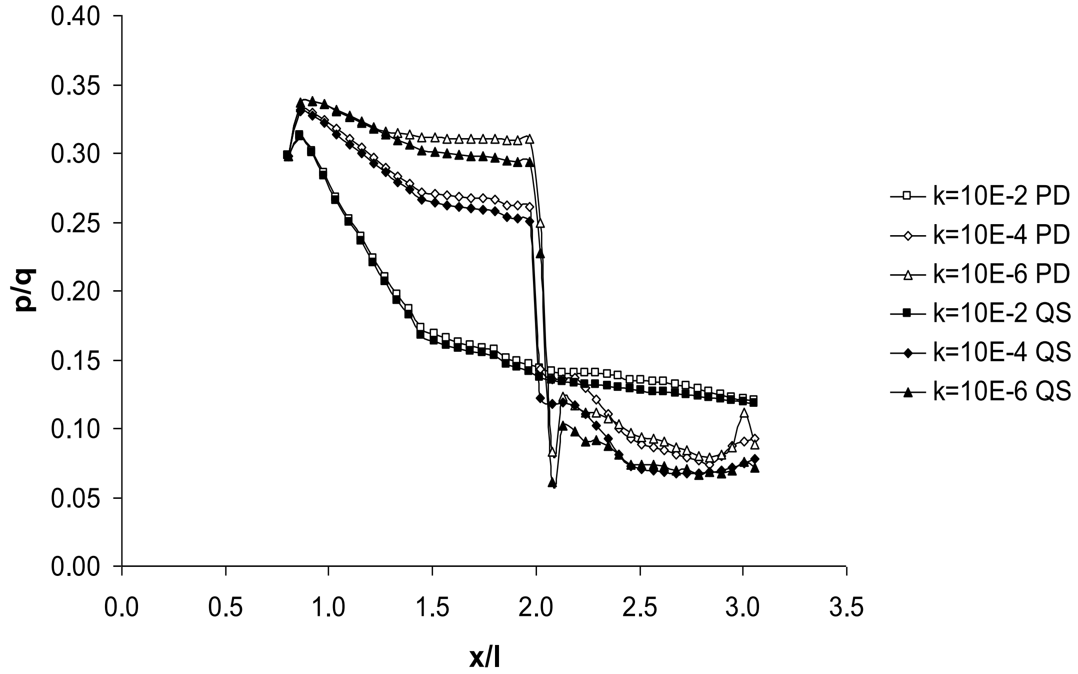

Figure 7.7: Effect of permeability on pore pressure in section 2-2.

When we examine section 2–2, it is also observed that there is a gradual decrease in the pore pressure in the rubble area under the caisson. This reduction continues along the entire section. At a point away from the wall, the decrease diminishes slightly at this section 2-2. In general, the increase in permeability values causes the pore pressures to decrease. Again, for this region it is possible to say that dynamic effects become more important when inertial terms are introduced. In addition to this, we can read the slight increase in discrepancy. In contrast, we see an opposite situation in the rubble. At the rubble - seabed layer intersection, difference in the pore pressures increases due to decrease in permeability values. As we can see, the increase in pore volumes in material does not directly mean an increase in pore pressures according to Figure 7.7. In addition, the sudden and large decline of pore pressures at the back toe of the caisson wall may explain a possible piping behavior for k=10E-4 m/s and k=10E-6 m/s.

In section 3 – 3, it can be said that as we move towards the top, especially after leaving the seabed layer, there is a decrease in the horizontal displacement values but the increase tendency in displacement generally continues. Even if the permeability value is as high as $k=10^{-2}$ m/s, very little increase in horizontal displacement is observed. As the differences between the values of seabed permeability increase, the dynamic effects become pronounced. In particular, the response of horizontal displacements obtained for $k=10^{-6}$ m/s is considerably higher than the results of the analyses which are worked for $k=10^{-4}$ m/s and $k=10^{-2}$ m/s.

Figure 7.9 shows that the vertical displacements increase rapidly especially in the seabed layer for $k=10^{-2}$ m/s in section 3 – 3. Dynamic effects are noticeable there. Also, in this figure, the results in QS solutions for $k=10^{-4}$ m/s and $k=10^{-6}$ m/s are not very different, nevertheless for $k=10^{-2}$ m/s there seems to be a large alter. Thus, the largest effect of dynamic terms is seen for $k=10^{-4}$ and $k=10^{-6}$ m/s.

Figure 7.10 shows the variation of the pore pressure values for different permeability values in section 3 – 3. Since seabed permeability is close to the rubble mound fill layer, we see a persistent change in the graph for $k=10^{-2}$ m/s. When the permeability decreases, pore pressure variation between the layers increase. This is apparent for $k=10^{-4}$ m/s and $k=10^{-6}$ m/s. Bottom line is, as permeability decreases, the effect of inertial terms increases correspondingly.

Depending on the rocking motion of the caisson wall, we see the stress accumulation at the front and back toe. The same applies to the rubble fill behind the caisson wall. These effects become even more pronounced due to reductions in soil permeability. As we move along the section 2 – 2, we can see that the stress values are gradually decreasing in the seabed layer. It is also noticeable that the values in the z direction give close results in the front and back of the caisson wall. Although the inertial terms have an effect on that reduction, it is a slight effect (Figures 7.14, 7.15, 7.16).

The normal stress values in the x direction continuously increase in the seabed layer, although they show a variable distribution in the rubble layer. On the other hand, the shear stress and the normal stress values in the z-direction go down after reaching at the bottom of the caisson. This decline is in a certain area and then the stress responses ascend again towards the fill. Then, it suddenly gets reduced again. Furthermore, in the rubble layer, there is no effect on the shear stresses of the soil permeability (Figures 7.17, 7.18, 7.19).

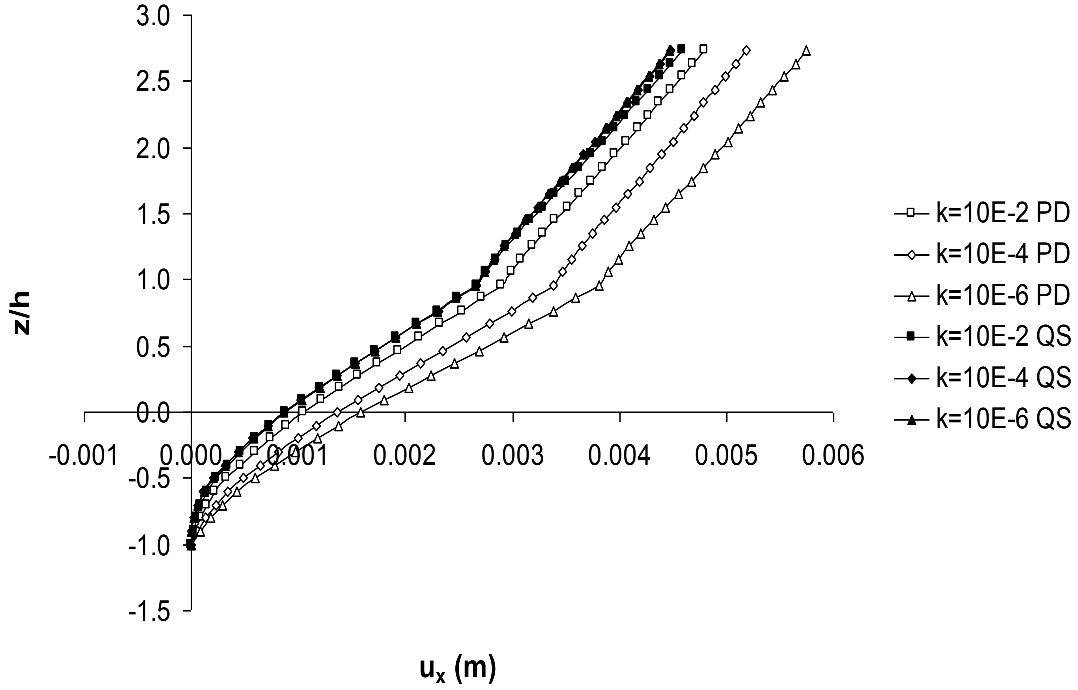

Figure 7.8: Effect of permeability on horizontal displacement in section 3-3.

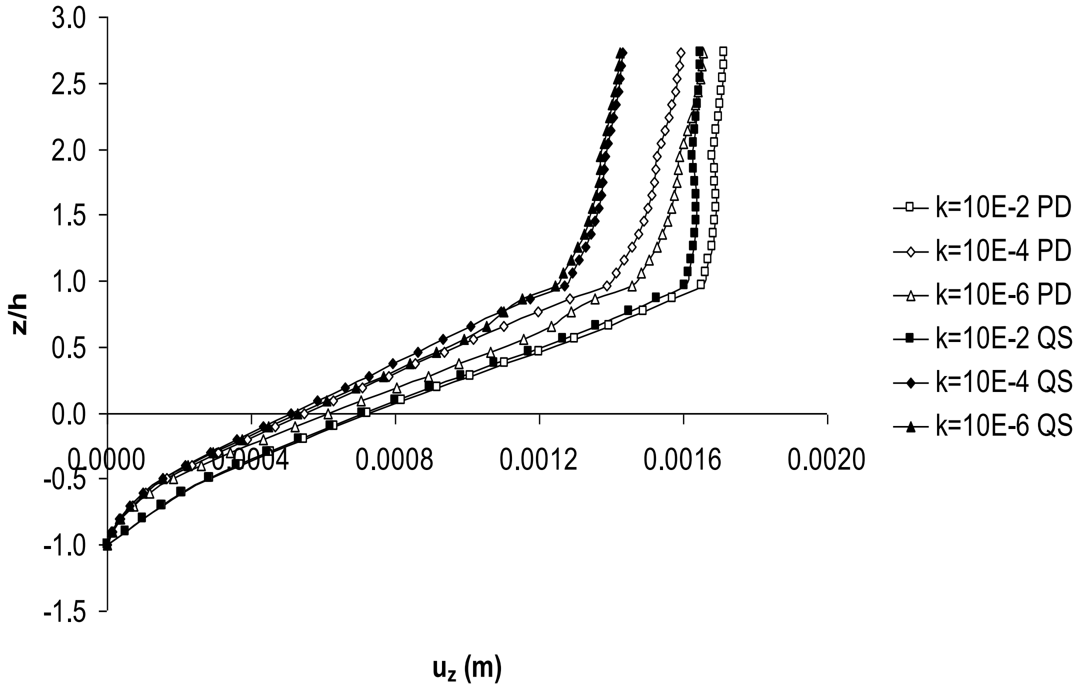

Figure 7.9: Effect of permeability on vertical displacement in section 3-3.

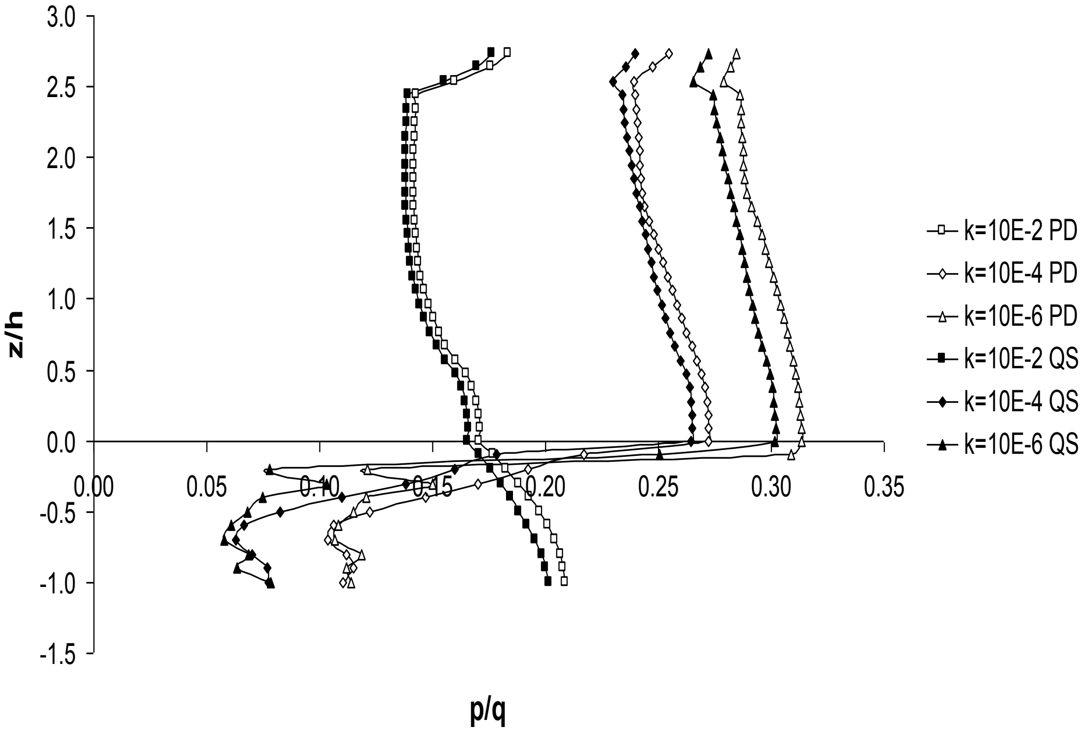

Figure 7.10: Effect of permeability on pore pressure in section 3-3.

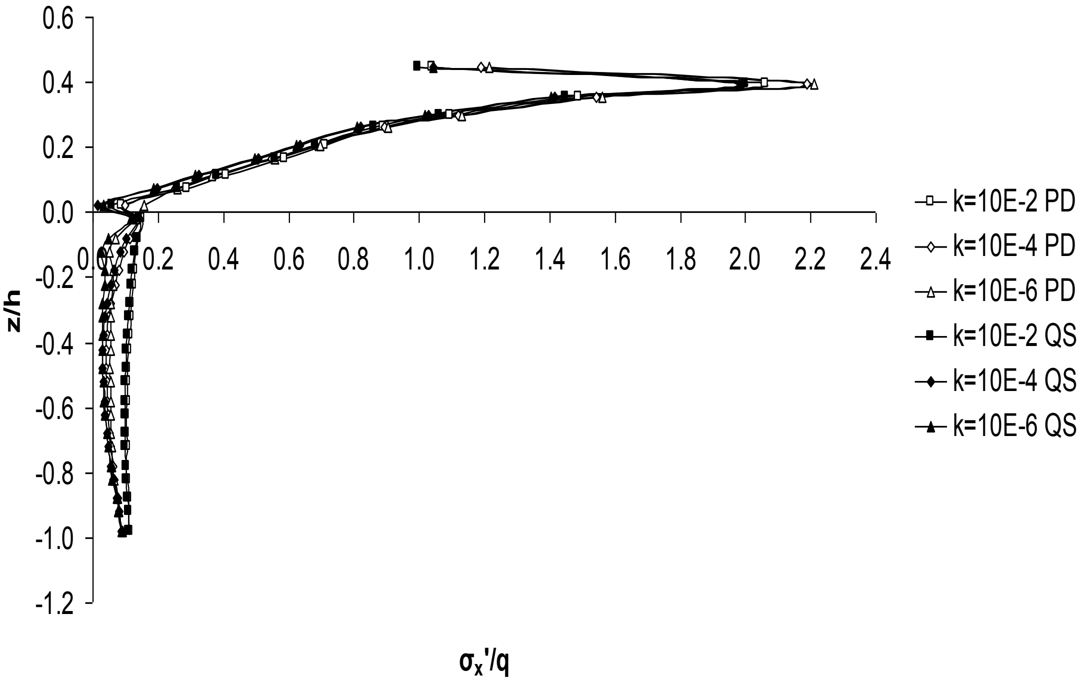

Figure 7.11: Effect of permeability on normal stress in x direction in section 1-1.

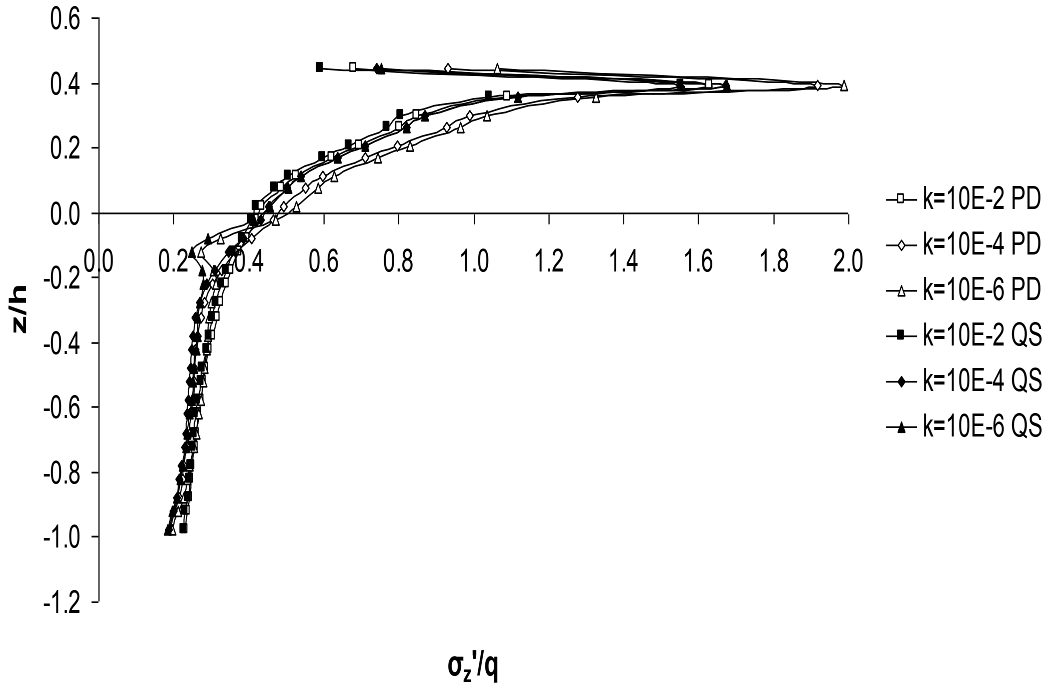

Figure 7.12: Effect of permeability on normal stress in z direction in section 1-1.

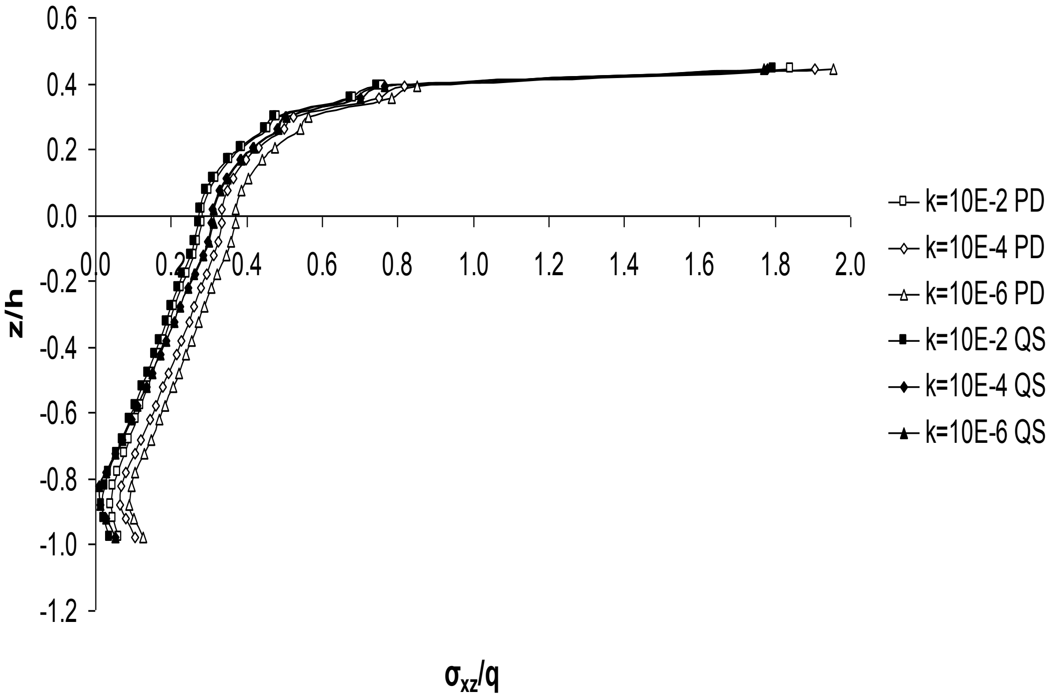

Figure 7.13: Effect of permeability on shear stress in section 1-1.

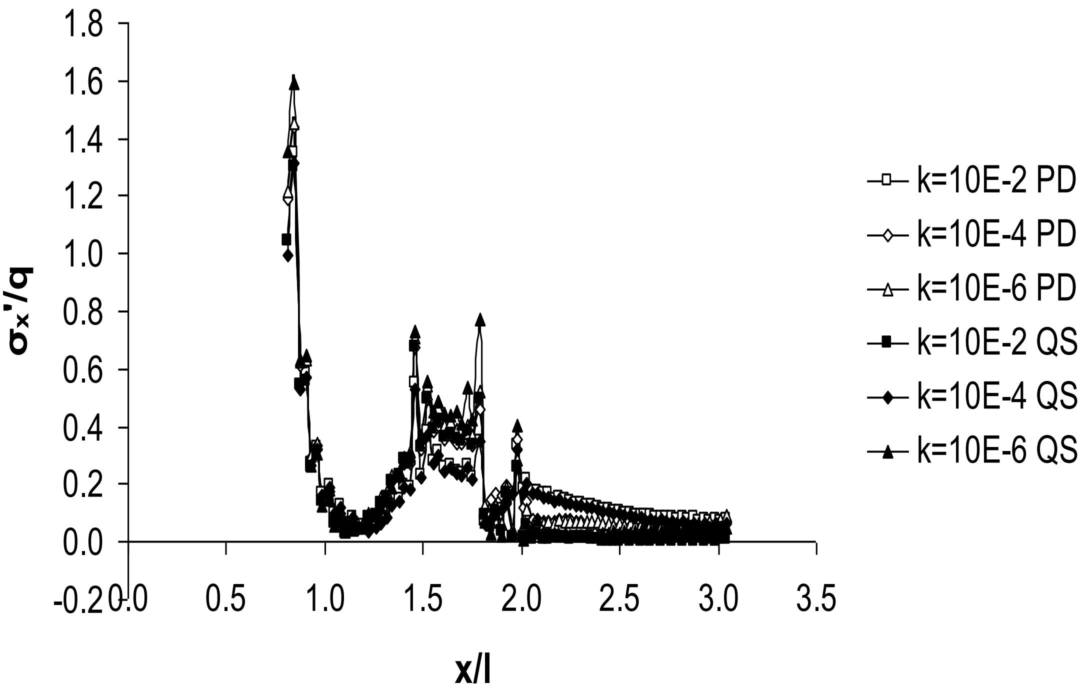

Figure 7.14: Effect of permeability on normal stress in x direction in section 2-2.

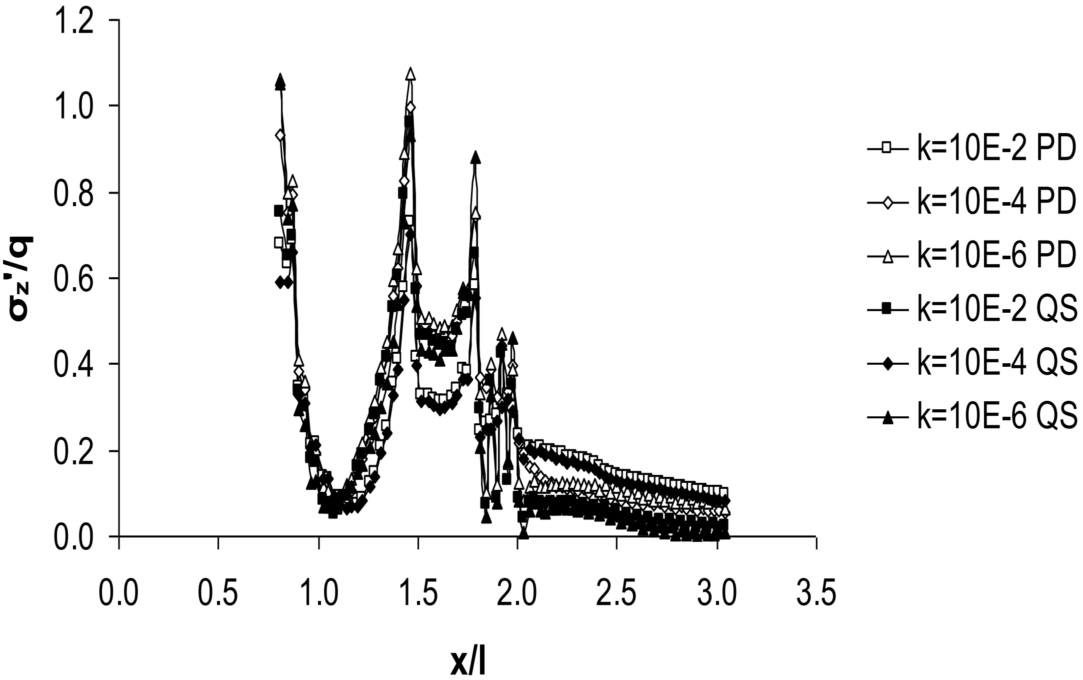

Figure 7.15: Effect of permeability on normal stress in z direction in section 2-2.

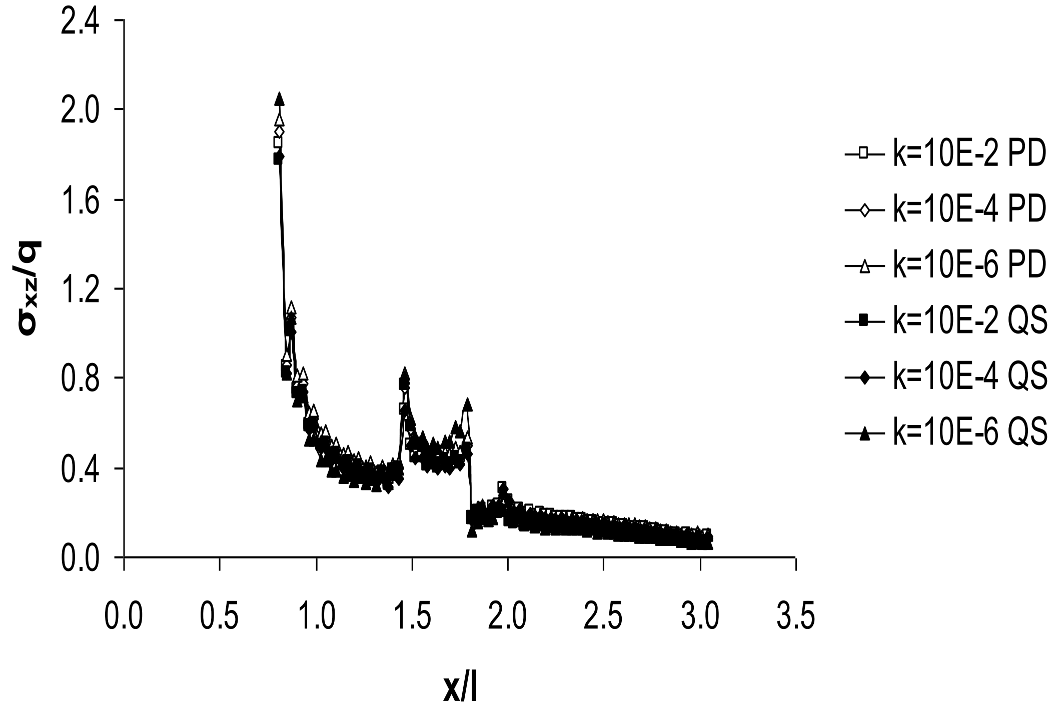

Figure 7.16: Effect of permeability on shear stress in section 2-2.

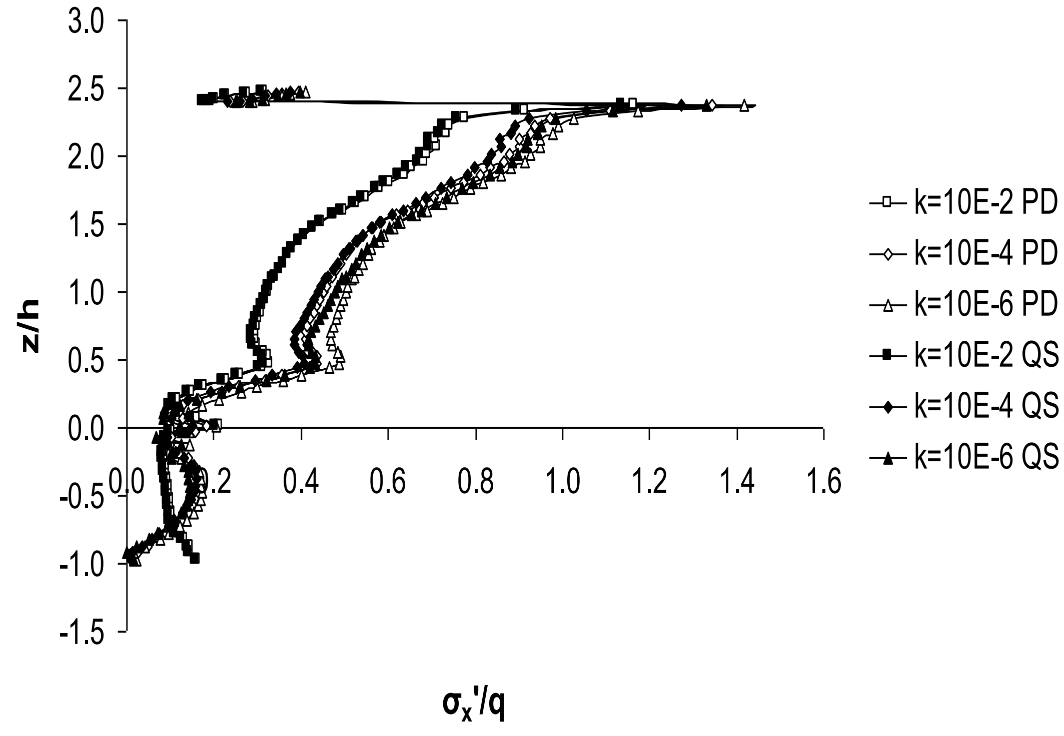

Figure 7.17: Effect of permeability on normal stress in x direction in section 3-3.

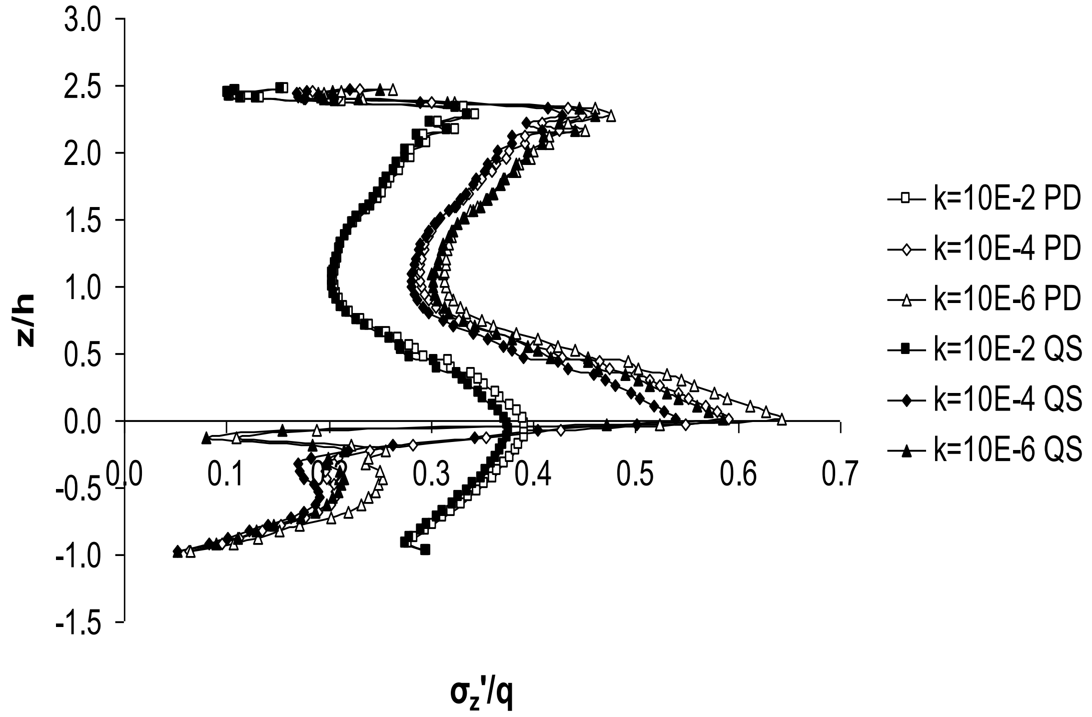

Figure 7.18: Effect of permeability on normal stress in z direction in section 3-3.

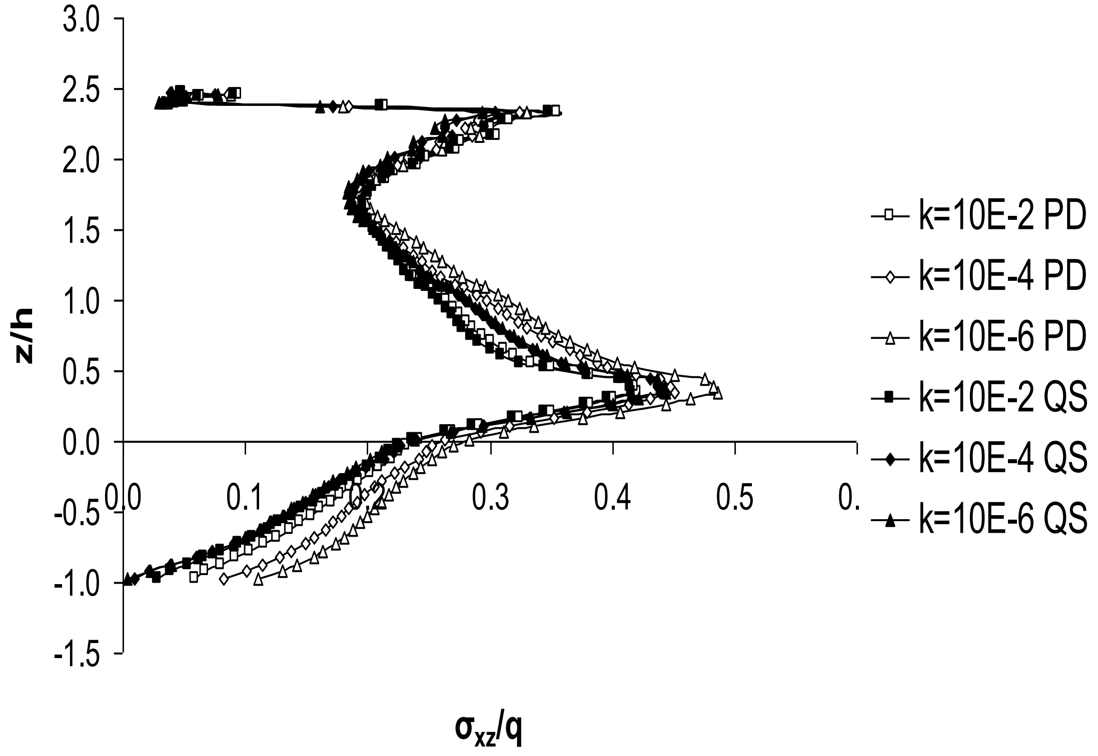

Figure 7.19: Effect of permeability on shear stress in section 3-3.

7.3.2 Effect of seabed soil type

Physical soil properties are often found in laboratory experiments on disturbed samples and make a significant source to engineers in terms of accountability. Classification systems are established by considering mainly the grain diameters of soil samples. In order to find the transition between clay, silt, sand, gravel and boulders etc. various systems have different assumptions (i.e. ASTM, USCS etc.).

The types of soil that are commonly found in coastal structures are sand and gravel. Occasionally, it is known that there are clayey sand layers or that there is thin clay layer overlying a granuler medium (Ulker, 2012; Soltanpour et al., 2010). In this work, therefore, different graded mixtures are used which are usually produced by these types. Silty sand – gravel mixture (GM), poorly graded sand (medium dense, SP) and well-graded sand – gravel mixture (GW) are chosen for this parametric work. These are also pretty much similar the soils found in the Kobe port soil. It should be note here that such soil types are loosely defined as the only parameter used to make a distriction between them are elasticity modulus, E, poisson's ratio, v and unit weight, γ. Table 7.4 are used to select the appropriate values of these parameters. Thus, although there is not clear cut transition from one soil type to anotherbased on these parameters (especially for soil symbols as no grain size is considered in the analyses) such soil types of well-graded gravel; poorly graded sand, silty sand gravel mixture etc. will still give the same idea about how much granular soil types will affect the overall dynamic response. In this chapter, the results of a parametric study for these three soil types is evaluated and presented.

Table 7.4 : Soil type parameters used in analyses.

Parameter	**Symbol**	**GM**	**SP**	**GW**
Elasticity Modulus	E	16 MPa	40 MPa	260 MPa
Poisson's Ratio	v	0.33	0.33	0.30
Unit Weight	γ	1.75 t/m^3	1.72 t/m^3	2.07 t/m^3

When the displacements are examined, the effect of inertial terms in the PD solution becomes more pronounced with the change of soil types. In section 1 – 1, between PD and QS solutions, low differences occur in the response for well-graded dense sand – gravel mixture (GW). It can be said that the reason for this is that the GW contains less space than other types of soil, although the permeability values are the same. According to the results from analyses made specifically for poorly graded sand (SP) and silty sand – gravel mixture (GM), inertial terms play an effective role on both horizontal and vertical displacements. In addition, the increase in discrepancy, especially in vertical displacements, can be emphasized and is more pronounced in the variation of horizontal displacement. Another result that can be deduced from these figures is the observable decrease in displacement when moving to the rubble zone (Figure 7.20 and 7.21).

Figure 7.22 shows the changes in pore pressure normalized by the standing wave amplitude in the rubble mound fill and seabed layers compared to the different soil types in section 1 – 1. In view of that, changes in soil types do not lead to a significant difference in the rubble mound layer. In this context, it can be said that what is important for the rubble mound layer is its granulometry. So, no matter how much the soil type in the lower layer varies, the upper rubble layer is not affected by this, considering the pore pressure differences. In addition, the dynamic terms have little effect in that section also. Alternatively, the effect of these terms is apparent in the seabed layer.

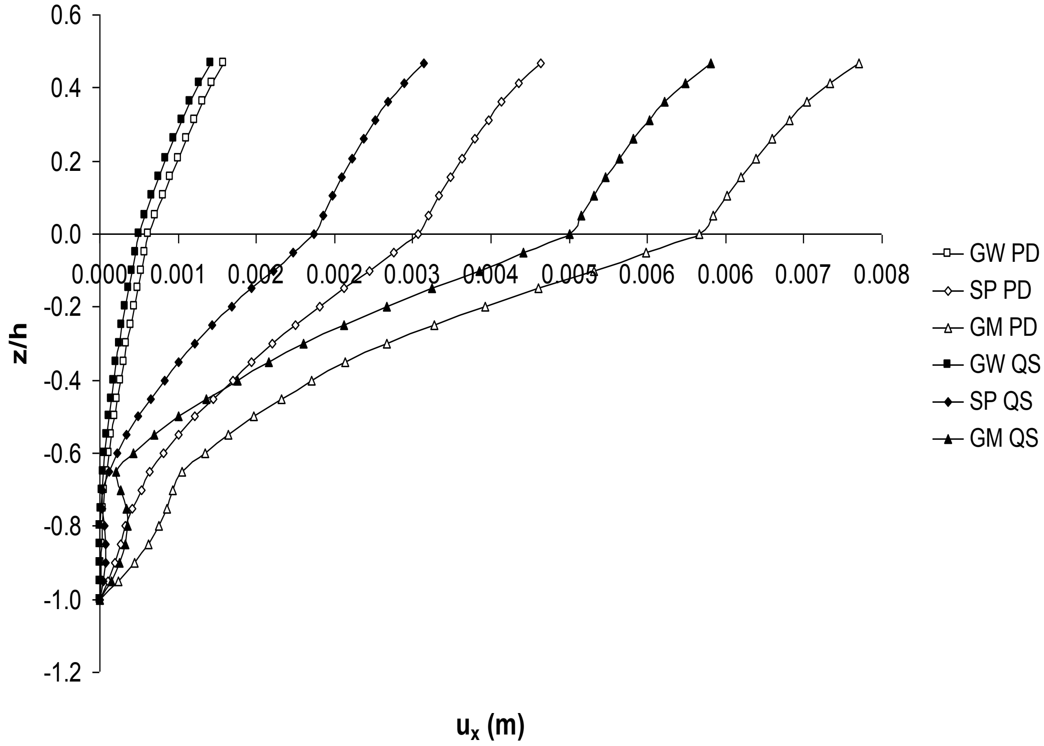

Figure 7.20: Effect of soil type on horizontal displacement in section 1-1.

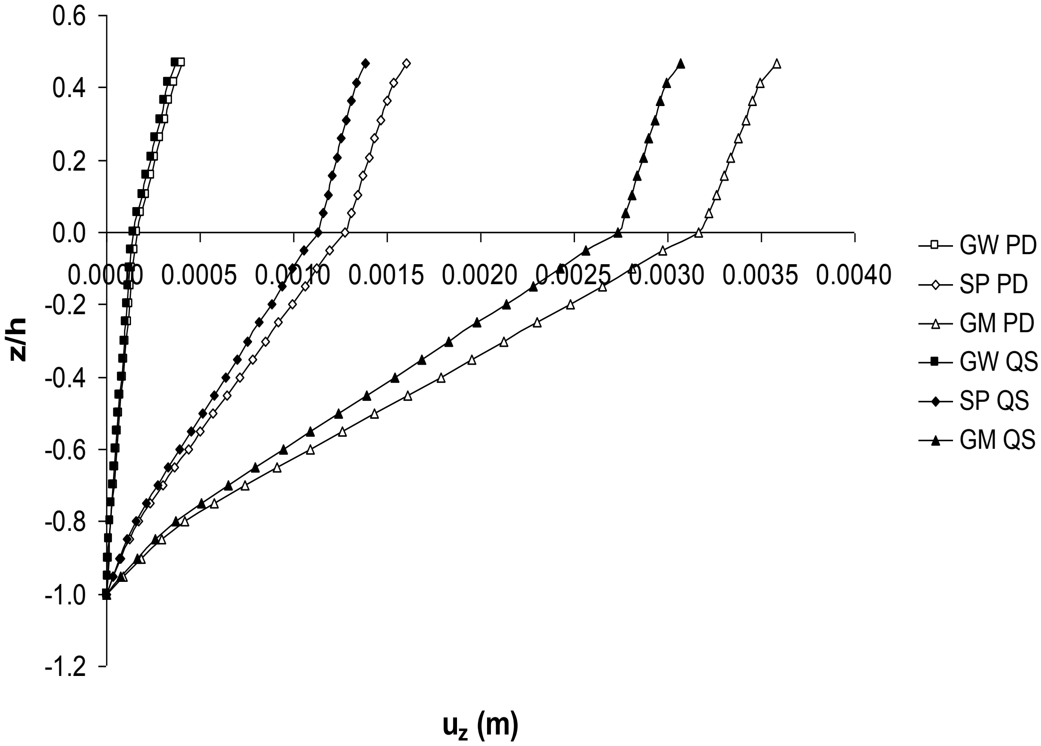

Figure 7.21: Effect of soil type on vertical displacement in section 1-1.

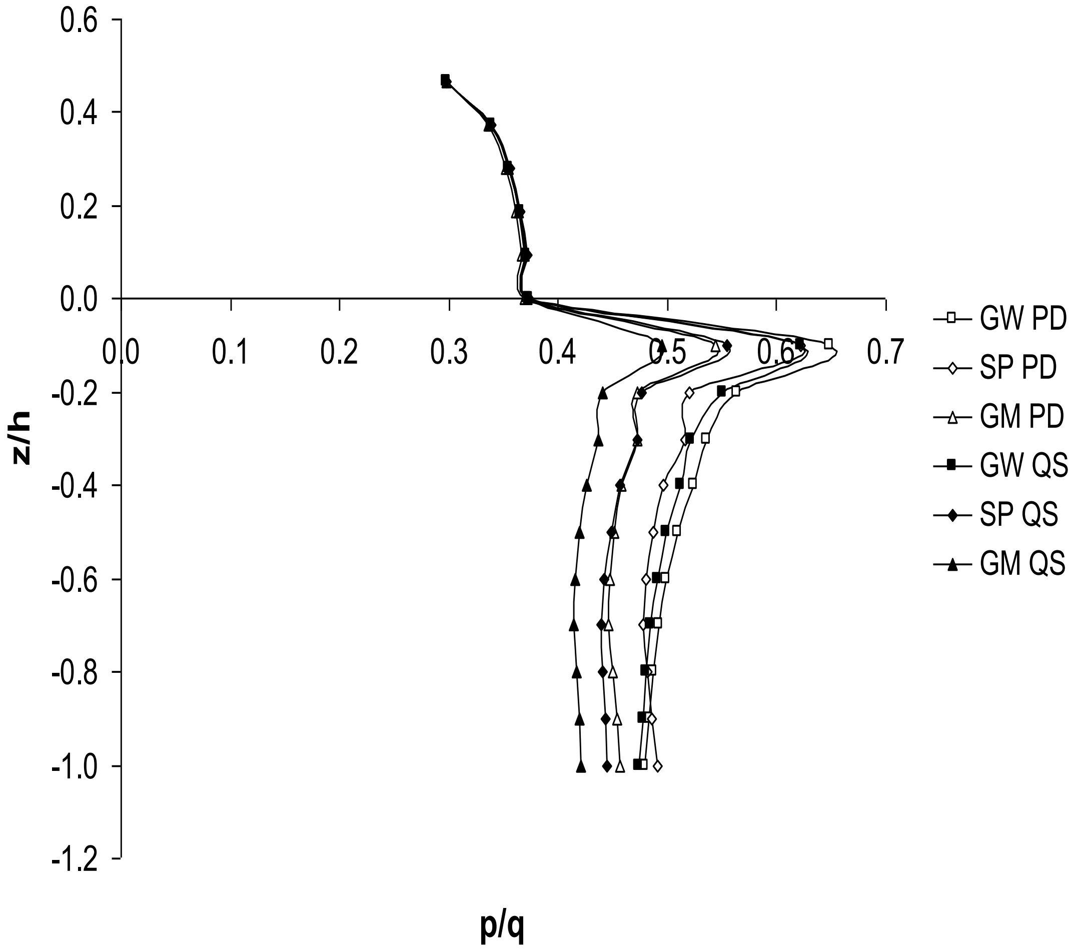

Figure 7.22: Effect of soil type on pore pressure in section 1-1.

In section 2 – 2, we see that the vertical displacements are low in the GW soil type, along the entire section line. In addition, inertial terms are negligible. In the case of SP soil type, it is visible that dynamic effects become very noticeable. It can be said that these vertical displacement values increase when compared to GW. As for GM, vertical displacement values increase further and reach to a maximum when combined with the dynamic effects. This level is at the intersection of "rubble backfill - seabed". In this graph it is also possible to observe the vertical displacement alterations and discrepancy increases caused by the rocking effects. (Figure 7.23).

As seen in Figure 7.24, the change in soil types does not cause large changes in the pore pressure in the lower part of the caisson wall in section 2 – 2. In particular, assuming no dynamic effects, we see negligible changes between GW and SP. In addition, there is a slight decrease in GM type soil. If we take into account the inertial terms, we get different patterns such that the maximum pore pressure occurs in the SP soil. After leaving the rubble zone under the caisson, all the pressure values decrease suddenly. Because the granulometric distribution in the rubble mound is such that there are more voids distributed more uniformly essentially increasingthe permeability in comparison to seabed. Therefore, the pore pressure values that are normalized with respect to the wave amplitude become higher also. The largest values in the seabed section are observed for the GM soil type. Within the seabed layer, dynamic effectsare more pronounced.

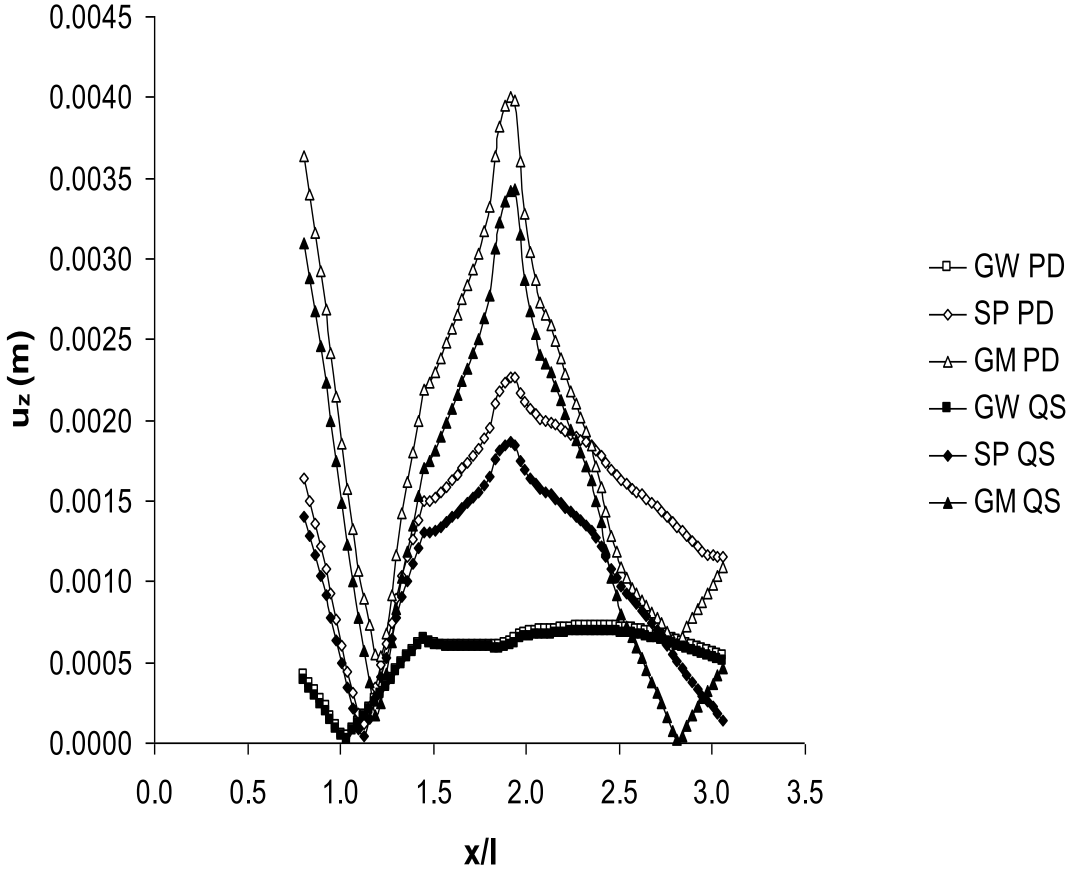

Figure 7.23: Effect of soil type on vertical displacement in section 2-2.

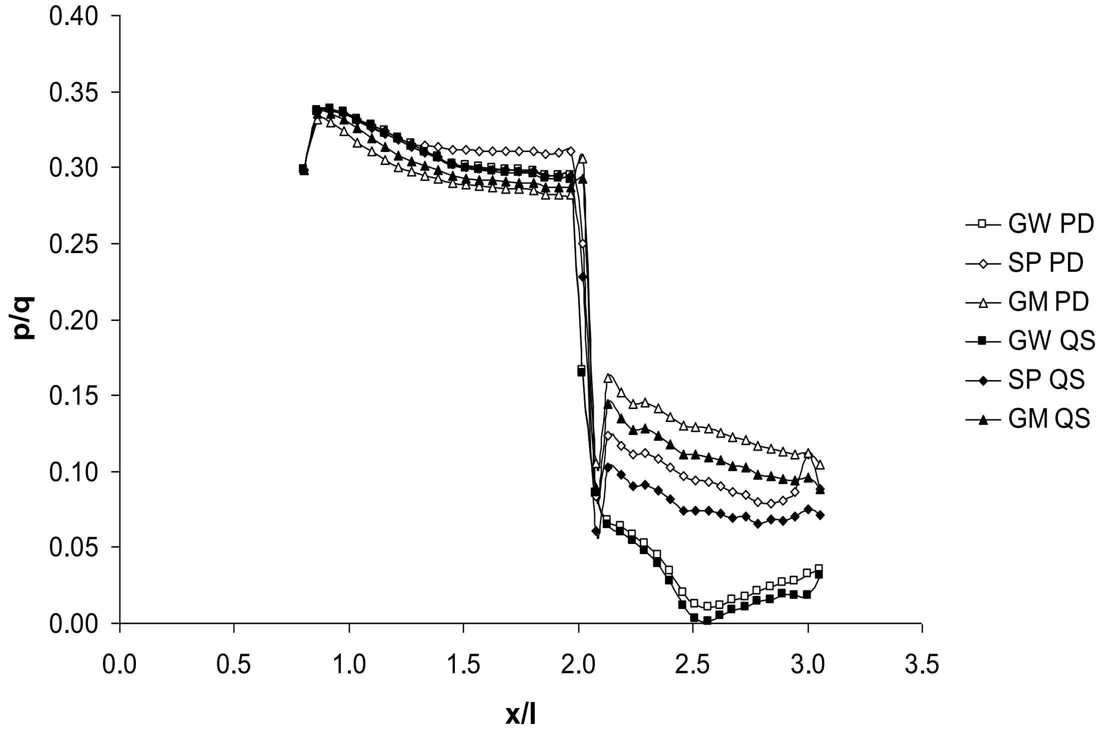

Figure 7.24: Effect of soil type on pore pressure in section 2-2.

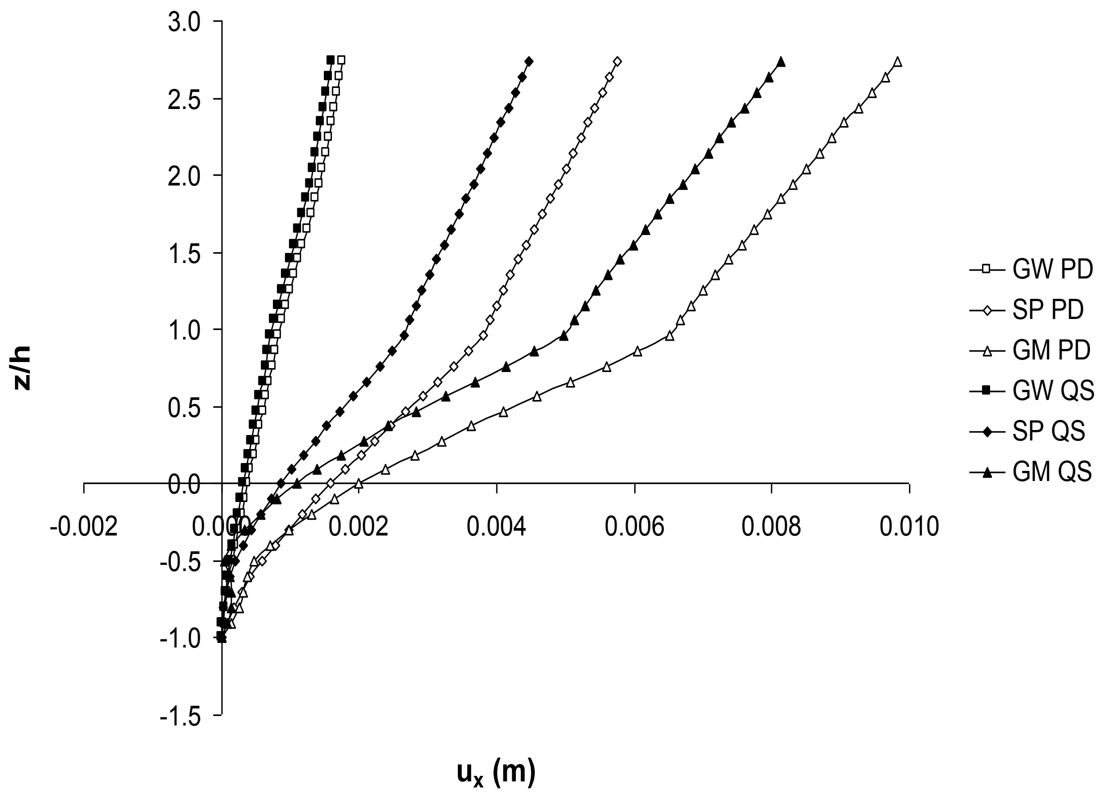

Figure 7.25: Effect of soil type on horizontal displacement in section 3-3.

The variation of horizontal displacements in section 3 – 3 according to soil types is shown in Figure 7.25. In the case of S = 1, these pores become filled with water as much as possible. This is a factor that facilitates the movement of the soil parts in the horizontal direction, especially. For this reason, the analysis results obtained for the GM soil type reveal the highest values of horizontal displacements as expected. Moreover, it is possible to see that the horizontal displacement values are decreasing as the soil type goes from GM to GW. The inertial terms for GW have little effect, but we cannot say the same thing for SP and GM. Therefore, in this figure, we can also clearly observe the increase in discrepancy.

In Figure 7.26, we can see that the QS – PD difference is very small compared to the GW soil type, and at the same time it allows us to read the minimum vertical displacement values for these two solutions in section 3 – 3. As the soil type changes from GW to GM, the vertical displacements increase. Besides, the QS - PD difference is increasingly rising and therefore, there is a grow in discrepancy. Especially in the rubble layer, when the pore pressure and soil type relation is examined, large differences are not seen. However, there are differences in the seabed layer. In addition, the difference between the largest and smallest values is much higher than the other results. According to the solutions of SP and GM soil types; excluding GW, dynamic effects matter. So the QS – PD difference can be neglected. On the other hand, when we look at the rubble mound fill, we can see that the pore pressure values tend to decrease, as they go up towards the surface. The maximum values are valid for the SP soil type and for the PD solution (Figure 7.27).

In section 1-1, when the effect of soil permeability on normalized effective stress distributions is examined, it is clearly seen that the maximum values occur for GM. Inertial terms contribute to this drastically. This also applies to shear stresses. Especially, it is seen that different soil types are effective for different areas in seabed layer. The maximum normal stress for SP soil is obtained in the x-direction and for GW soil in the z-direction. With the transition from seabed to rubble, stress values increase. Normal stresses suddenly decrease as we get closer to the surface of the rubble, but no similar situation is observed for shear stresses (Figures 7.28, 7.29, 7.30).

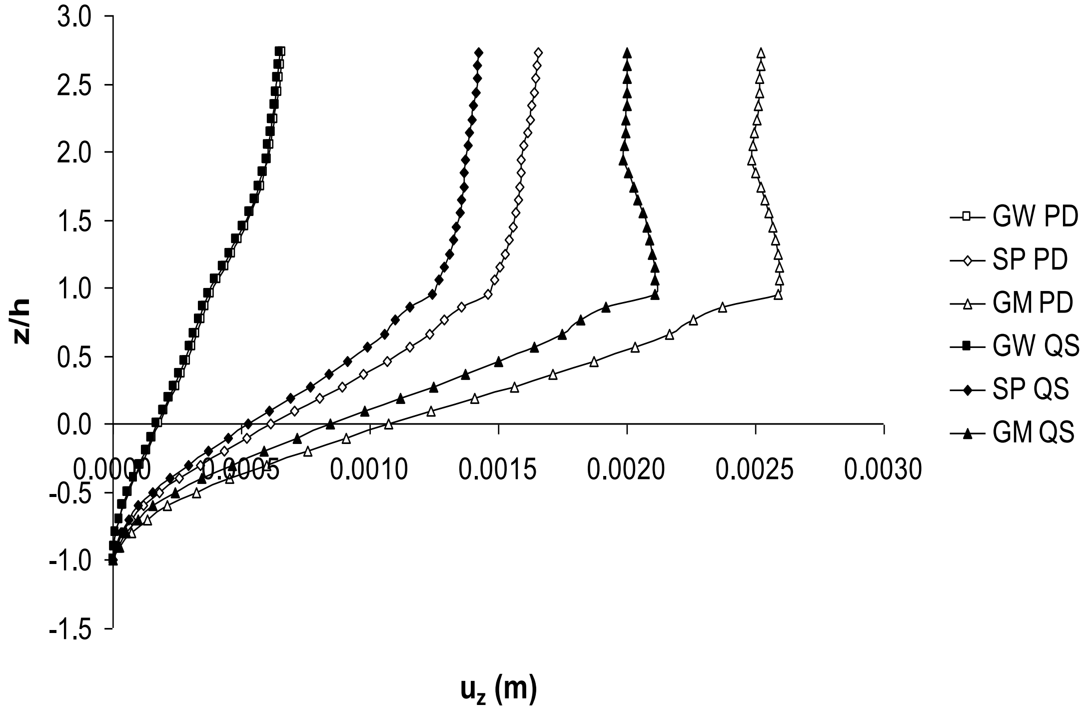

Figure 7.26: Effect of soil type on vertical displacement in section 3-3.

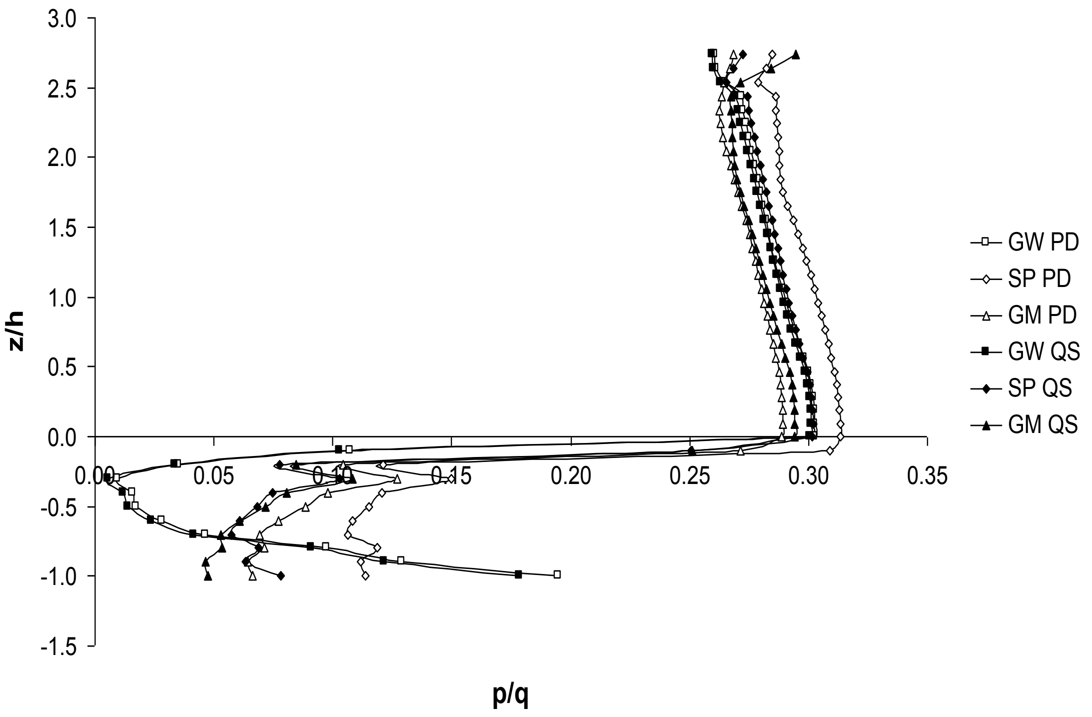

Figure 7.27: Effect of soil type on pore pressure in section 3-3.

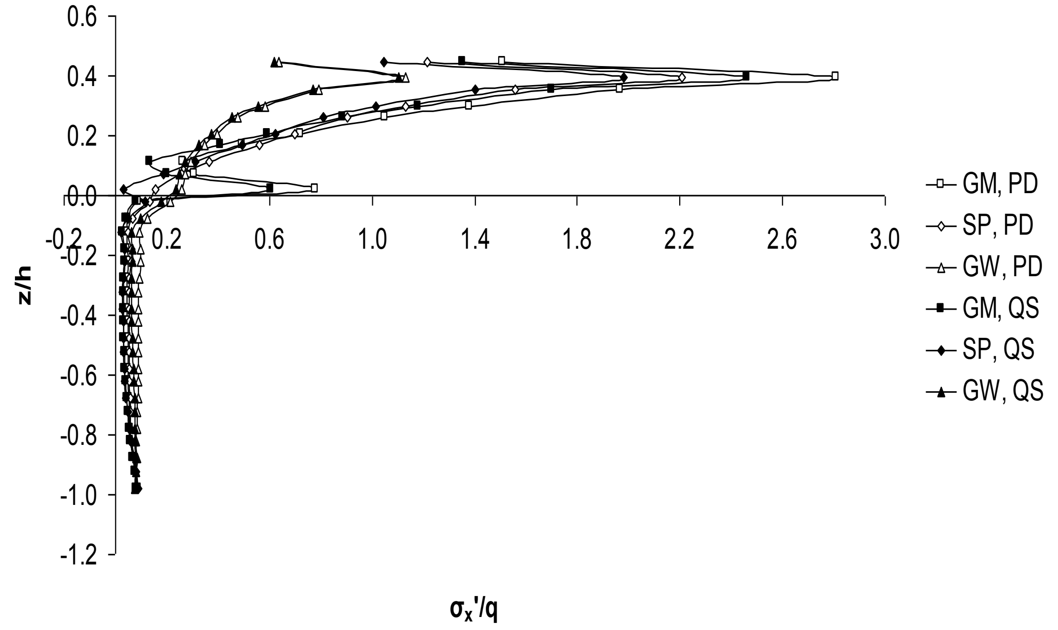

Figure 7.28: Effect of soil type on normal stress in x direction in section 1-1.

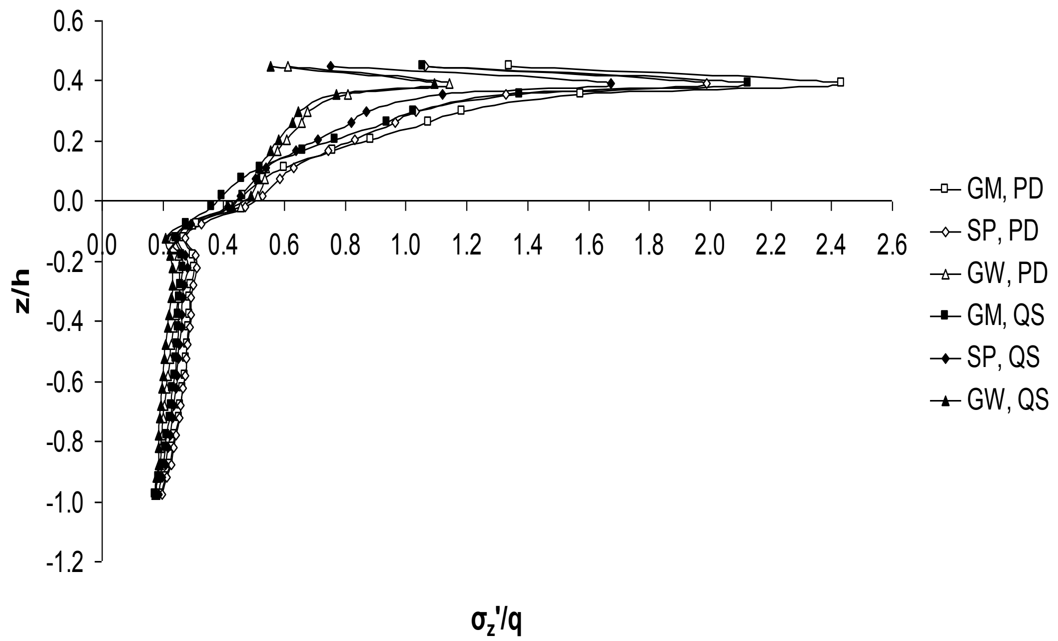

Figure 7.29: Effect of soil type on normal stress in z direction in section 1-1.

According to Figures 7.31, 7.32 and 7.33, the stresses around the front toe of the caisson are excessive in Section 2 – 2. This can be interpreted as that, the rocking motion under the standing wave effect is more effective for the GM that has the lowest modulus of elasticity in this parametric study. The wave motion affects the system in such a way that the SP and GW soils generate less stresses. Soil-type variations generally have a slight effect on normal and shear stresses. We also see that the discrepancies in inertial terms are not always increasing, and sometimes there is a diminutive effect (Figures 7.34, 7.35, 7.36).

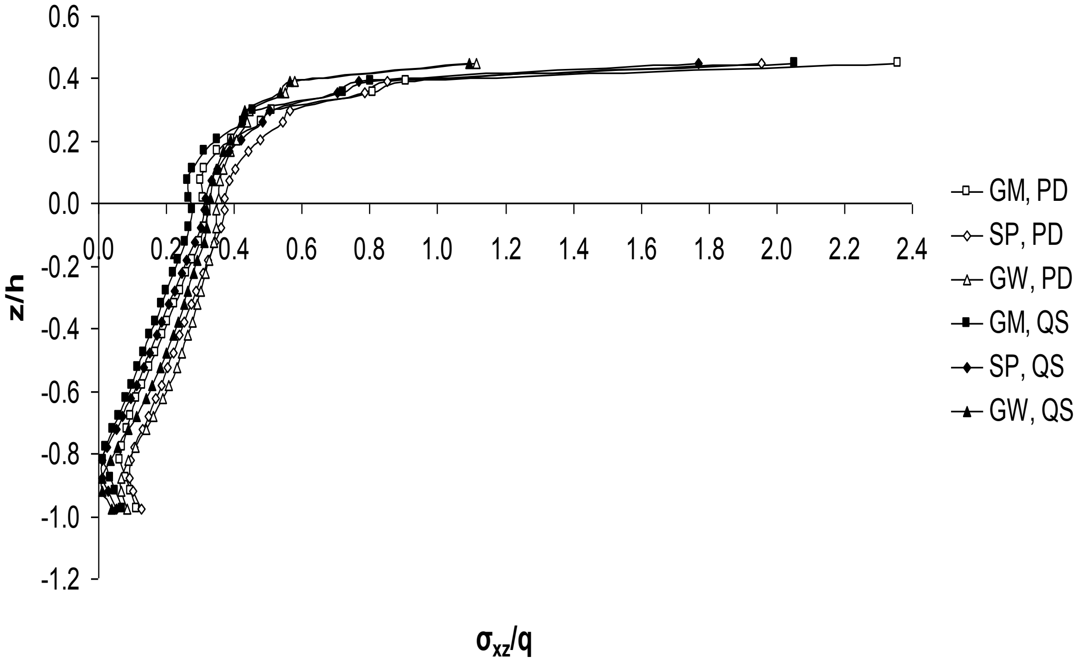

Figure 7.30: Effect of soil type on shear stress in section 1-1.

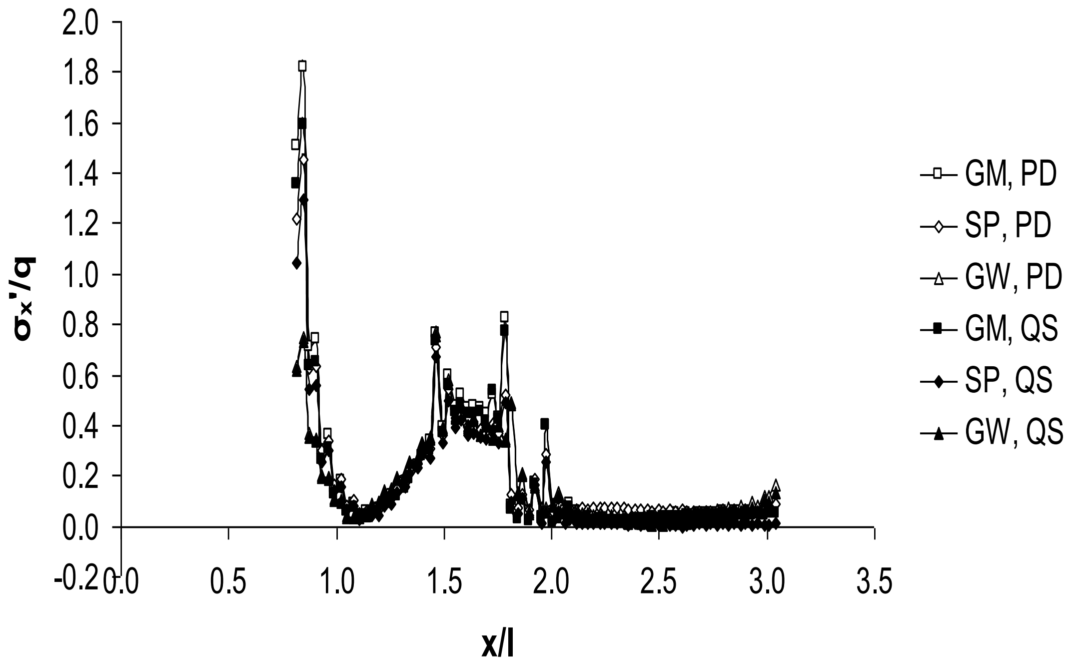

Figure 7.31: Effect of soil type on normal stress in x direction in section 2-2.

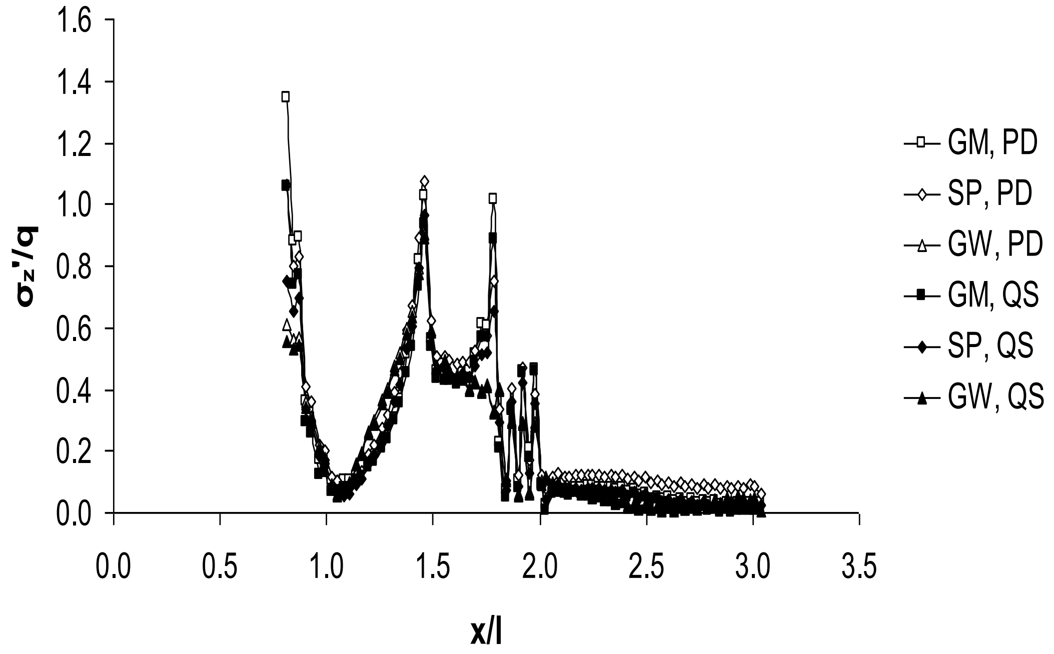

Figure 7.32: Effect of soil type on normal stress in z direction in section 2-2.

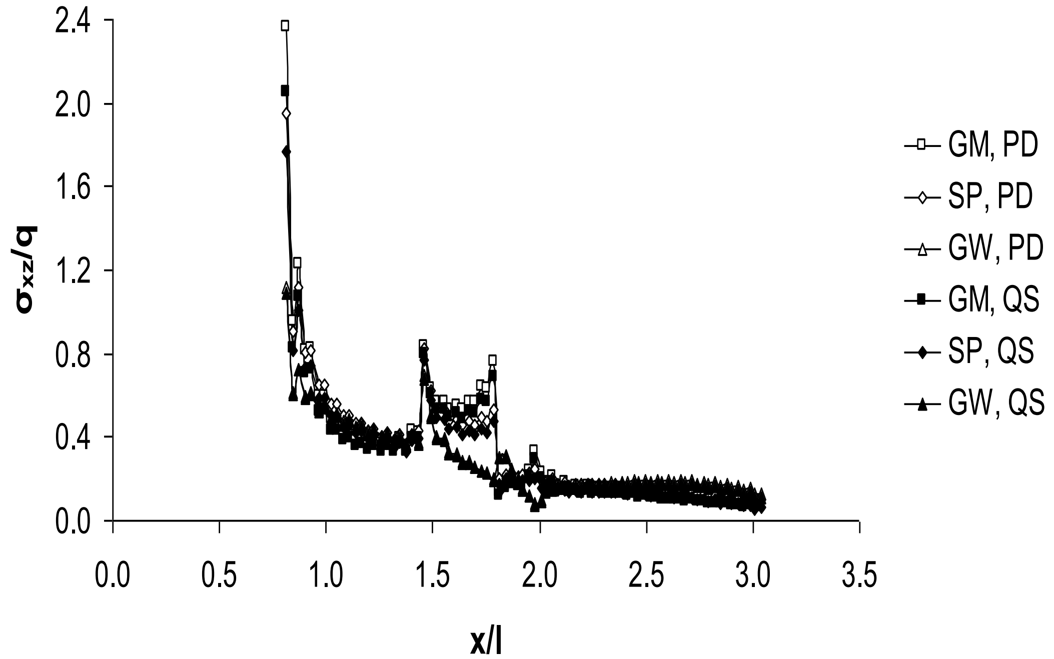

Figure 7.33: Effect of soil type on shear stress in section 2-2.

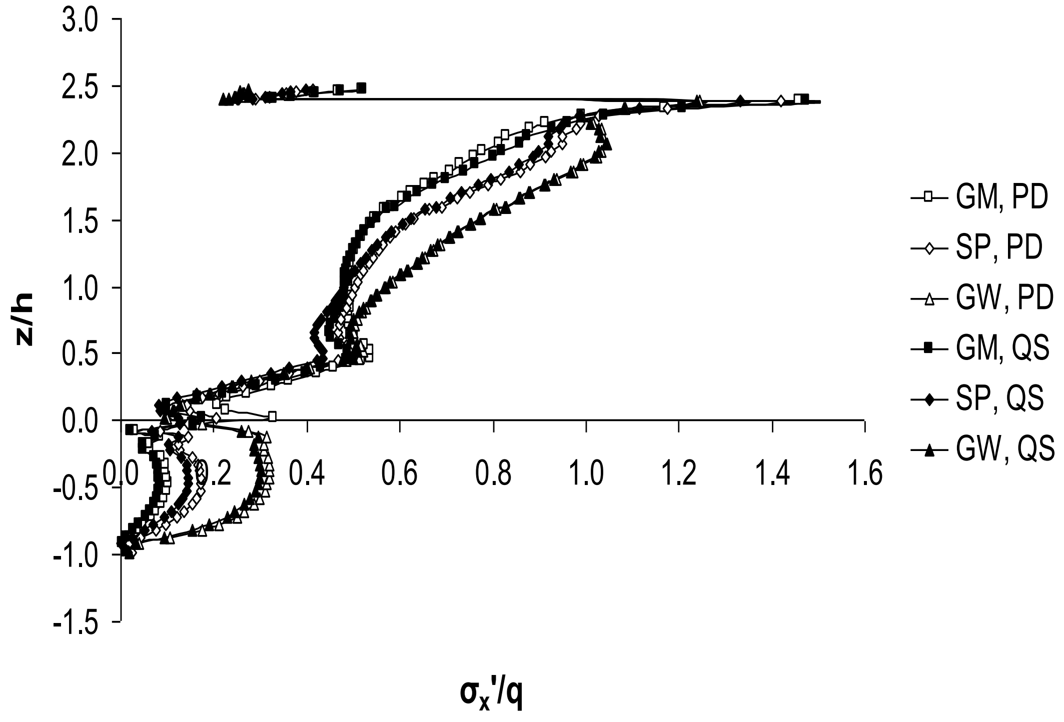

Figure 7.34: Effect of soil type on normal stress in x direction in section 3-3.

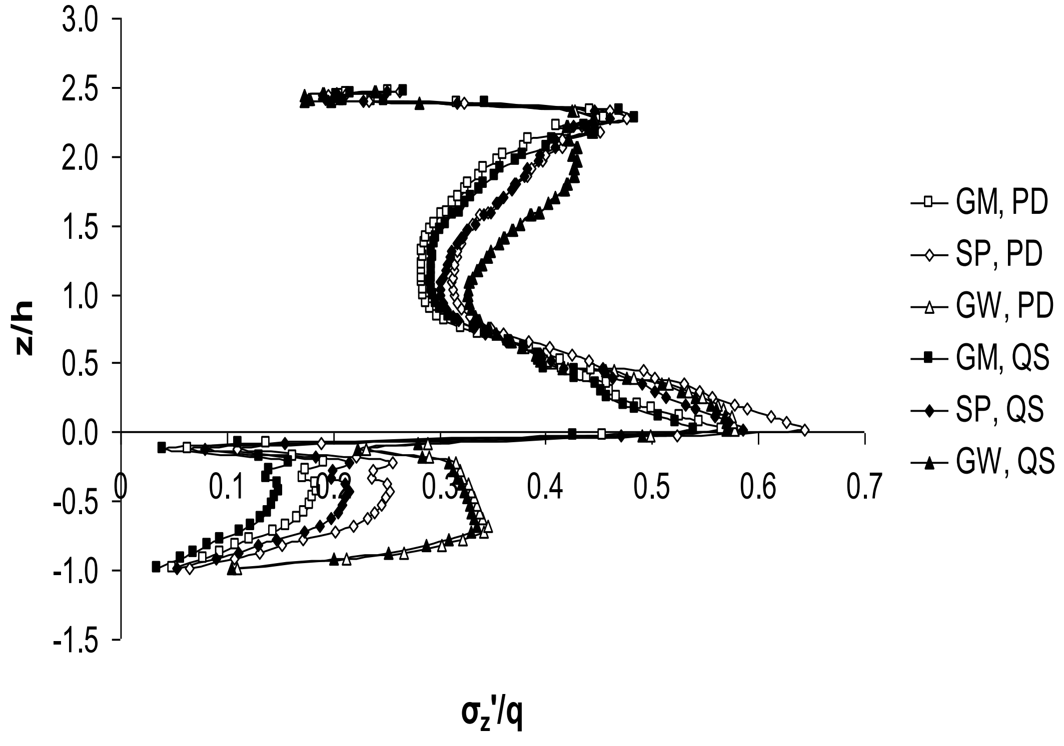

Figure 7.35: Effect of soil type on normal stress in z direction in section 3-3.

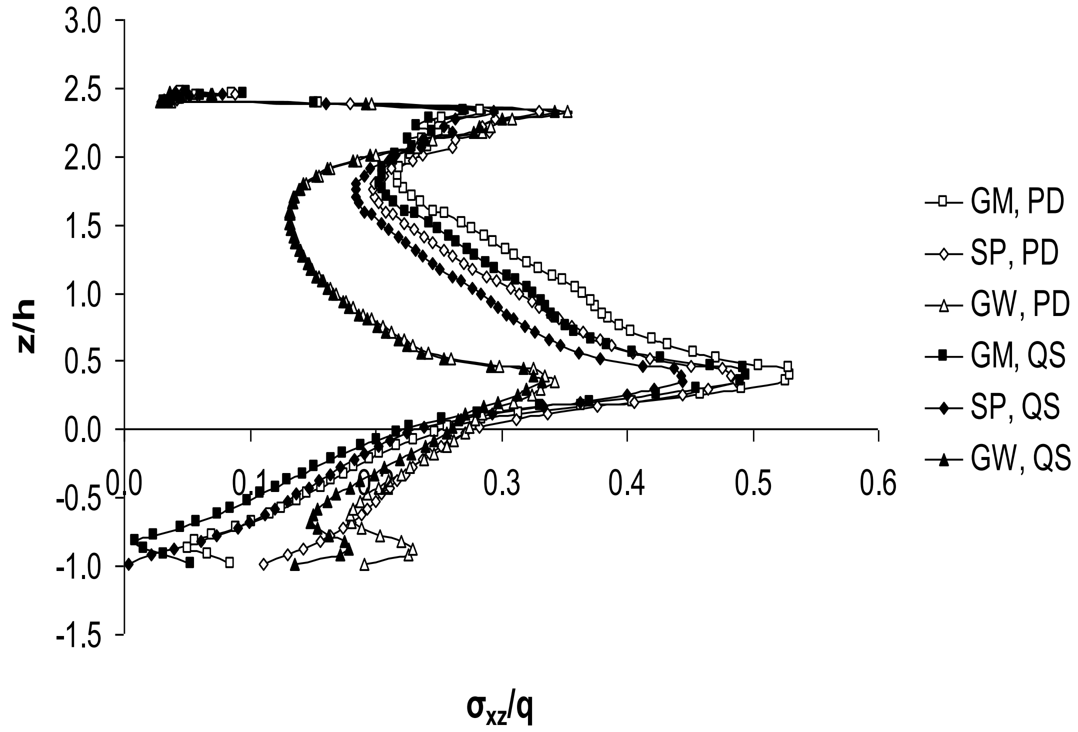

Figure 7.36: Effect of soil type on shear stress in section 3-3.

7.3.3 Effect of standing wave period

When we examine the effects of changes in standing wave periods on horizontal and vertical displacements in section 1 – 1, we notice that the response figures do not change in parallel with the parametric changes. That is, the peak values of the reactions occur between certain period values. For example, the dynamic effects observed for T=10 s are greater than those observed for T=5 s and T=15 s (Figure 7.37 and 7.38). It is also noticed that the changes in both horizontal and vertical displacements are reduced in the rubble area. The results obtained for periods of T=5 s and T=15 s show an expected variation of soil response, especially for the horizontal displacement. However, for standing wave period T=10 s the corresponding value drops sharply in the seabed. This shows that there does not necessarily have to be an “expectedly increasing” or “expectedly decreasing” variation of DOF under standing waves in the seabed. As in our case, the system dynamic response seems to be altered for T=10s wave period and further elaborations on such a rather interesting result continue with further analyses.

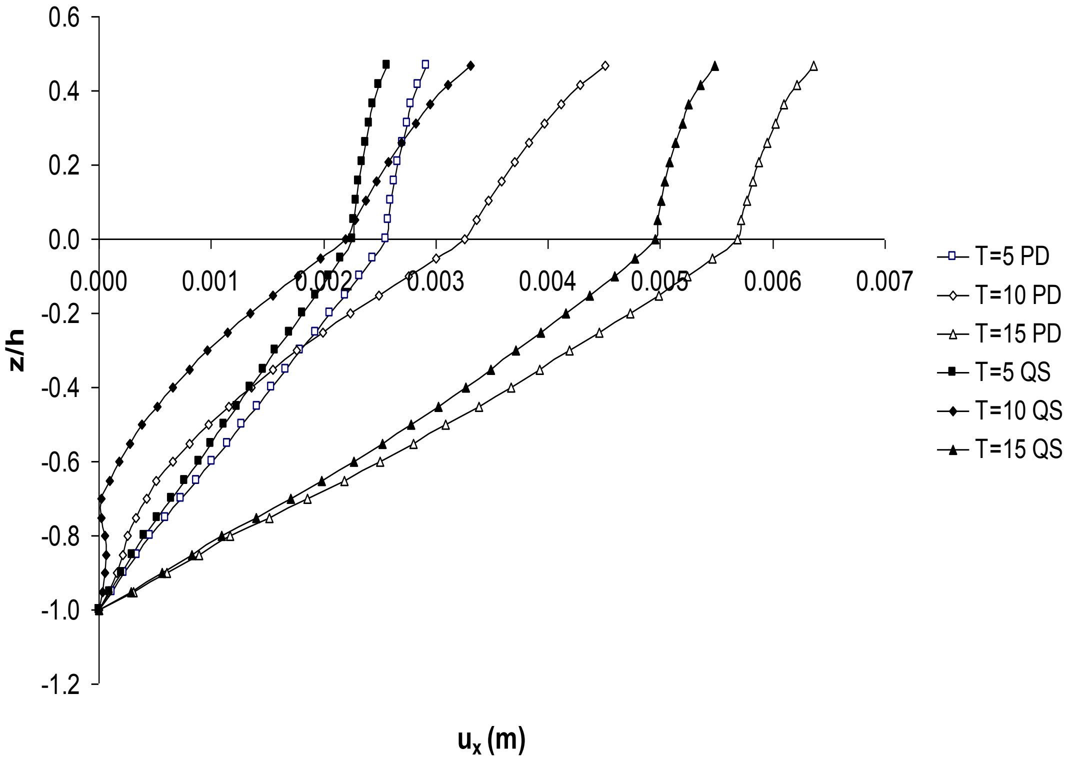

Figure 7.37: Effect of wave period on horizontal displacement in section 1-1.

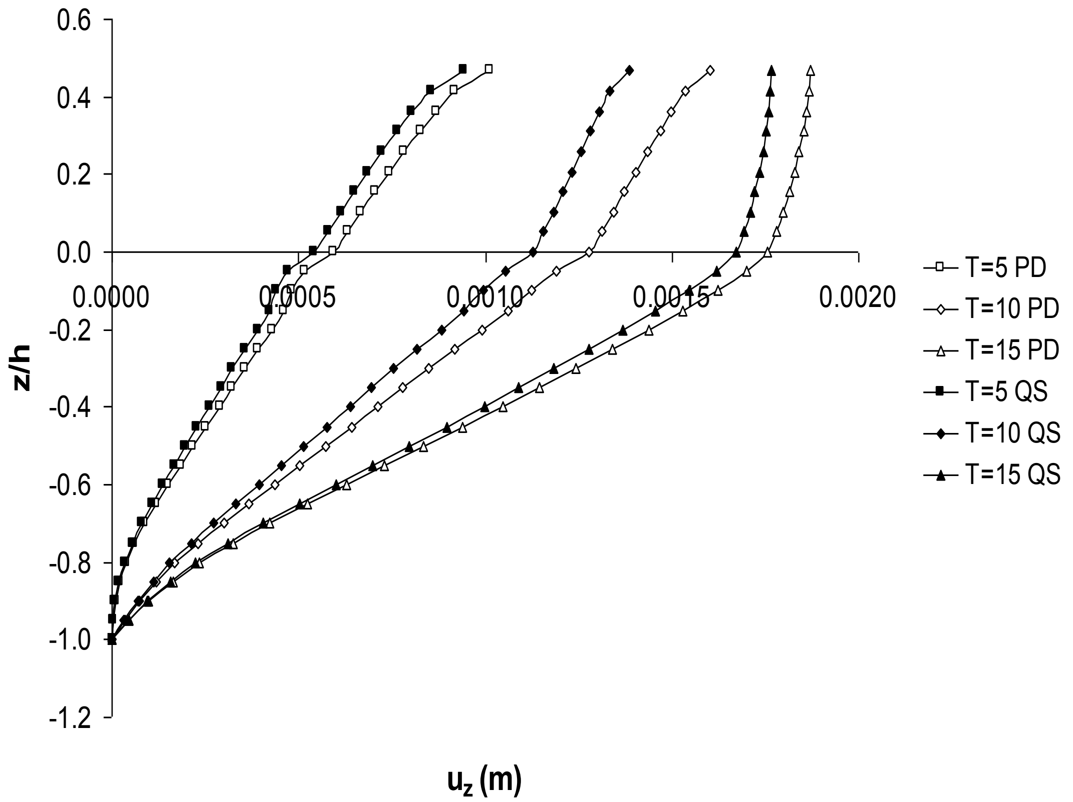

Figure 7.38: Effect of wave period on vertical displacement in section 1-1.

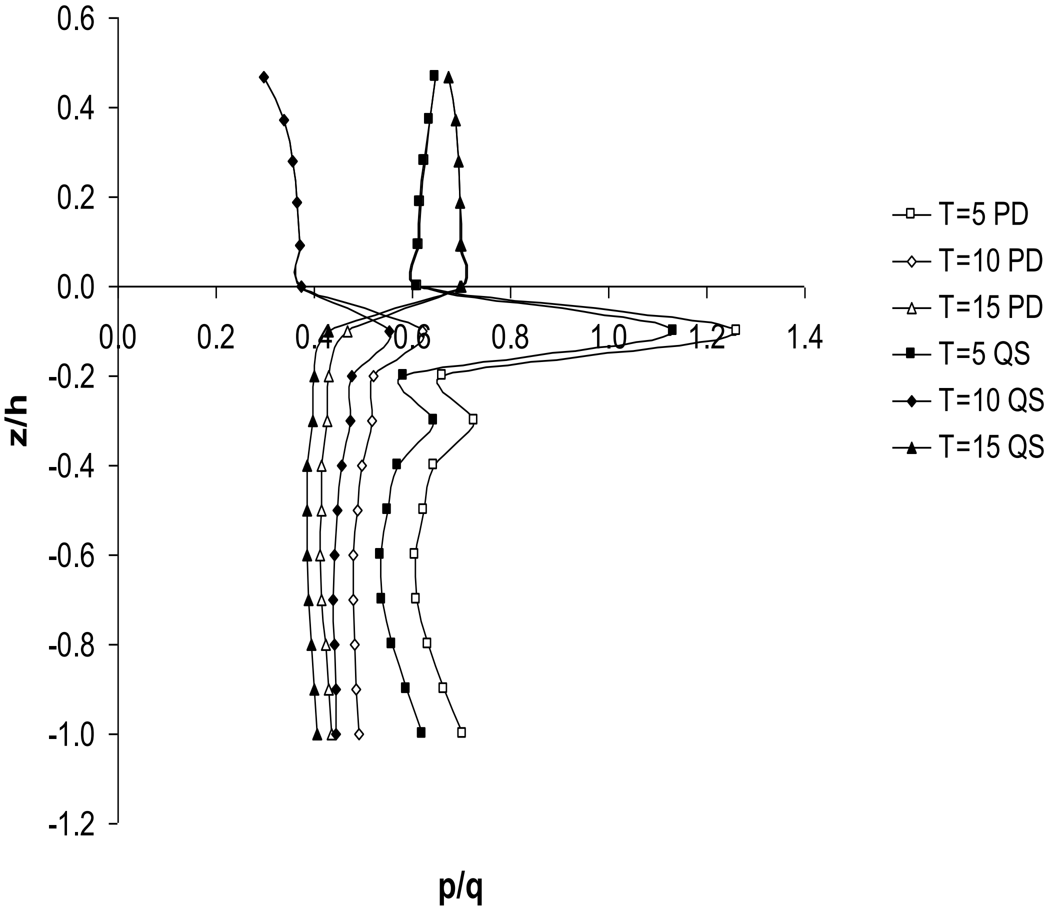

Figure 7.39: Effect of wave period on pore pressure in section 1-1.

Figure 7.39 presents the results of analyses for different standing wave periods. It shows that inertial terms are increasingly influential on the dynamic response, especially in the seabed at section 1 – 1. On the other hand, in the rubble mound, these terms have absolutely no effect. That is, the inertial terms associated with the motion of the solid phase included in the seabed do not affect the rubble motion. Moreover, as the standing wave periods decrease a respective increase in the pore pressures is observed in the seabed. My take on from these response curves is, considering the possibility of being near or getting closer to the natural period of the CTQ-seabed system, results of the T=10 s analyses may just be revealing such a dynamic response in the problem.

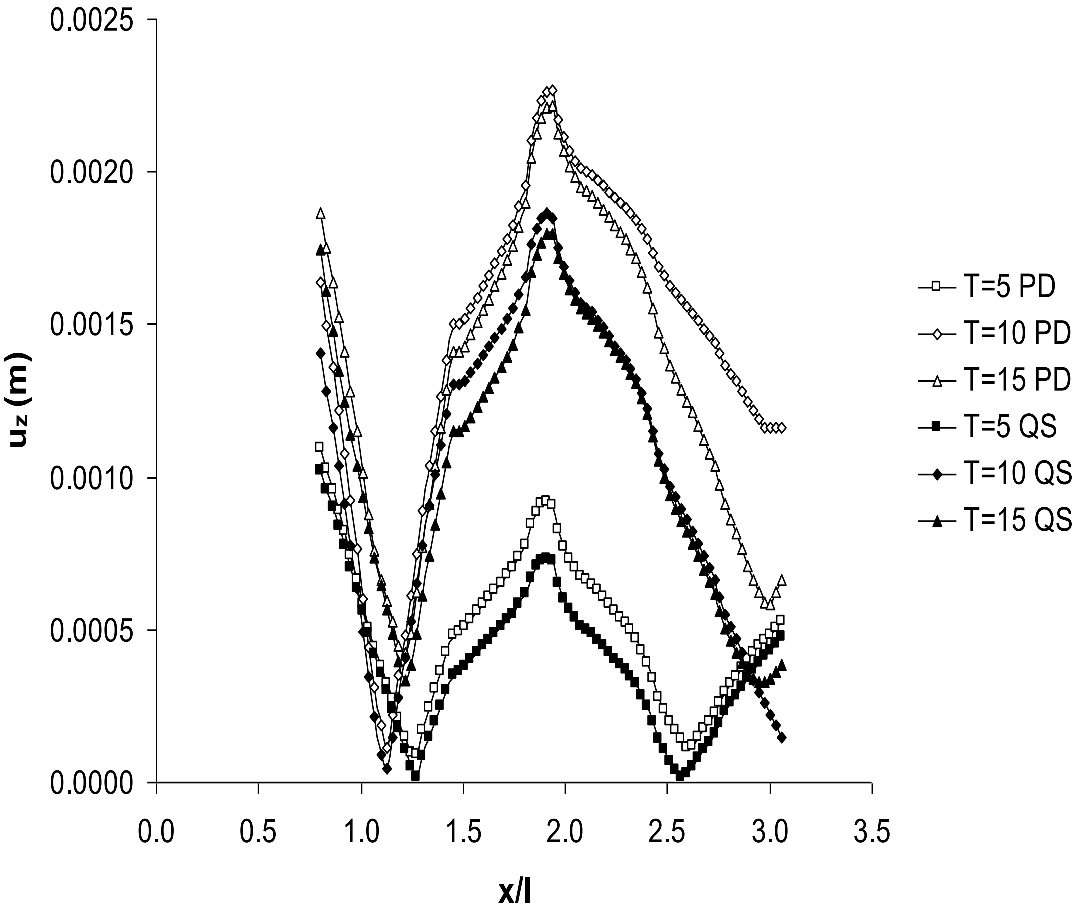

Figure 7.40: Effect of wave period on vertical displacement in section 2-2.

Figure 7.40 shows that the increase in the standing wave periods makes it also possible to observe the dynamic effects on the response of the entire system in both the caisson region and in the seabed for section 2 – 2. In particular, we observe that the vertical displacement values obtained for the T=10 s and T=15 s periods in the seabed layer within the section are close to each other. These values, which tend to increase with the addition of dynamic effects remain close to one another at the point where the maximum displacement occurs. It is seen that the vertical displacement values obtained for t=5s are lower than the other studies. It is one of the interesting results in this chart that the vertical displacement values of the seabed layer are increasing again after a definite point for each parametric studies. That is, it is not very accurate to say that as moving away from the wall, the amount of deformation decreases regularly. This shows that; even if there is not any collapse behind the wall, even more damage can occur to the interior of the harbor, for instance. This is essential to know prior to any design to be made such that even in a poroelastic model it may reveal important information about how the vertical settlement is distributed around the CTQ. In this particular case for $k=10^{-6}$ m/s, settlements are larger for the outlier 10s period in the dynamic analysis (PD).

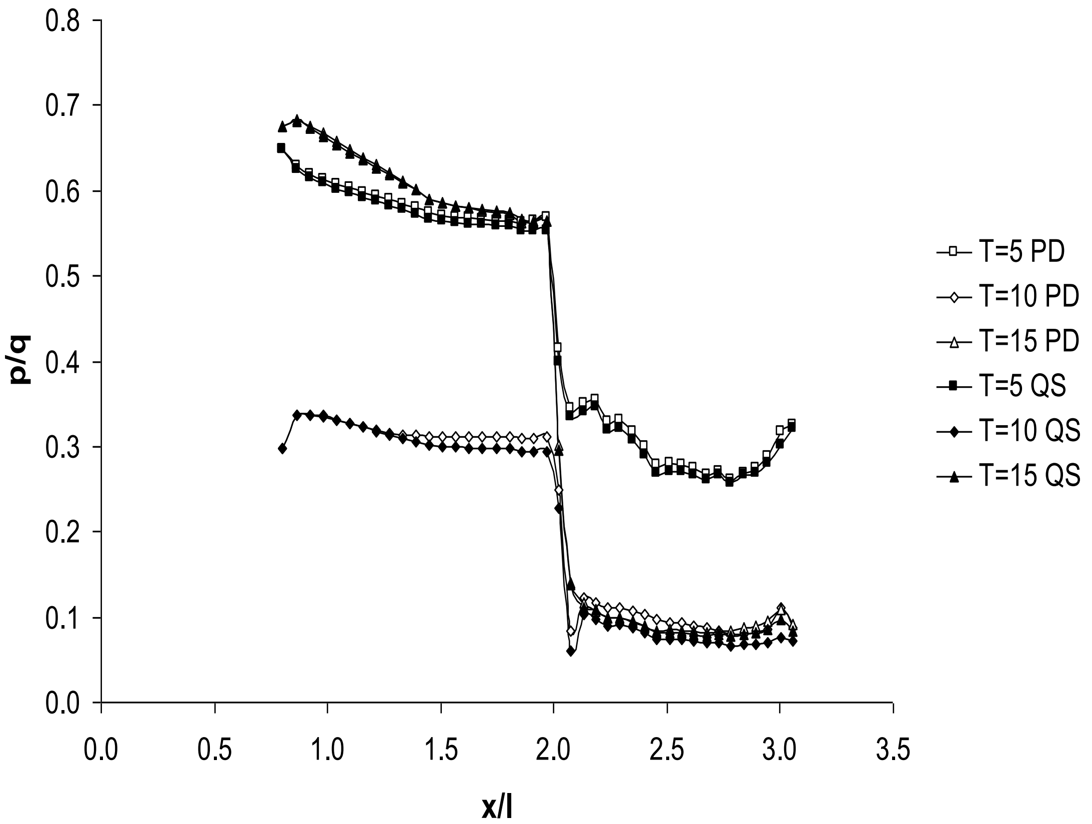

Figure 7.41: Effect of wave period on pore pressure in section 2-2.

On the lower part of the CTQ and in the rubble, the large difference between the pore pressures is obtained for section 2 – 2 in Figure 7.41. Especially the values obtained for standing wave period T=10 s are considerably lower than others. Although it is possible to observe dynamic effects, we cannot say that it has made excessive changes. In particular, it is one of the consequences that, as the reduction in pore pressure for the standing wave period (T=15 s is too considerable and the values fall almost at the same level as T=10 s. This graph shows us once again that the maximum or minimum values for different specific standing wave period intervals can occur in a dynamic analysis.

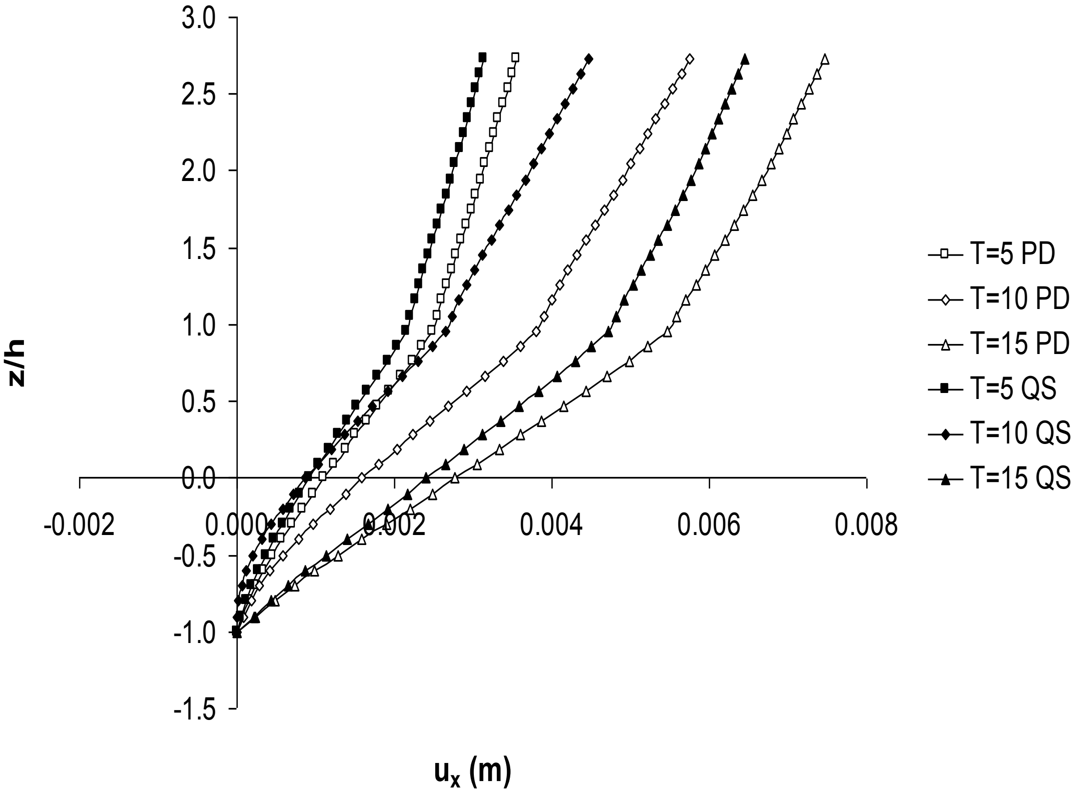

Figure 7.42: Effect of wave period on horizontal displacement in section 3-3.

In general, it can be seen that the horizontal displacement values obtained for standing wave period T=10 s are closer to those obtained for T=15 s as they go towards the top of the rubble mound (Figure 7.42). The dynamic effects are obvious in the analyses for the 3 different standing wave period values. However, for horizontal displacements, the largest difference between the QS and PD solutions is for T=10 s. Seabed displacements also decrease in the rubble mound in section 3 – 3.

The variation of vertical displacement values with varying standing wave periods gives interesting results in section 3 – 3, unlike previous figures (Figure 7.43). According to the results obtained from PD solutions minimum displacement values are obtained for T=5 s and there is a noticeable increase in the values when the effect of dynamic terms is taken into consideration. On the other hand, the displacements obtained in the QS solution, especially for T=10 s and T=15 s are higher in the rubble layer than they are in the PD solution.

Figure 7.44 shows the effects of wave period on pore pressure variation along section 3-3. While the response is again similar to Figure 7.10, since permeability is now much less for seabed as opposed to rubble, its effect can be seen for z/h < 0 giving the largest values for T=5s. Rubble response gets also affected by the wave period with a distinct variation for T=10s.

Although the standing wave periods may directly affect the stresses in the seabed, since according to the linear wave theory change in wave period also causes a change in wavelength, it is possible that such an effect could be as a result of changes in wavelength at a particular water depth. Such a change may or may not yield a steady decline or increase in stress values in response to increasing wave periods. For example, there are cases where the lowest values in the rubble layer occur for the T = 10s wave period (Figures 7.45, 7.47, 7.53). In addition, the minimum values of stresses generated under the caisson can be for T = 10 sec (Figures 7.48, 7.49). Such an argument will be finalized once additional FE analyses are finished.

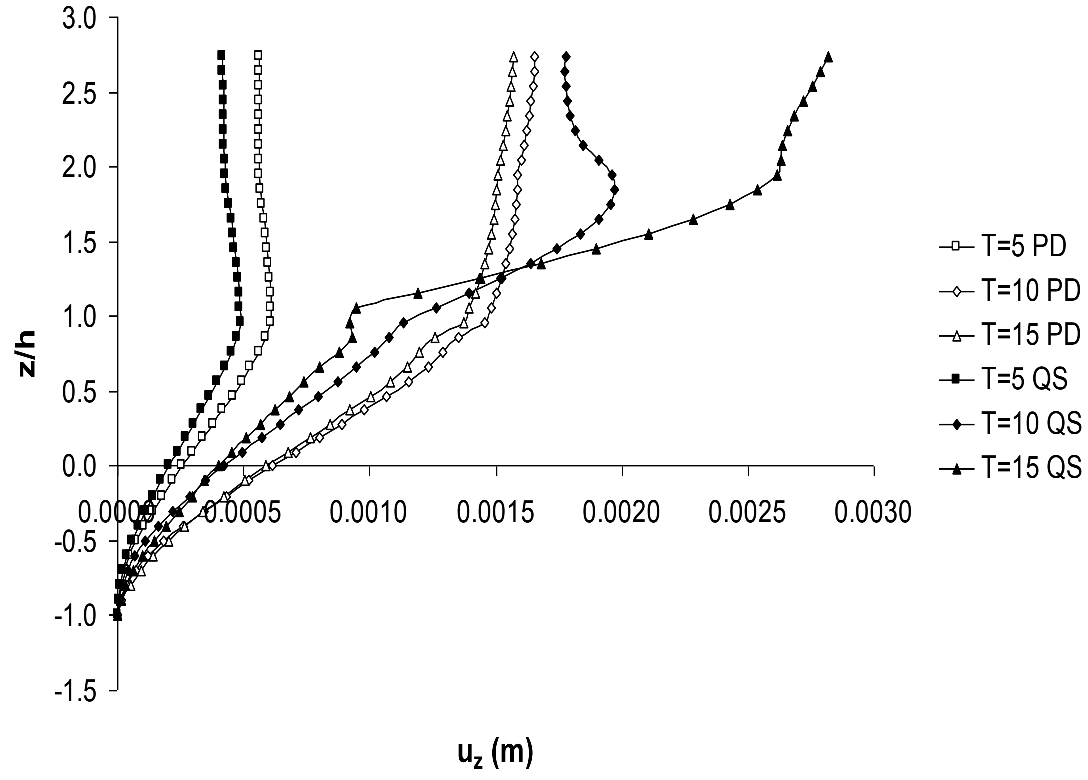

Figure 7.43: Effect of wave period on vertical displacement in section 3-3.

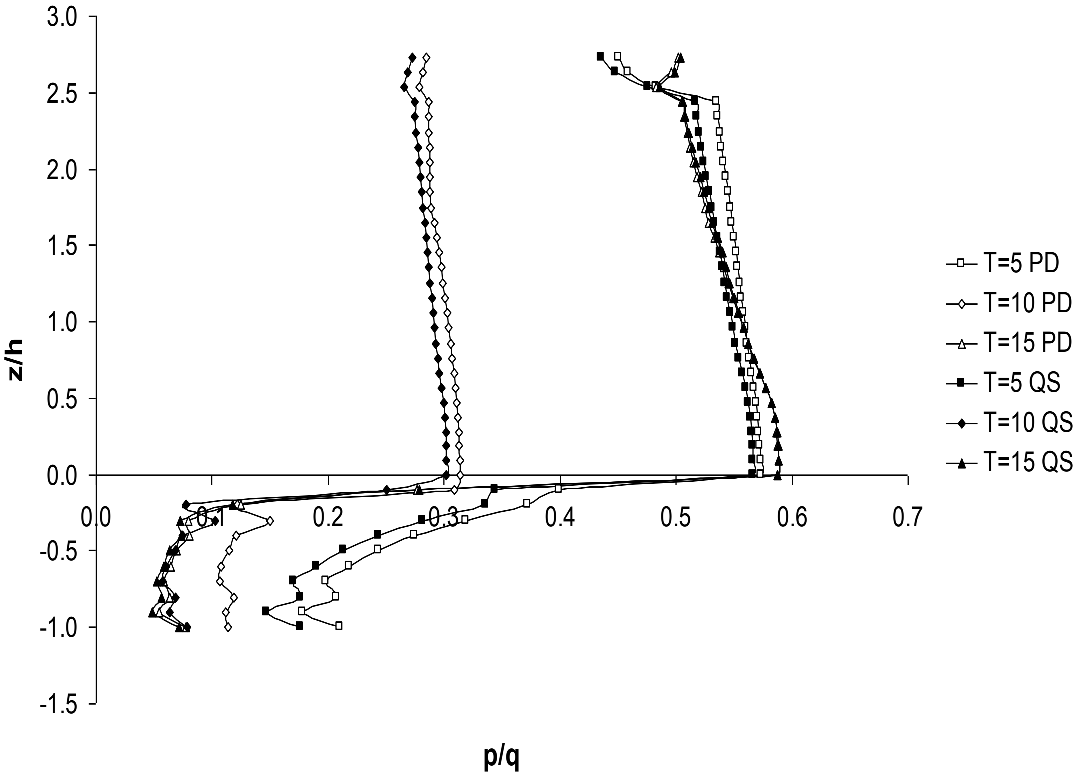

Figure 7.44: Effect of wave period on pore pressure in section 3-3.

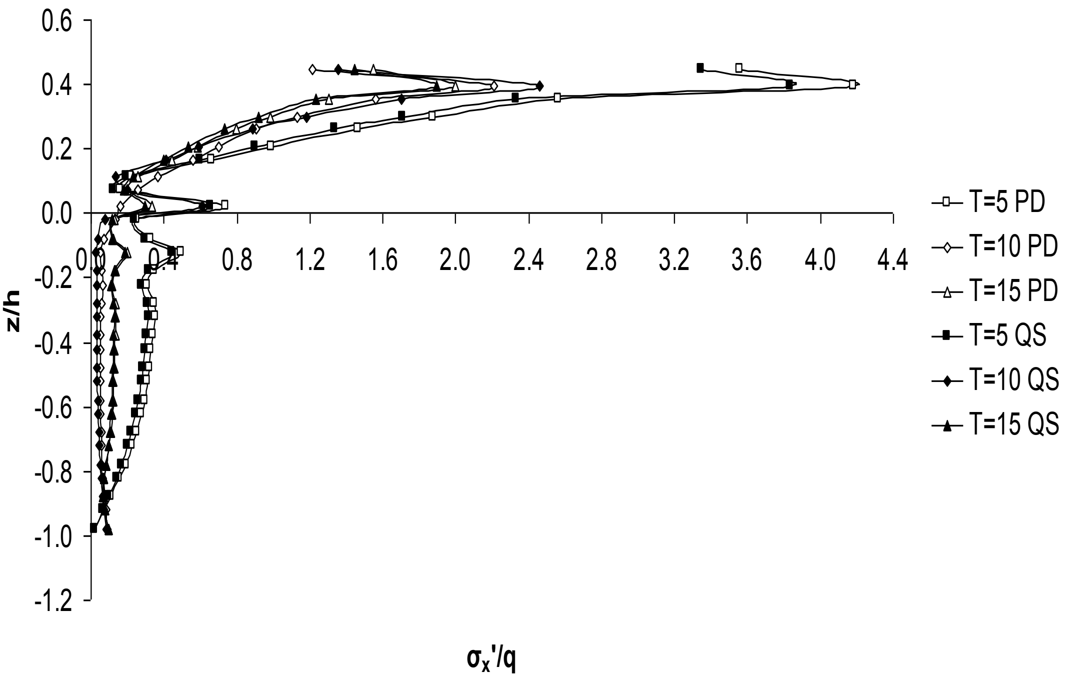

Figure 7.45: Effect of wave period on normal stress in x direction in section 1-1.

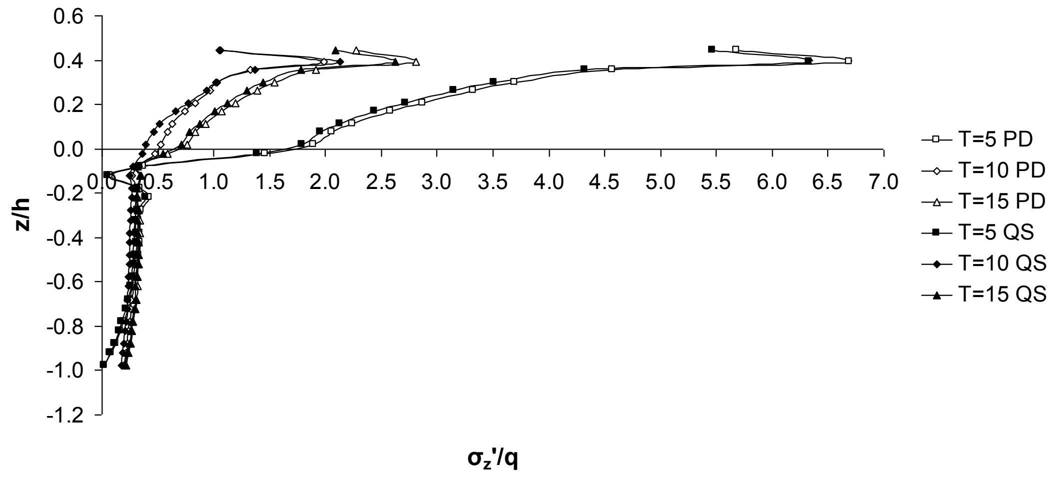

Figure 7.46: Effect of wave period on normal stress in z direction in section 1-1.

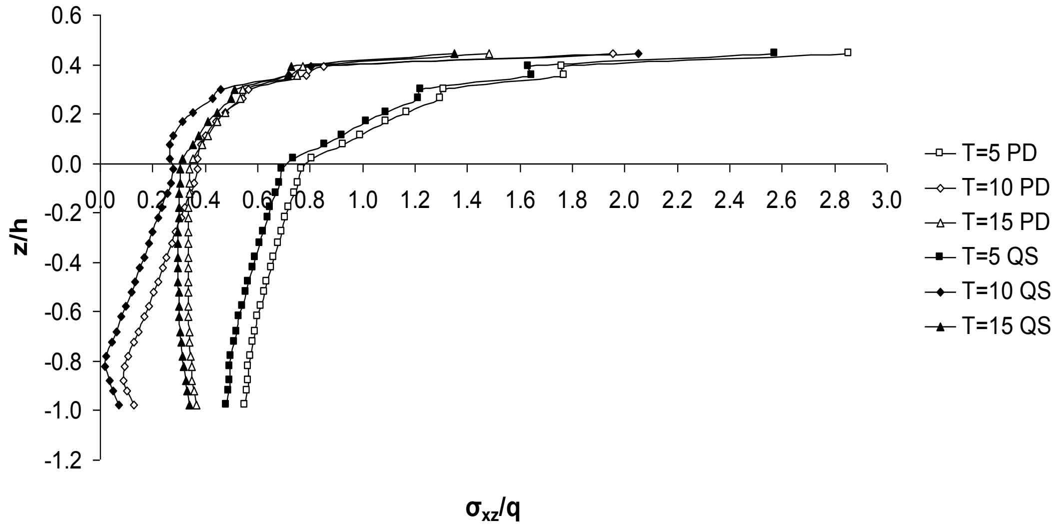

Figure 7.47: Effect of wave period on shear stress in section 1-1.

We observe that the existence of inertial terms play an important role on the increase in the shear stresses at the front and back of the caisson wall (Section 1-1 and Section 3-3). It should also be emphasized that sudden increases in shear stresses occur when T = 10s and T = 15s, when the rubble layer moves to the seabed layer (Figure 7.52). The maximum shear stresses occur at the front of the wall for T = 5 s wave (Figures 7.48, 7.49, 7.50). This circumstance suggests that due to the decrease of the standing wave period, the damage at those area which the front toe of the caisson wall locates is too much. But still, this interpretation is not satisfactory. Therefore, it is noticeable that further studies are required for low wave period values. In some cases, as the wave periods increase, it is another important result that the inertial terms lose their effect (Figure 7.51).

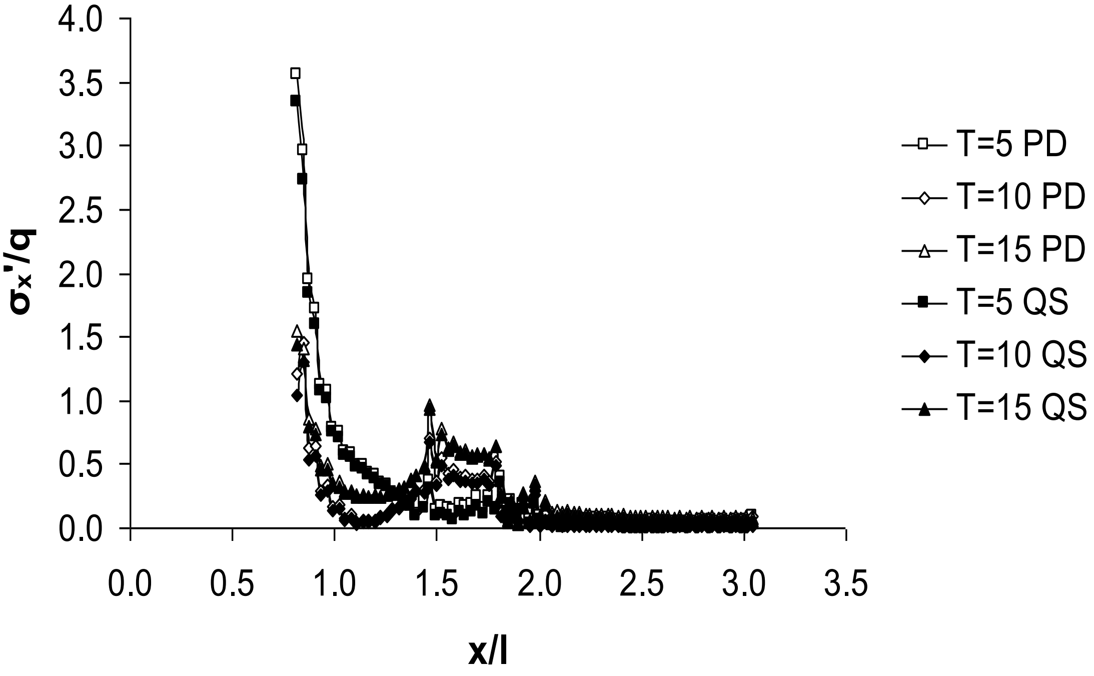

Figure 7.48: Effect of wave period on normal stress in x direction in section 2-2.

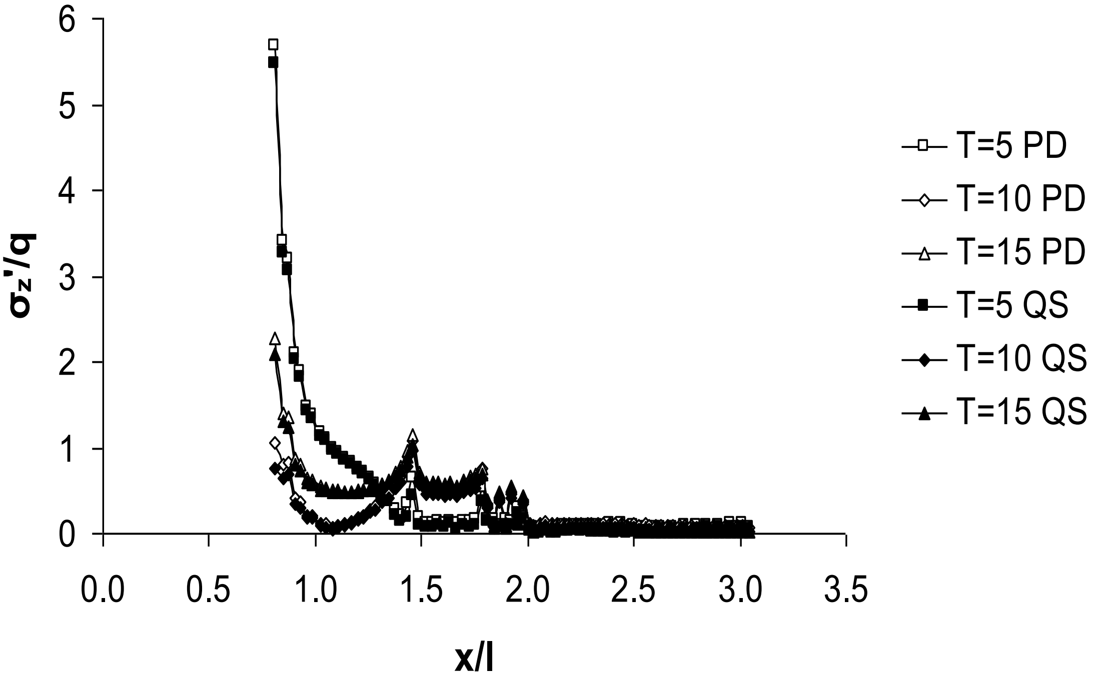

Figure 7.49: Effect of wave period on normal stress in z direction in section 2-2.

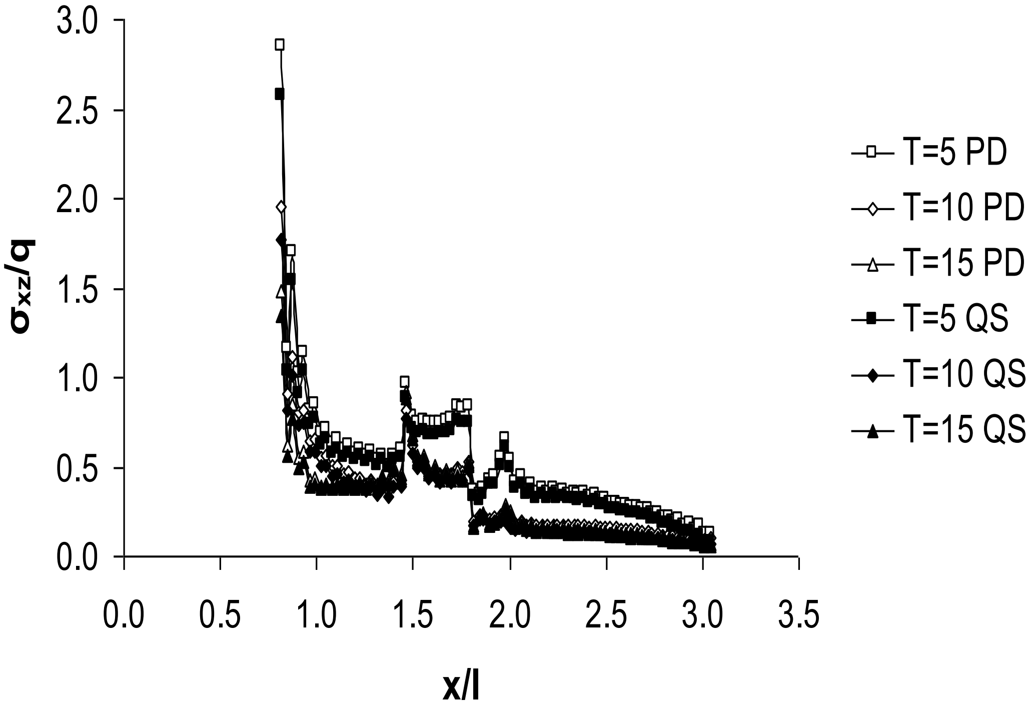

Figure 7.50: Effect of wave period on shear stress in section 2-2.

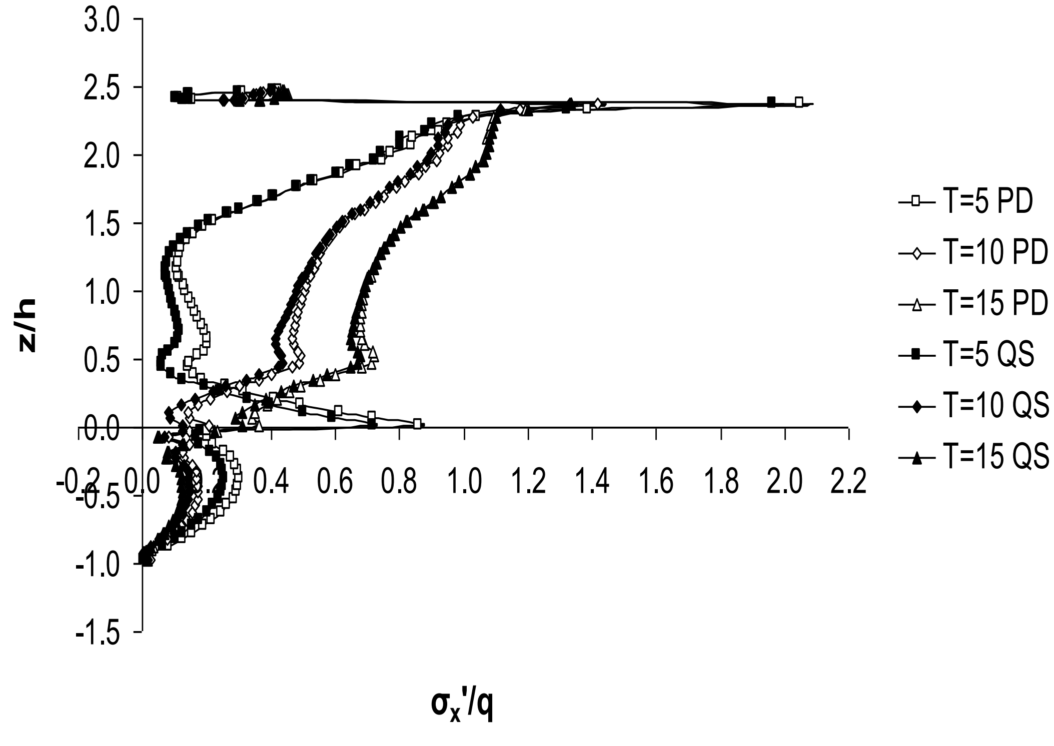

Figure 7.51: Effect of wave period on normal stress in x-direction in section 3-3.

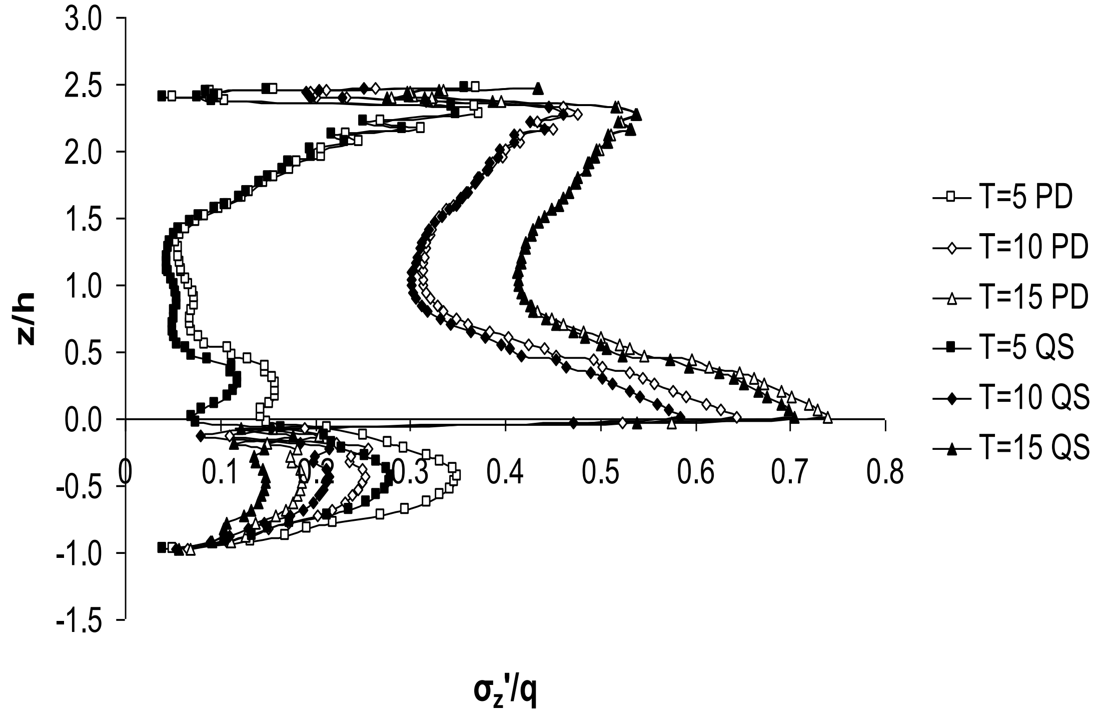

Figure 7.52: Effect of wave period on normal stress in z direction in section 3-3.

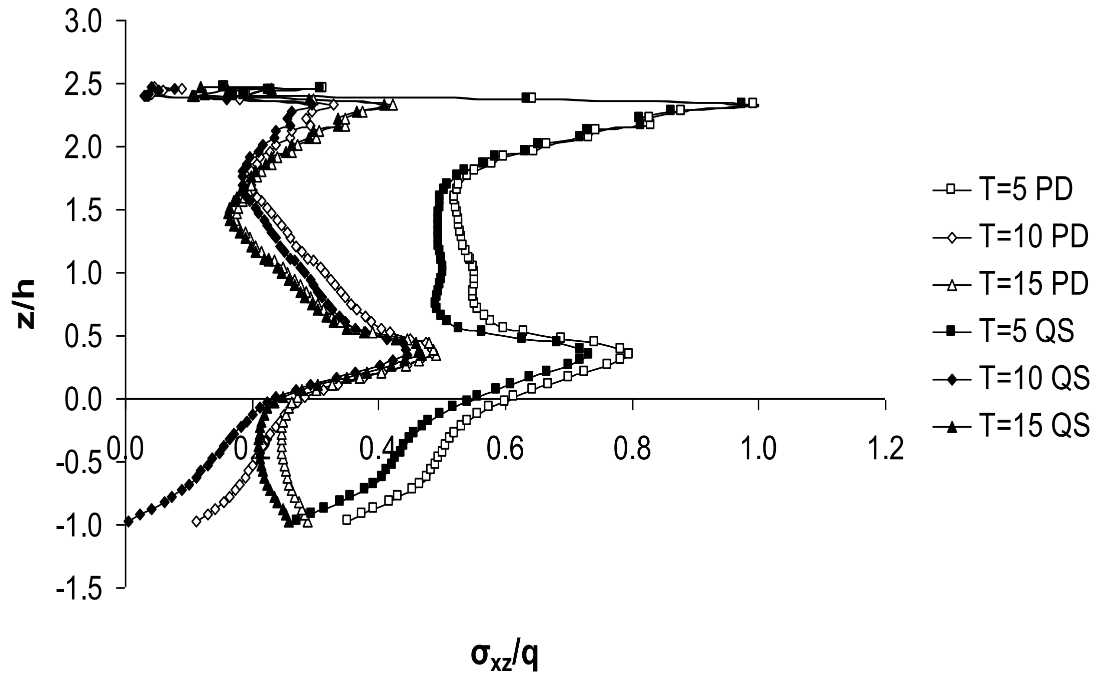

Figure 7.53: Effect of wave period on shear stress in section 3-3.

8. INSTABILITY OF CTQ–SEABED SYSTEM UNDER STANDING WAVES

Just like for all coastal structures, CTQs are under constant attack of wave loads. This effect not only changes the physical conditions (displacements, stresses etc.) of the underlying soil layers and hence their stabilities, but also the existing structureitself. It is important that coastal geotechnical engineering studies such changes that may occur in the system under severe wave action. The reason for this is, marine soils are susceptible to “wave-induced liquefaction” resulting in failure in coastal structures. Liquefaction is an important phenomenon that occurs in saturated loose sandy seabed soils where effective stress in the soil skeleton becomes zero due to continuous build-up of pore pressure under wave actions. Hence, the soil as a whole acts like a fluid without having any shears strength. Therefore, once seabed is liquefied under wave action, any object resting on the liquefied seabed sinks immediately deep into soil.

When progressive waves propagate over a sandy seabed, a shear deformation is induced in the seabed. This deformation rearranges the sand grains and thus seabed soil experiences compressive normal stresses under each wave crest and similarly tensile stresses under each wave trough. As a result, pore pressure builds up in the sandy layer with the tendency of contraction behavior (Figure 8.1).

In this chapter, instantaneous liquefaction potential is studied around the CTQ - seabed system and a number of parametric studies is conducted to understand the effect of key physical and wave parameters on the instability.

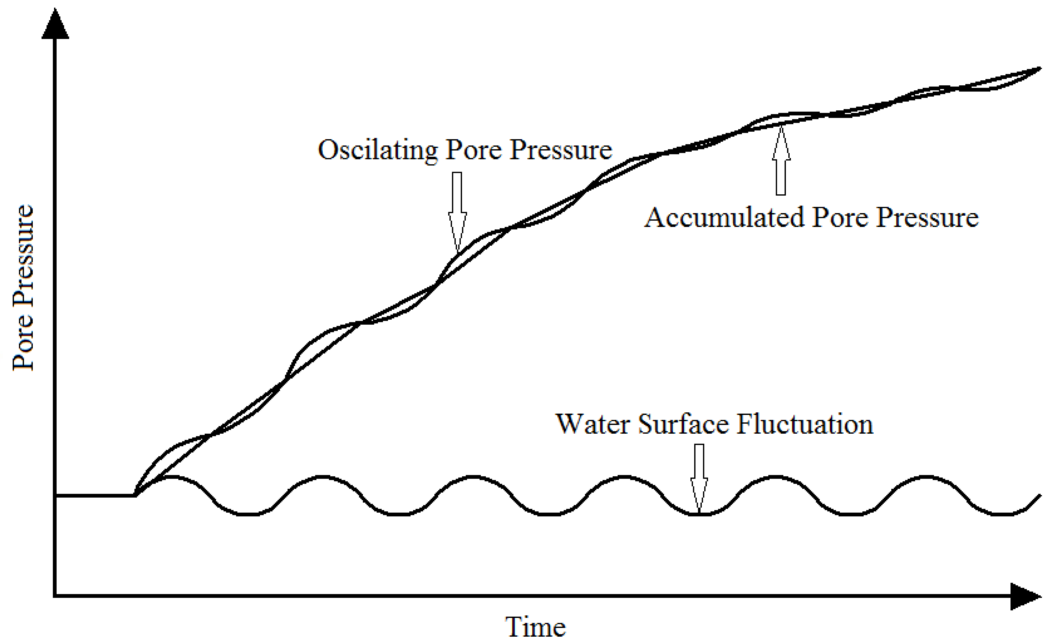

Figure 8.1 : Pore pressure builds up and accumulation.

8.1. Instantaneous Liquefaction

During passage of wave trough, upward pressure gradient develops at the top surface of the sandy seabed. This pressure gradient is not large for fully saturated seabed surface, but could be extremely large for the seabed containing air/gas bubbles and cavities (unsaturated conditions) because of fast dissipation rate. Therefore, top layer of the sandy seabed feels tremendous upward gradients of drag force. If the upward drag pressure exceeds the effective mean overburden pressure, then the seabed liquefies for an instant of time (only the passage time of trough of a wave) and any object resting on it sinks into seabed instantaneously. This phenomenon of seabed is called “instantaneous liquefaction” (Sakai et al., 1994; Sumer and Fredsøe, 2002; Ulker et al., 2010; Ulker et al., 2012; Ulker 2012). The liquefaction criterion for a 3-D elastic analysis that is applicable to a short-crested wave system as described by Tsai (1995). It is perceived that a soil skeleton will be liquefied when its mean effective normal stress becomes zero. Thus, the criterion of soil liquefaction based on 3-D elastic analysis can be expressed as,

$$\sigma_m' = \frac{1}{3}\gamma' z\left(1+2K_0\right)+\frac{1}{3}\left(\sigma_x' + \sigma_y' + \sigma_z'\right)=0 \qquad (8.1)$$

where K_0 is the coefficient of lateral earth pressure at rest and $\left(\sigma_x^{'} + \sigma_y^{'} + \sigma_z^{'}\right)$ is the sum of normal effective stresses induced by wave on the sea floor. Elastic equilibrium requires,

$$K_0 = \frac{\upsilon}{1-\upsilon} \tag{8.2}$$

where υ is the Poisson's ratio. If we write $\sigma_y^{'} = \upsilon\left(\sigma_x^{'} + \sigma_z^{'}\right)$ for plane strain, the relation (5.4) is written as,

$$\sigma_m^{'} = \frac{1}{3}\left[\gamma' z\left(1+2K_0\right) + \left(1+\upsilon\right)\left(\sigma_x^{'} + \sigma_z^{'}\right)\right] = 0 \tag{8.3}$$

In this study, the comparison of the instability of seabed is made with the available results in the literature for a seabed layer based on the effective mean stress criterion described in (8.3) to predict the region of instantaneous liquefaction. Then the actual seabed instability around and underneath the caisson is evaluated based on the total (i.e. including the in-situ effective mean stress of soil) effective mean stresses in the seabed due to wave-action are calculated. This criterion simply states that when the effective mean normal stress in the seabed under wave load becomes zero, the soil liquefies. Most of the time seabed will have some air in its voids due to deposition characteristics as well as grain size distribution but there are some studies that suggest that some air/gas may also be produced by marine micro-organisms in the seabed such as bacteria (Sumer and Fredsøe, 2002). It should be noted here that instantaneous liquefaction occurs even if there is not permanent deformations in the soil. That is, pore water pressure oscillates in time (either harmonically or in the case of irregular waves following closely the induced wave pattern) without any accumulation essentially carried by pore water. However, in order for instantaneous liquefaction to exist, there must be some air present in the voids of the porous seabed such that any upward gradient of induced wave motion will not be balanced by gradual rise of corresponding pore pressure but it will basically overcome the effective stress of the soil. Therefore degree of saturation, $S<1$ must hold. When that happens, the soil cannot resist the tension induced by wave trough and the soil liquefies. In this chapter, the potential of instantaneous liquefaction is investigated through FE analyses for the CTQ – seabed system.

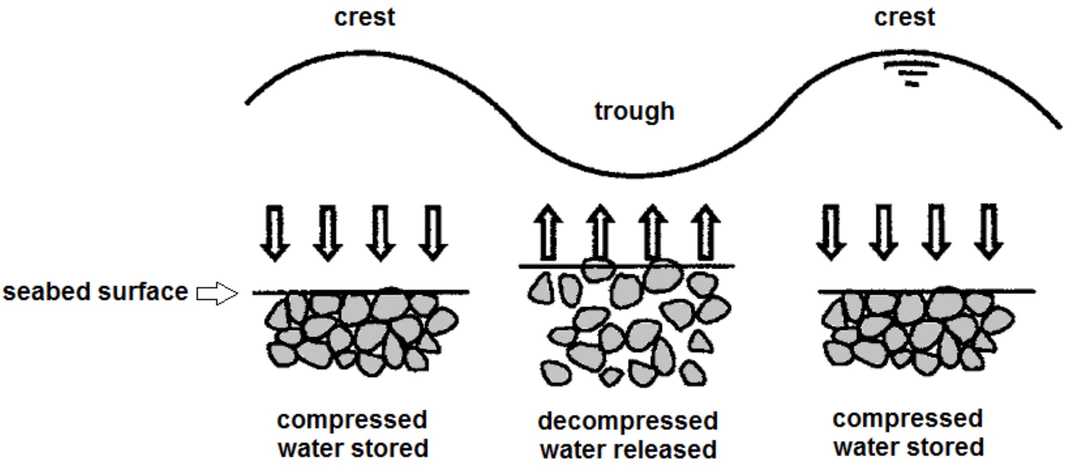

Figure 8.2: Instantaneous liquefaction caused by waves (after de Groot et al., 2006)

8.2 Numerical Analysis of Liquefaction

Numerical results are obtained by using the FEM the basics of which are outlined in Chapter 4. Plane-strain analyses are performed and the linear elastic behavior for the deformation of the soil skeleton and the quay wall is assumed. The FE model of the CTQ-seabed-rubble system is same as the one used previously for the standing wave action. The QS and PD formulations require the horizontal and vertical displacements, u_x and u_z and the pressure, p specified as DOFs at the nodal points. However, now the numerical aspects of the FE analyses in terms of the duration and time history of loads as well as output parameters are different. In the case of wave-induced hydrodynamic pressures caused by standing wave loads, the seabed and rubble boundary is under hydrostatic wave load followed by standing pressures (Figure 8.3). The standing wave amplitude, q_0 and wave pressure, p are calculated as:

$$q_0 = \frac{\gamma_w g H}{2\cosh(k.d)} \tag{8.1}$$

$$p = \gamma_w d + q_0 \cosh(kz)\cos(kx)\cos(wt) \tag{8.2}$$

in which γ_w is the unit weight of water, g is the gravitational acceleration, H is the wave height of the standing wave, d is the water depth and k is the wave number ($k = 2\pi / L$, in which L is the wavelength).

In evaluating the instantaneous liquefaction, first, a layer of seabed soil is constructed and the DOF values along the lateral boundaries are computed in separate free field FE analyses. These DOF results are then applied to the actual CTQ-seabed model as single point constraint time histories. Once all the boundary conditions are evaluated, then actual standing wave pressures are calculated and converted into consistent nodal loads and are applied at nodes.

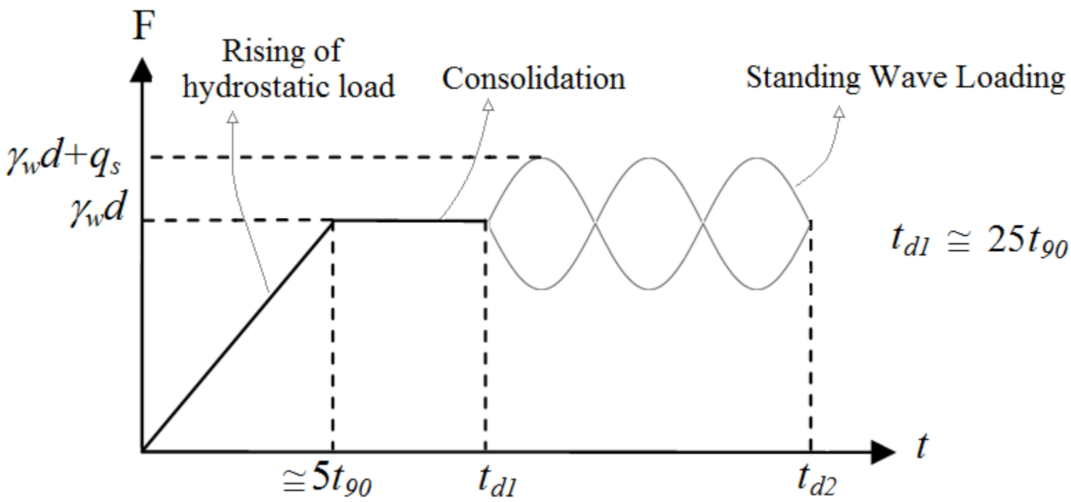

Figure 8.3: Time history for loads in wave-induced response; hydrostatic load followed by standing wave applied on the seaward boundary.

Following this, the seabed is consolidated under hydrostatic water pressure applied on seabed top surface and caisson wall with a time history similar to the one presented in Figure 8.4. Here, t_{90} is the amount of time needed for the completion of 90% consolidation and is calculated as,

$$t_{90} = T_v \frac{H_d^2}{c_v} \tag{8.3}$$

where c_v is the consolidation coefficient, H_d is the drainage distance of the layer and the time factor, T_v, is 0.848 corresponding to 90% consolidation. The consolidation coefficient, c_v is calculated from,

$$c_v = \frac{k_z}{m_v \gamma_w} \tag{8.4}$$

where k_z is the vertical permeability, γ_w is the unit weight of water and m_v is the volumetric compressibility coefficient and is found from,

$$m_v = \frac{1-2\nu}{2G(1-\nu)} \tag{8.5}$$

where G is the shear modulus. The pore pressure values in the soil layer are dissipated imitating the condition actualising in the field by taking rise time of about 4-5 times the t_{90}. Hydrodynamic wave loads caused by standing waves for the cyclic response of seabed are applied to the seaward boundary after the completion of consolidation under hydrostatic pressure. The dynamic response of the system is attained until arriving steady state (Ulker, 2009).

8.3 Parametric Study Results

In this section, the results of a parametric study investigating the effect of some key wave and seabed parameters to the standing wave-induced liquefaction potential are presented. The results are presented in terms of the contour plots of effective mean normal stresses (S_m, σ_m') inside the domain. This way it is possible to identify the regions where it becomes zero, hence the instantaneous liquefaction. The analyses were carried out by using QS formulation where all the inertial terms are neglected and by PD formulation where only the inertial terms associated with the relative pore fluid displacement are excluded to examine the effect of the inertial terms on the instantaneous liquefaction. In addition, $S \cong 0.999$ is chosen for K_f=2GPa to identify the locations that may possibly liquefy even for a very small unsaturation.

8.3.1 Effect of seabed permeability

When the form of the system is evaluated by permeability changes, the first thing to notice is that the width of the instantaneous liquefaction area, including the seabed-landfill layers, locates at the back of the caisson type quay wall for $k=10^{-4}$ m/s (Figure 8.6). The upper half of the seabed layer and fill just above it reaches positive S_m values together. This indicates that there is instantaneous liquefaction in the region. We see that instantaneous liquefaction values do not show a direct or inverse proportion with seabed permeability, because the widest liquefactive zones are obtained for k=10E-4 m/s. However, since the rocking effect is somewhat greater for the k=10E-6 m/s study, the maximum S_m value is obtained in the rubble mound layer of the front toe region of the CTQ (Figure 8.8). Accordingly, an increase in the liquefied area is observed due to accumulation of tensile stresses during the wave motion behind the caisson in the upper part of the the fill. Results obtained according to all three different permeability values indicate that the inertial terms have negligible effect for reaching instantaneous liquefaction potential at the bottom of the caisson, system-wide. This does not apply to the back top of the CTQ. The presence of dynamic effects has greatly expanded the area of instantaneous liquefaction in this zone (Figures 8.5-8.6-8.8).

8.3.2 Effect of seabed soil type

We see a concentration of instantaneous liquefaction zones at seabed layer below the rubble (Figure 8.7). This, however, is not a result observed in this region in other cases. The poor grading of the soil is a triggering factor for reaching the positive pressure values. The main result of the other graphs is also seen here; the upper corner of the seabed layer under the sea has undergone instantaneous liquefaction. In addition, we can see this result for all seabed surfaces. It is possible to say that the rocking effect is lower for GW, which has a smaller amount of void space because of its well gradation in comparison to GP or GM. At the back of the caisson, there is some considerable liquefaction in the alluvial clay layer (Figure 8.9).

8.3.3 Effect of standing wave period

There is no significant effect of the wave period change on the instantaneous liquefaction potential, except for a few small locations in the seabed under the rubble and in the upper small area of the rubble mound (Figures 8.4, 8.8 and 8.10). However, some results indicate that for the period of T = 15 s, the PD solution result in the areas where negative pressure values are obtained in the back toe of the rubble mound in a decreasing manner and accordingly the instantaneous liquefaction behavior increases in the landfill layer. Some liquefaction response is also observed in the seabed layer behind the caisson (Figure 8.10).

8.4 Shear Stress Variations

In this study, the actual variations of shear stresses as developed along the cross sections of concerns are also computed. These are plotted in terms of their contours across the entire problem domain (i.e. CTQ-seabed-backfill). What we mean by "actual shear" here is that the shear stresses are calculated in this section while considering the body forces (i.e. weights) as well as the hydrostatic and more importantly hydrodynamic standing wave forces acting at the surface of the domain. Therefore, such calculations of the shear stresses are more realistic as opposed to the "excess" values where no body forces or hydrostatic forces are included. In the below, effects of seabed permeability, the soil type and the wave period on the variations of shear stresses are briefly presented. This way, it is possible to identify the locations of high shear concentrations that may possibly lead to shear failure around the CTQ in the soil.

8.4.1 Effect of seabed permeability

We note that there is some increase in shear stresses obtained in the seabed layer below the caisson corresponding to some decrease in permeability. Excessive water flow in the seabed somewhat reduces the soil shear resistance. The result we have obtained confirms this. It can be also said that the values obtained in PD solutions are slightly lower than QS. With the study of inertial terms, it can be thought that the passage of water may accelerate and consequently decrease the shear stresses (Figures 8.12, 8.13, 8.15).

8.4.2 Effect of seabed soil type

Most of the shear stresses are located at,

- the inclined part containing the clay;
- the front toe of the caisson wall;
- and in the seabed layer just below the intersection of CTQ and the rubble and just above the impermeable rock boundary.

It is complicated to measure the shear strength of the seabed in the field. Practically speaking, in coastal regions such a task is very tough to achieve. Therefore, the degree of water saturation, the initial stress state, loading parameters and drainage conditions must be carefully considered.

If we evaluate the shear stress distributions within the seabed layer around the caisson wall the results of the analyses with the GW soil show that the amount of coarse grains may be affecting the shear stress variations in the soil in comparison to the GM soil type with some silts present. However, this is a loose argument in this thesis as we did not literally model the seabed soil accounting for relative amounts of coarse and fine grain material but more we did in terms of permeability, rigidity and density. Although the stress magnitude is high, the shear resistance is also high in these regions because of the existence of well-graded soil (Özaydin, 2005). In the well graded gravel type seabed layer which allocates a large part of the bottom and back of the caisson wall, we see a tendency for the CTQ to lean forward with its rocking motion. Thus, in the rubble layer beneath the front toe of the wall, excess shear stress values and some decrease in magnitudes in the back toe are observed (Figures 8.14, 8.15, 8.16). The effect of inertial terms is negligible for shear stress distributions also.

8.4.3 Effect of standing wave period

In the analyses, we also consider the effect of wave period on the shear stress variations. Results indicate that the increase in the standing wave period do not cause much change in the distribution of shear stresses on the CTQ system for the QS solutions. However, although the effect is negligible, shear stress magnitudes increase in the seabed especially behind the caisson with increasing period for the PD solutions. While there is no difference for T=5 s and T=10 s, the results obtained for T=15 s make us think that more analyses need to be made by using higher standing wave periods to determine the actual behavior of the CTQ-seabed system in terms of inertial terms effects (Figures 8.11, 8.15, 8.17).

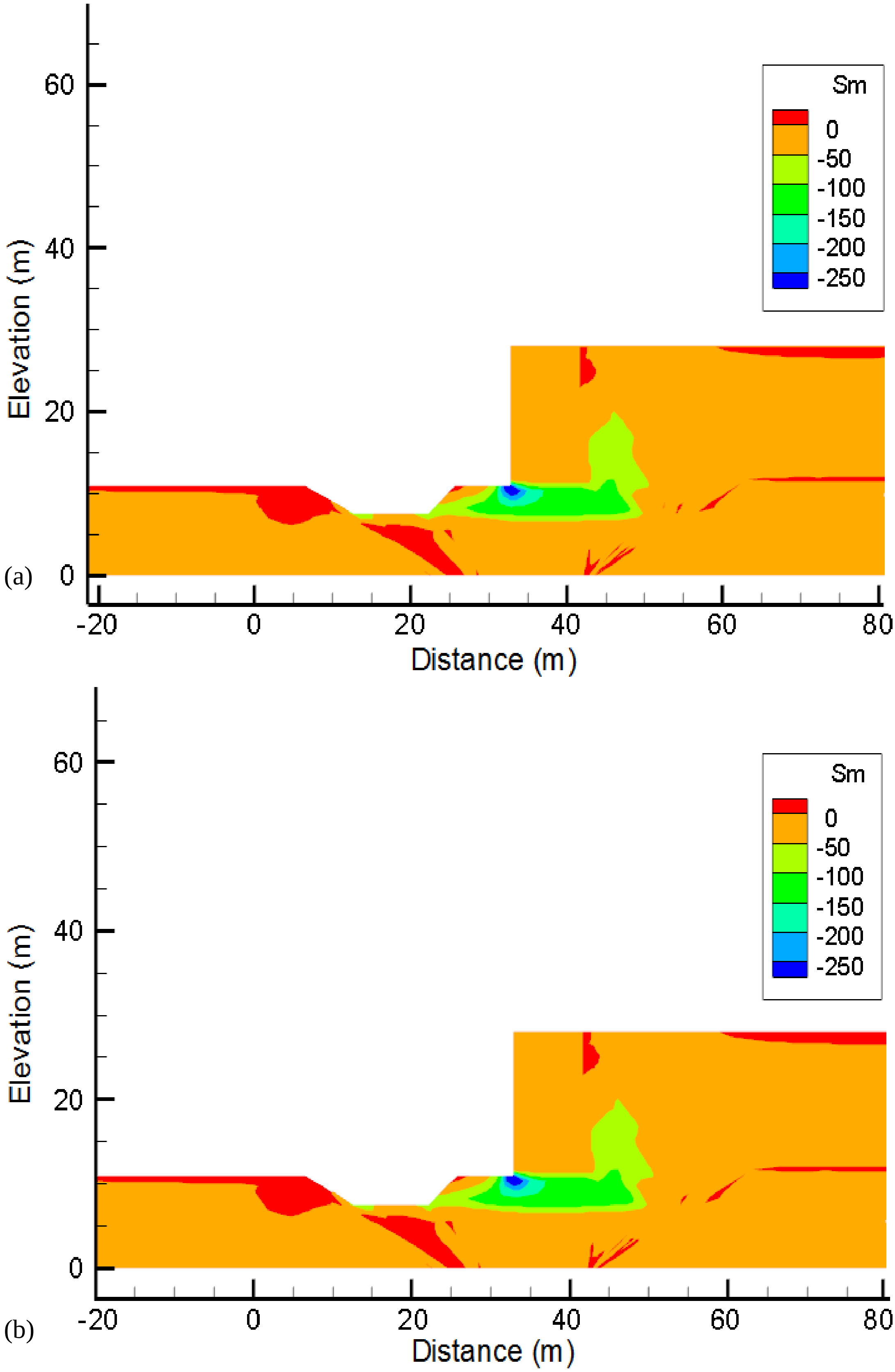

Figure 8.4 : (Sm, σ'_m) contours for SP, T=5 s, k_s=10E-6 m/s from

a) QS b) PD results, (units kPa)

(a)
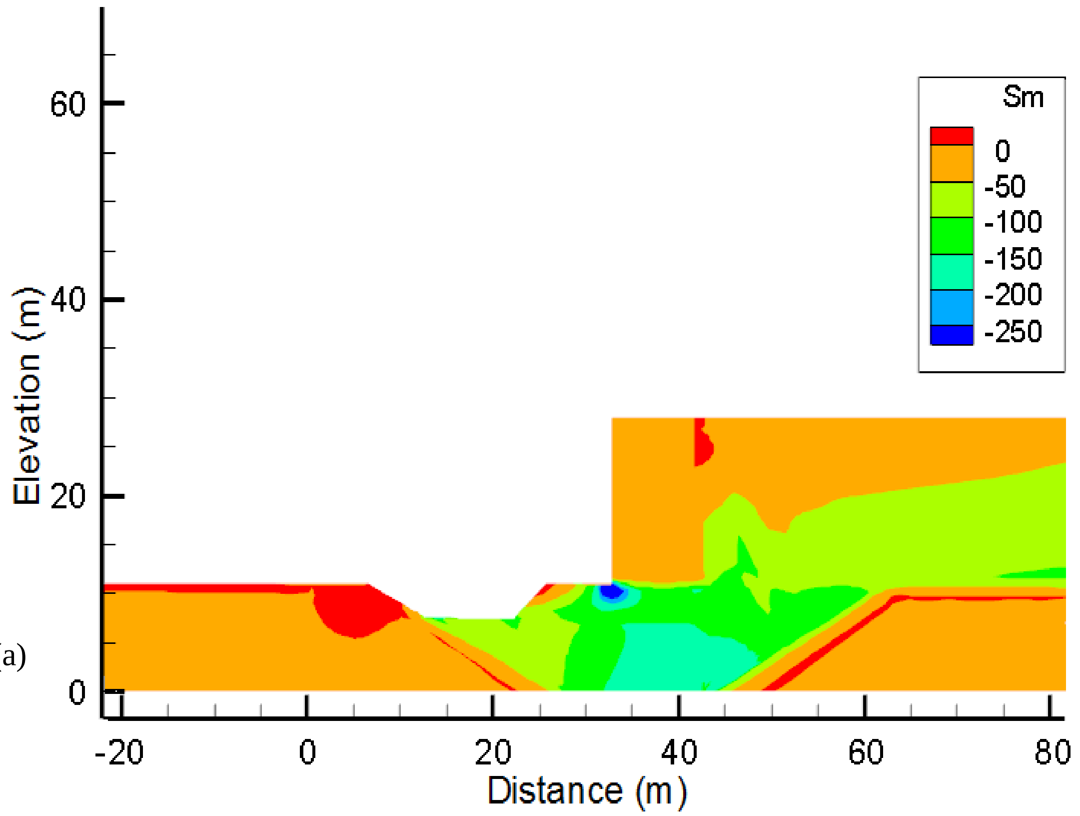

(b)
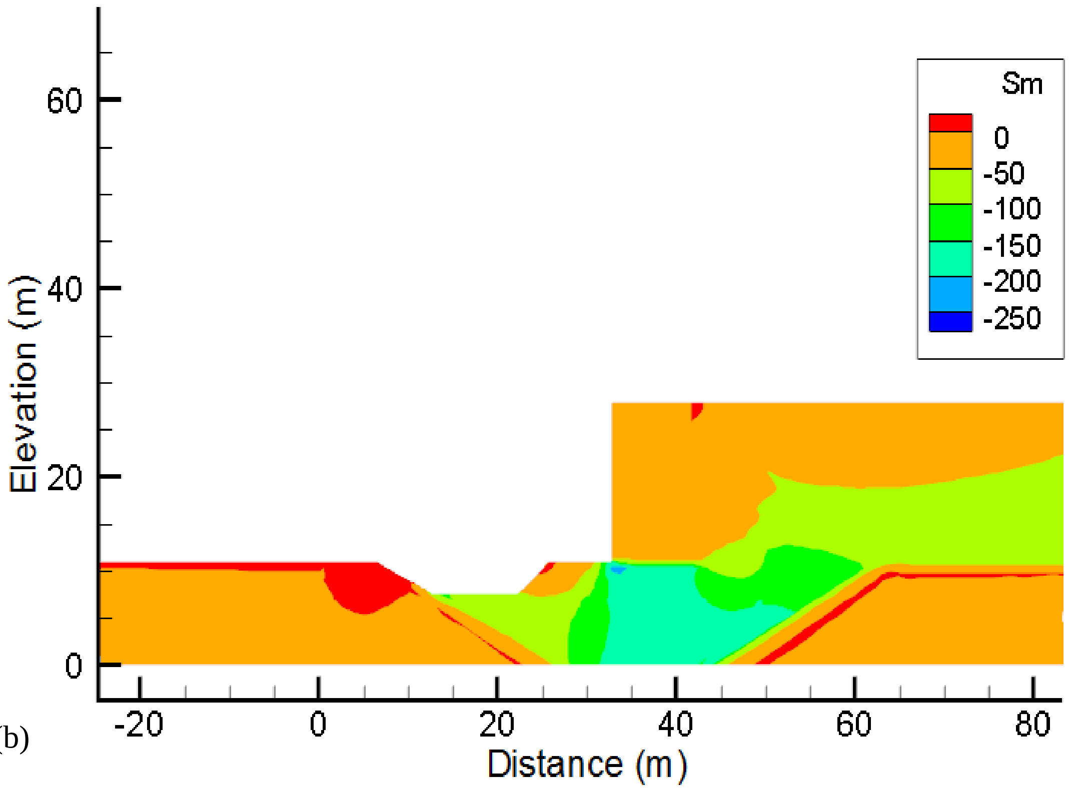

Figure 8.5 : (Sm, $\sigma_m^{'}$) contours for SP, T=10 s, k_s=10E-2 m/s from a) QS b) PD results, (units kPa)

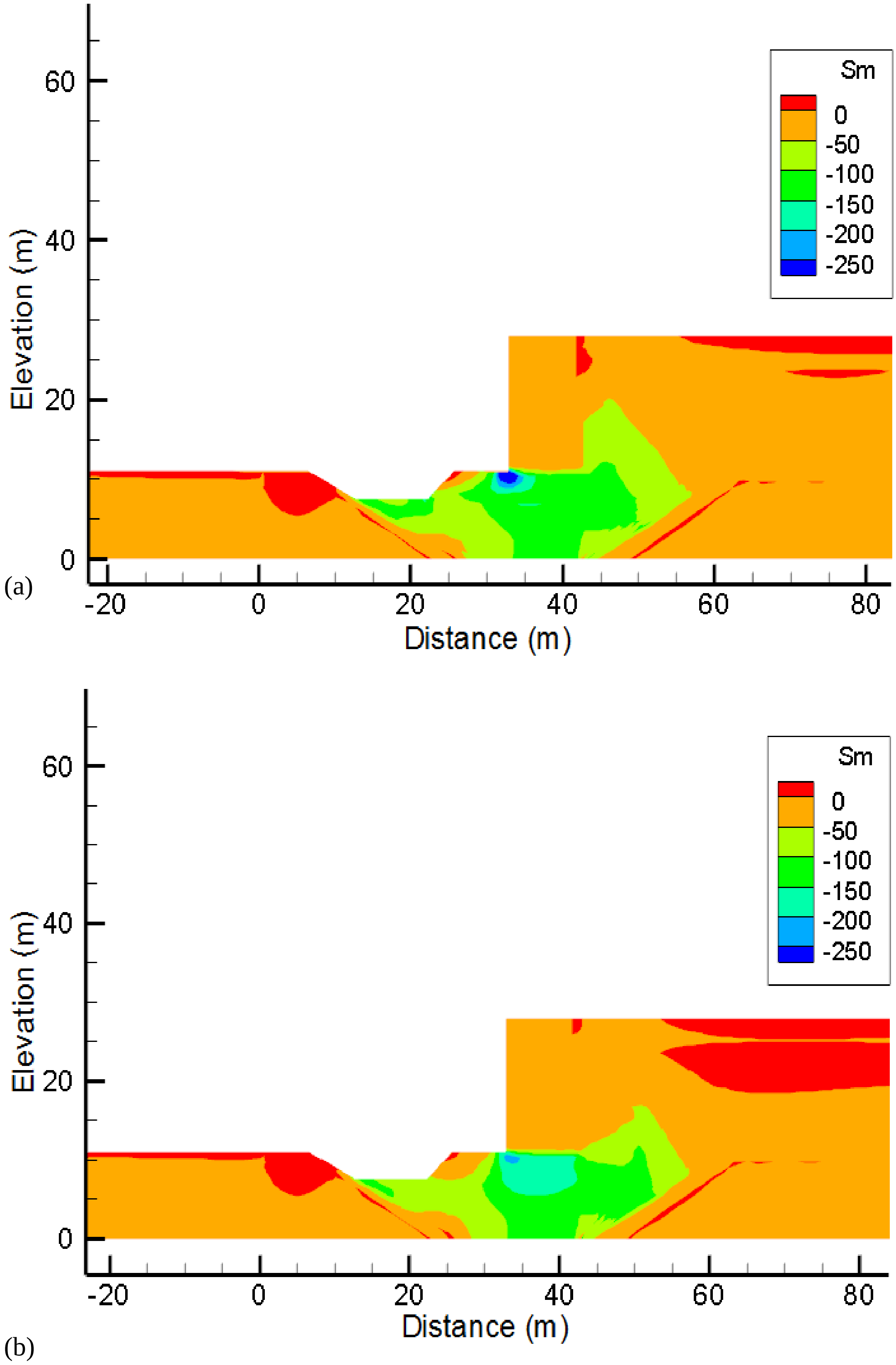

Figure 8.6 : (Sm, σ'_m) contours for SP, T=10 s, k_s=10E-4 m/s from

a) QS b) PD results, (units kPa)

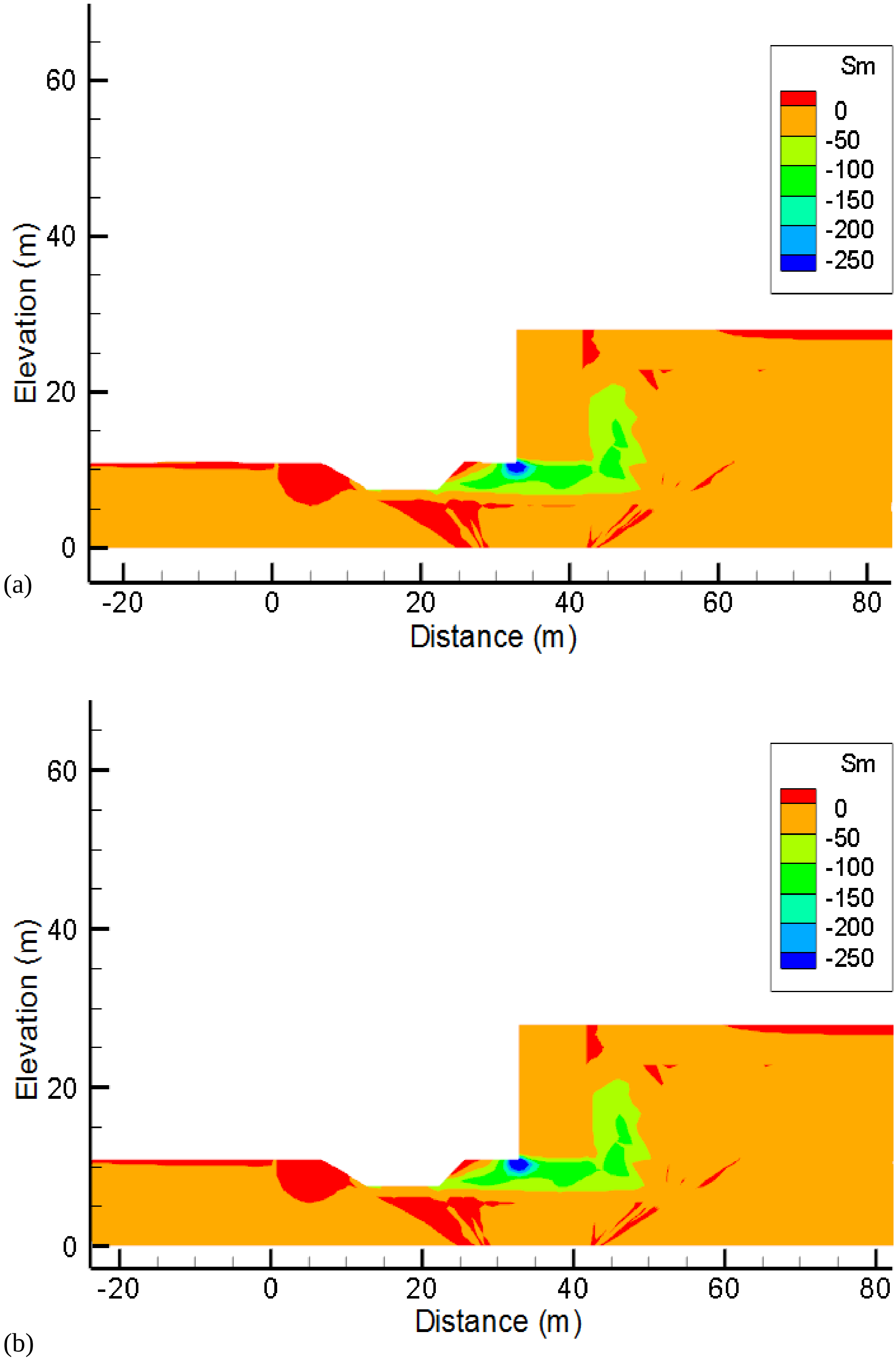

Figure 8.7 : (Sm, $\sigma_m^{'}$) contours for GM, T=10 s, k_s=10E-6 m/s from a) QS b) PD results, (units kPa)

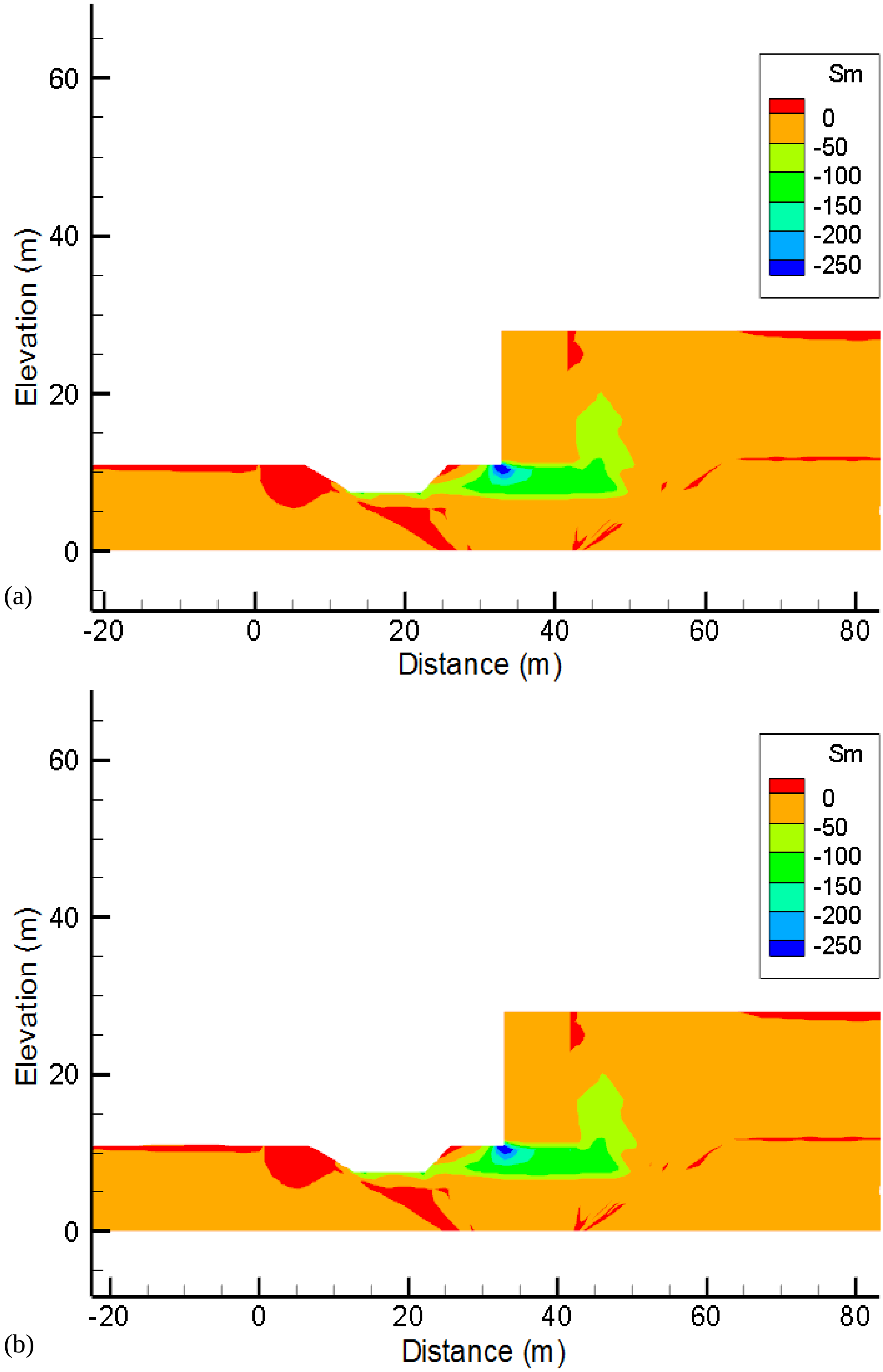

Figure 8.8 : (Sm, σ'_m) contours for SP, T=10 s, k_s=10E-6 m/s from a) QS b) PD results, (units kPa)

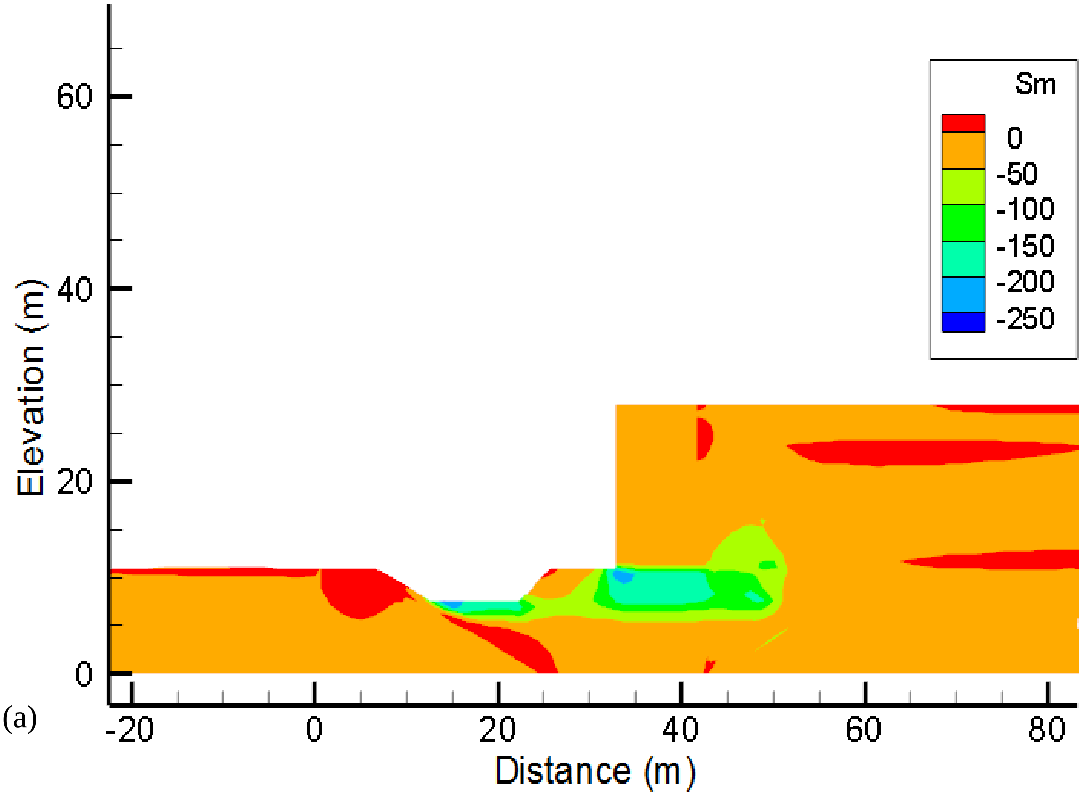

(a)

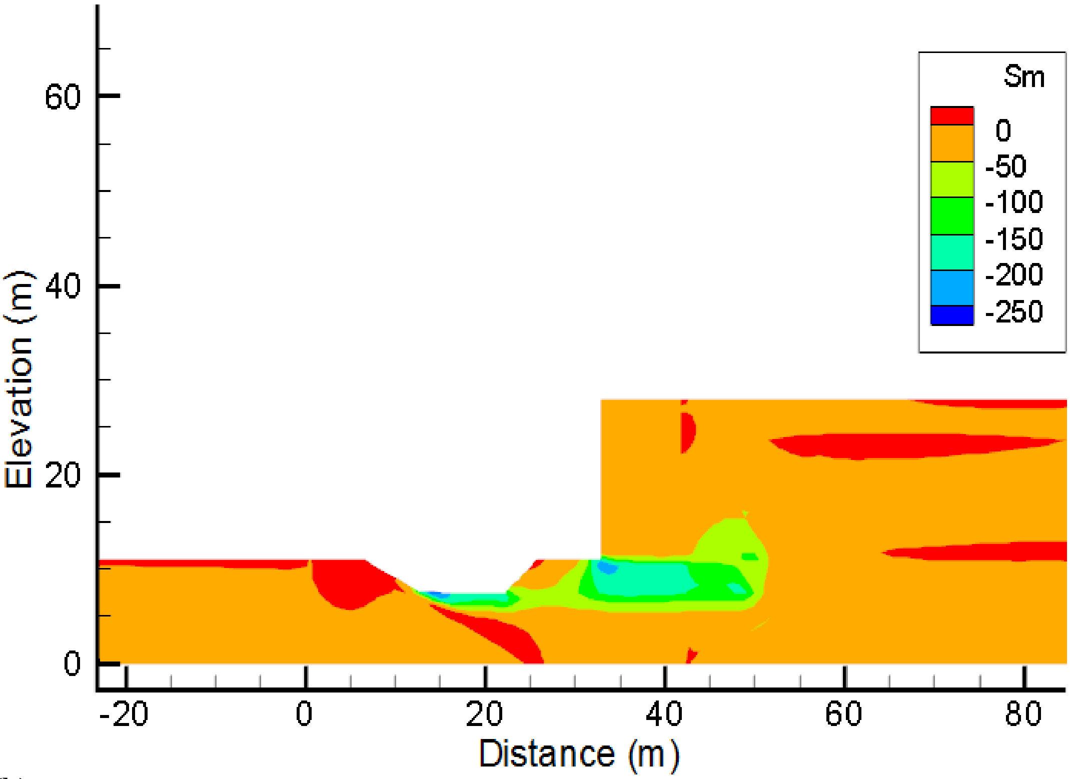

(b)

Figure 8.9 : (Sm, $\sigma_m^{'}$) contours for GW, T=10 s, k_s=10E-6 m/s from a) QS b) PD results, (units kPa)

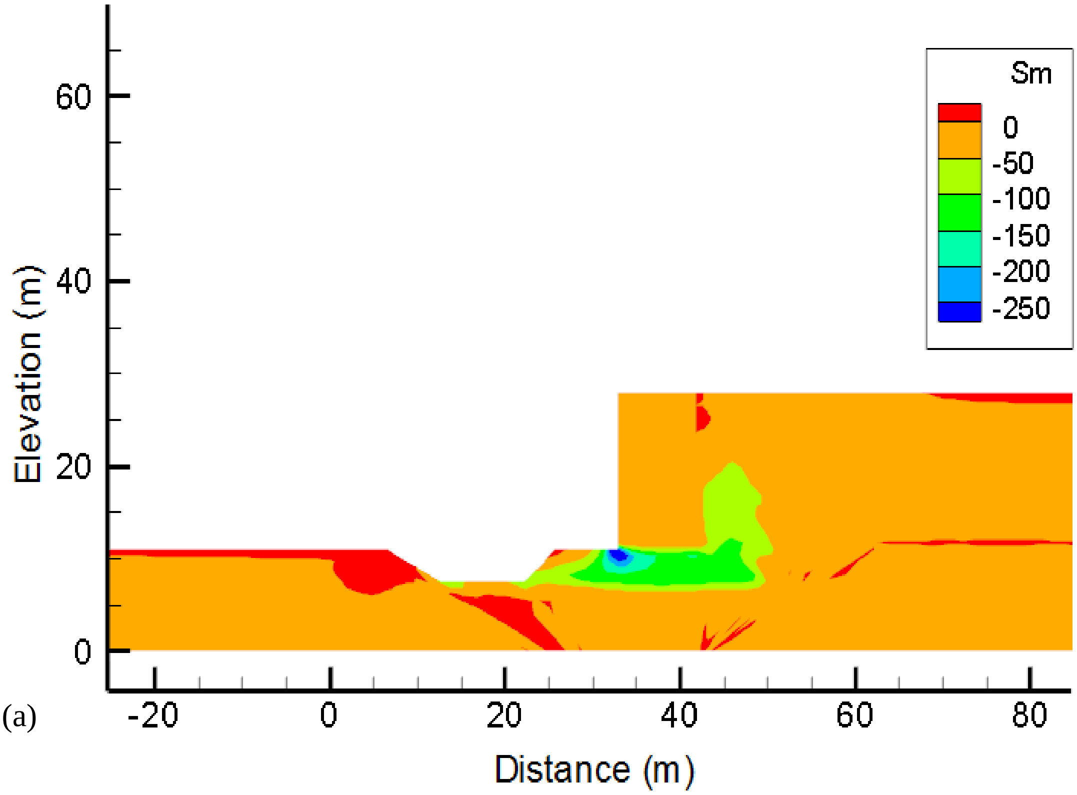

(a)

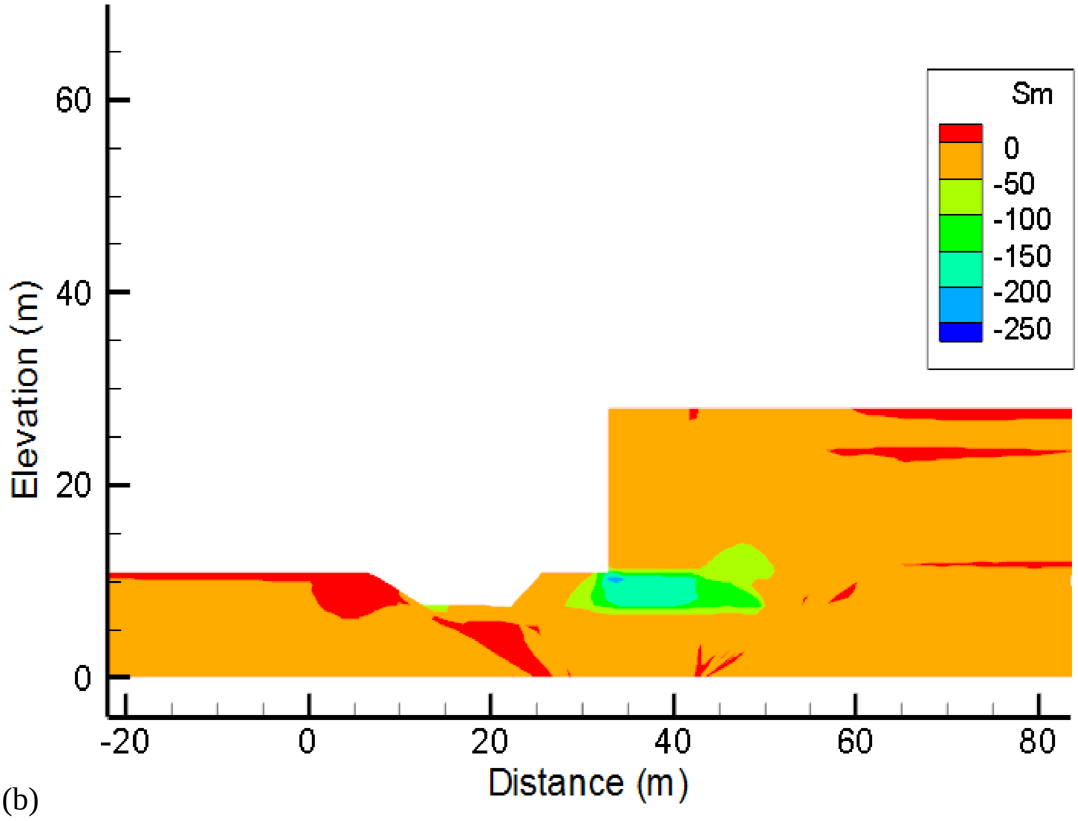

(b)

Figure 8.10 : (Sm, σ'_m) contours for SP, T=15 s, k_s=10E-6 m/s from a) QS b) PD results, (units kPa)

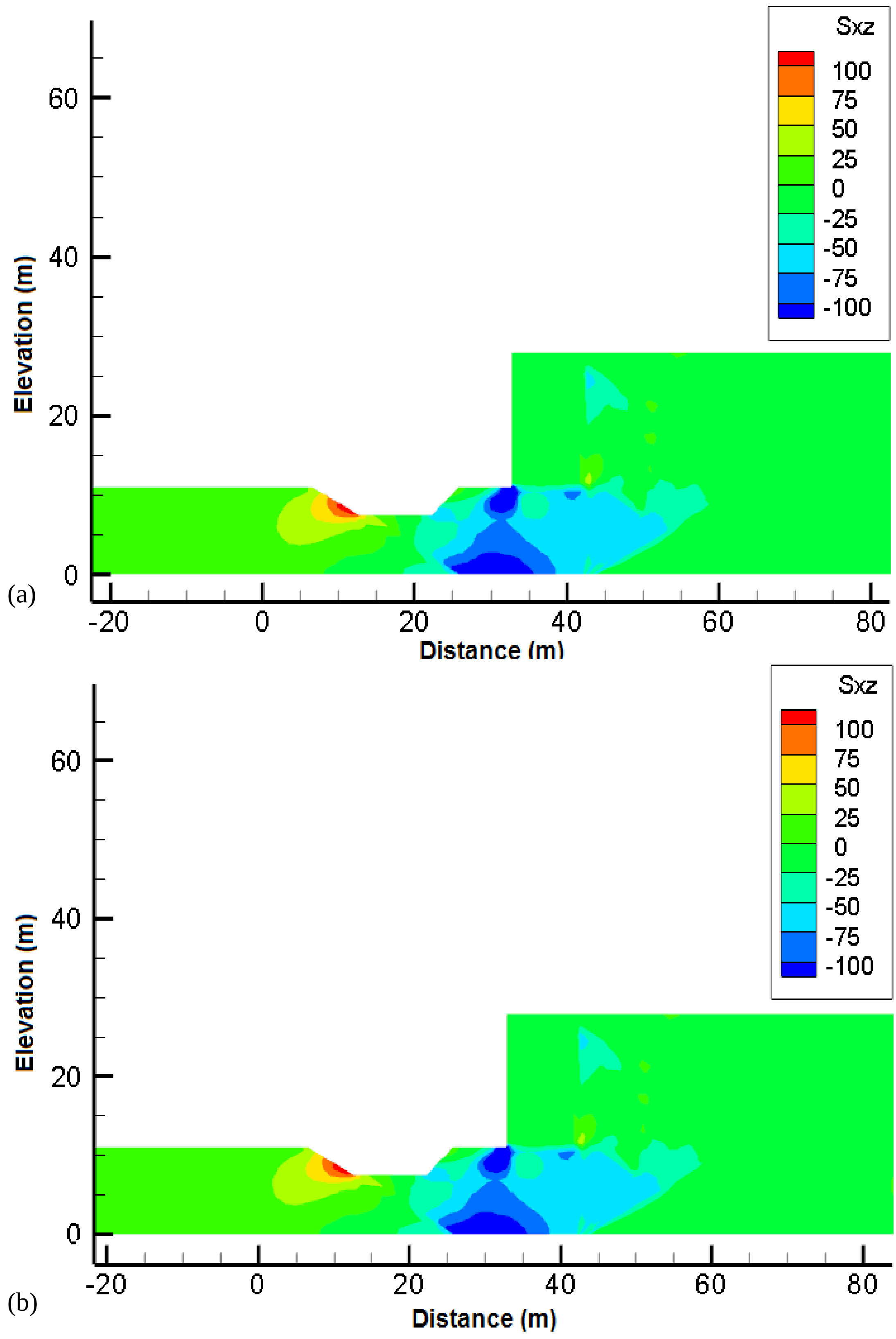

Figure 8.11: σ_{xz} contours for SP, T=5 s, k_s=10E-6 m/s from

a) QS b) PD results, (units kPa)

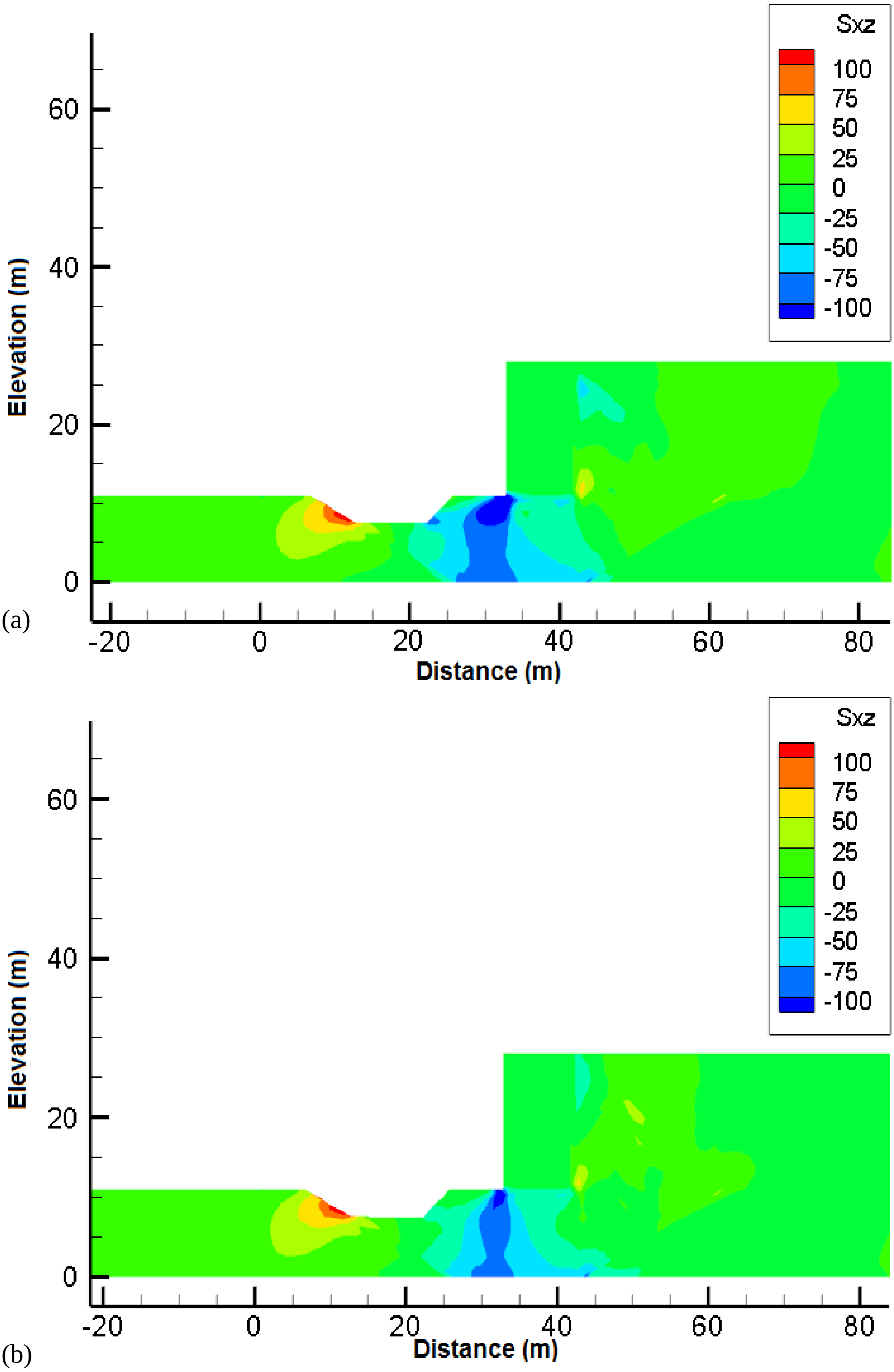

Figure 8.12: σ_{xz} contours for SP, T=10 s, k_s=10E-2 m/s from

a) QS b) PD results, (units kPa)

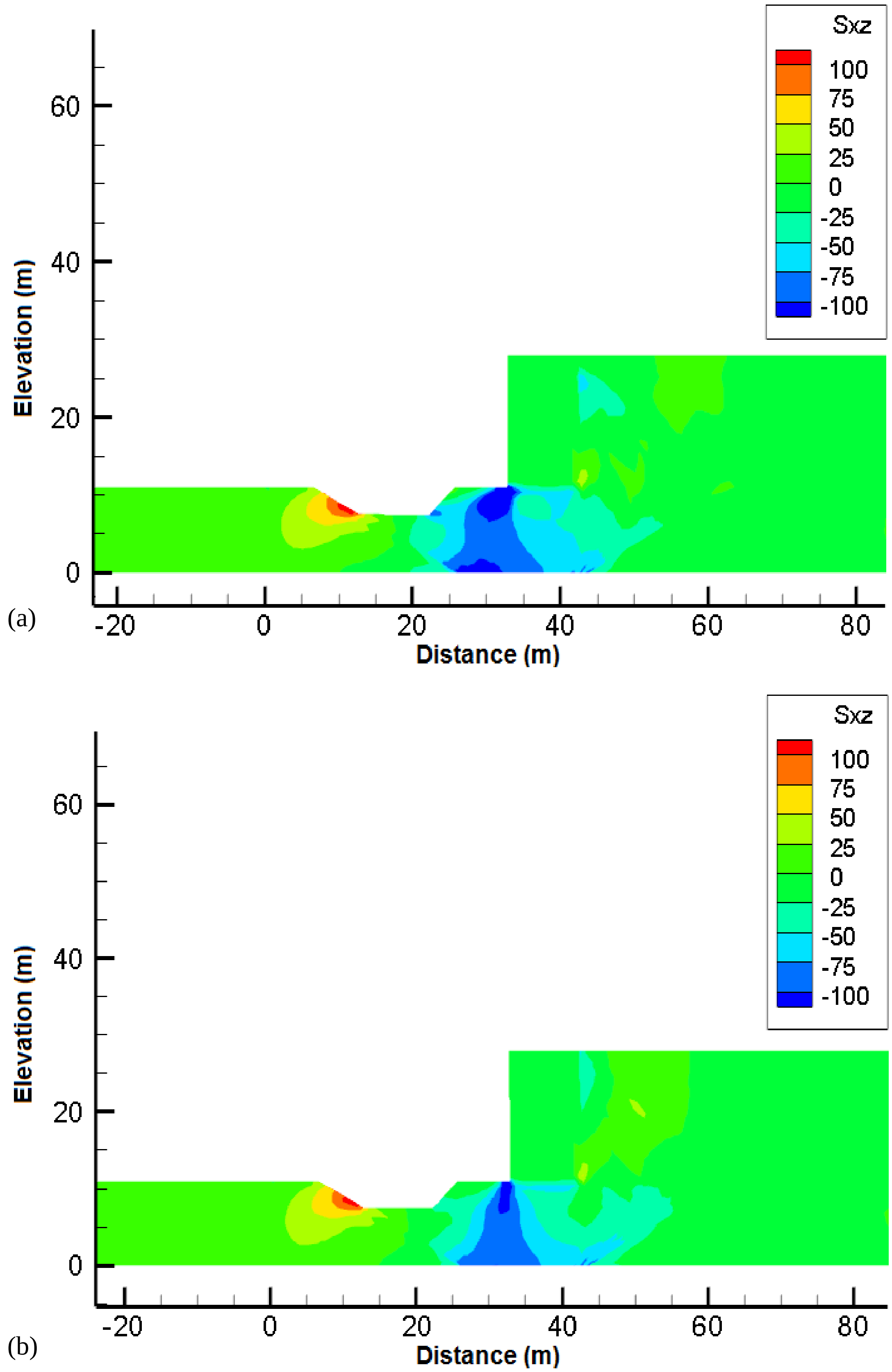

Figure 8.13: σ_{xz} contours for SP, T=10 s, k_s=10E-4 m/s from

a) QS b) PD results, (units kPa)

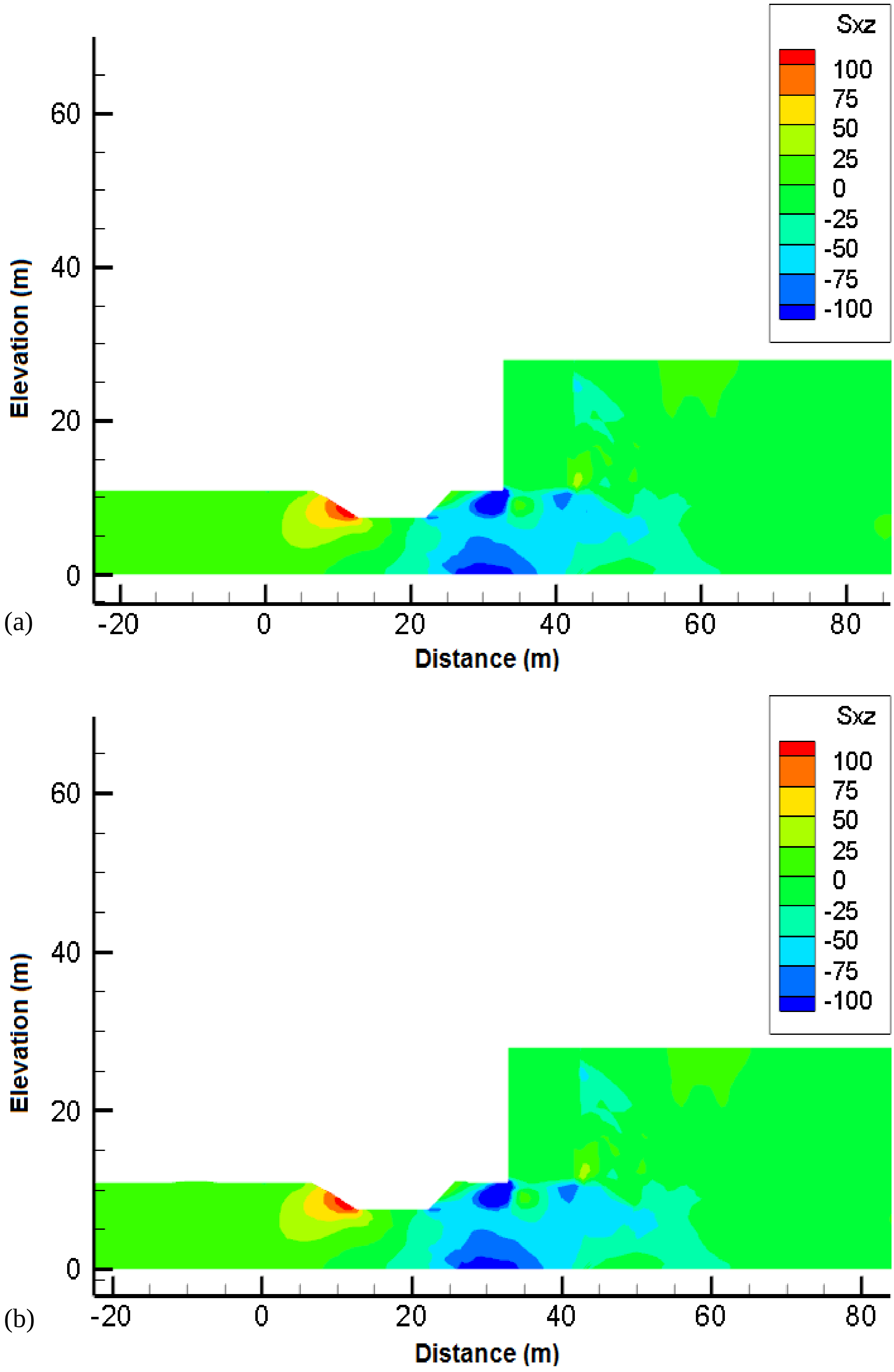

Figure 8.14: σ_{xz} contours for GM, T=10 s, k_s=10E-6 m/s from

a) QS b) PD results, (units kPa)

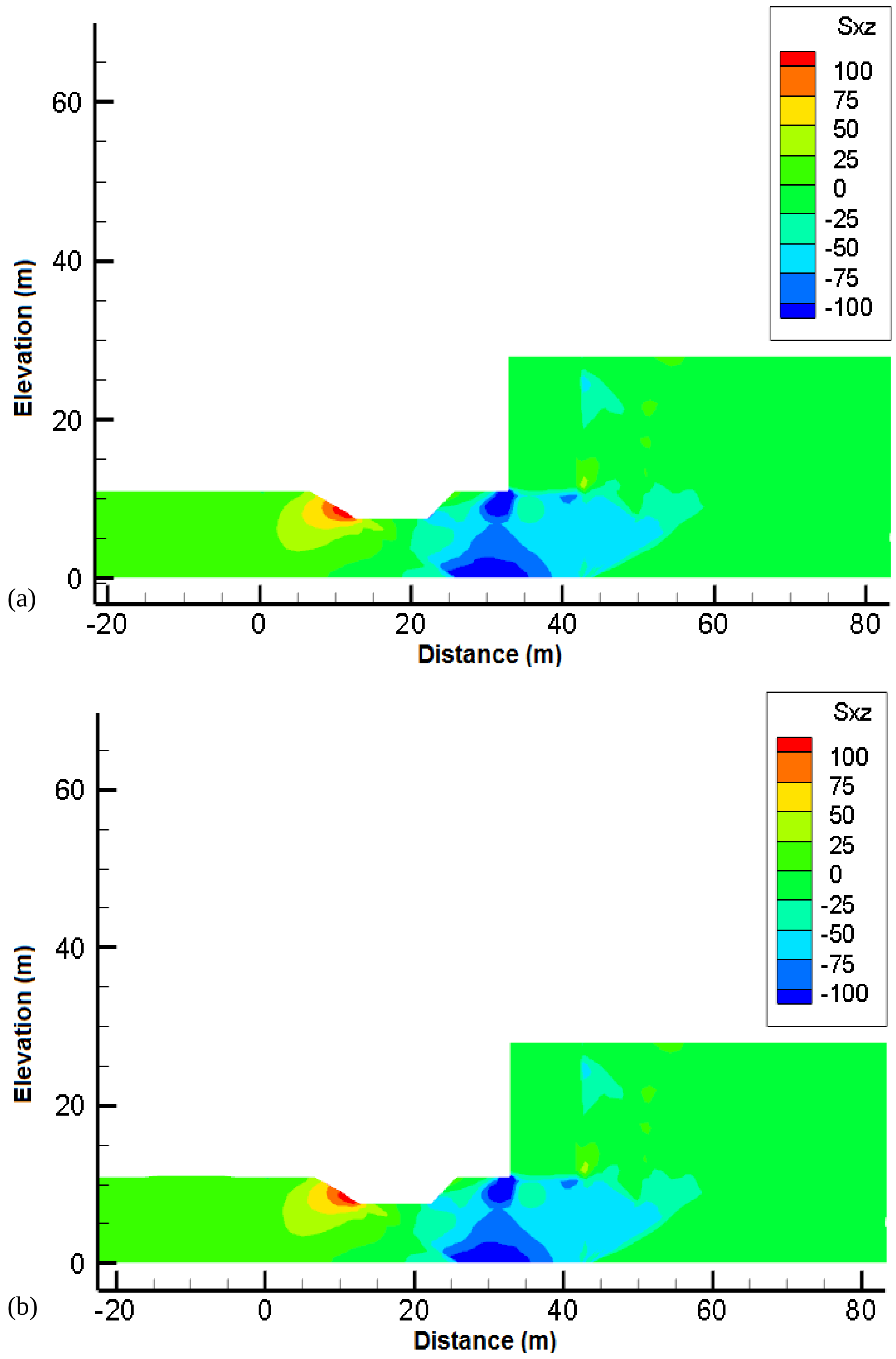

Figure 8.15: σ_{xz} contours for SP, T=10 s, k_s=10E-6 m/s from

a) QS b) PD results, (units kPa)

(a)

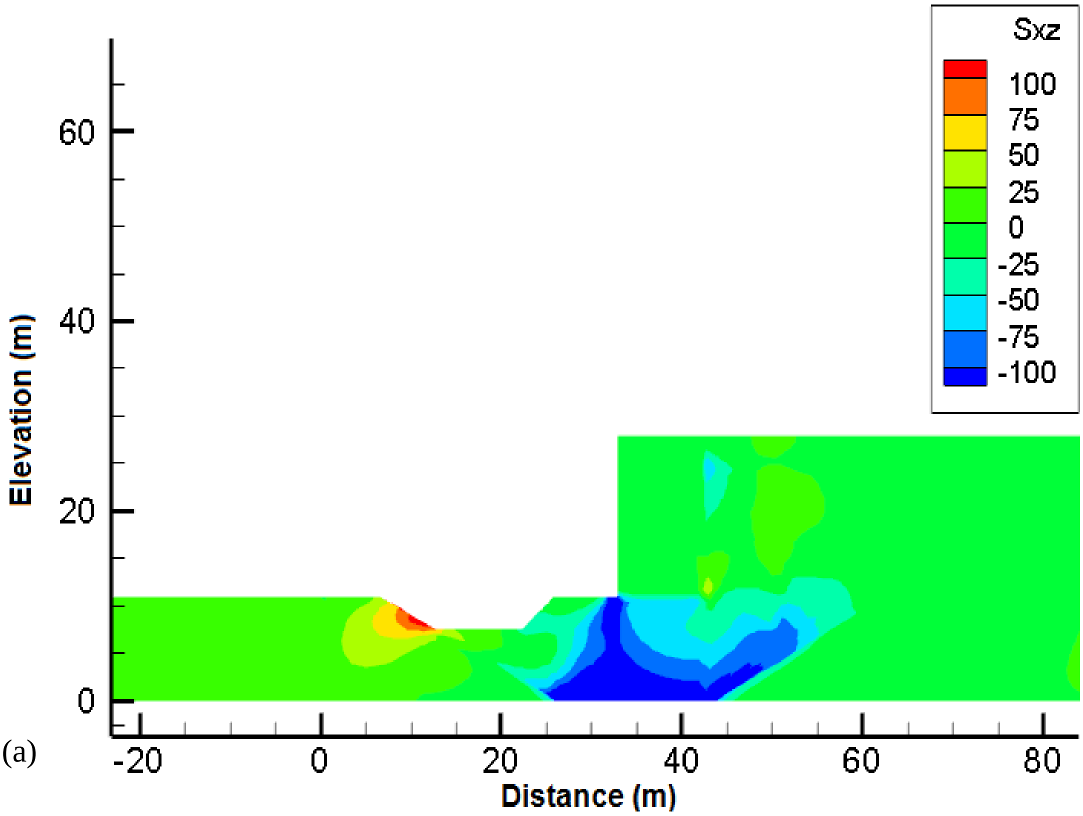

(b)

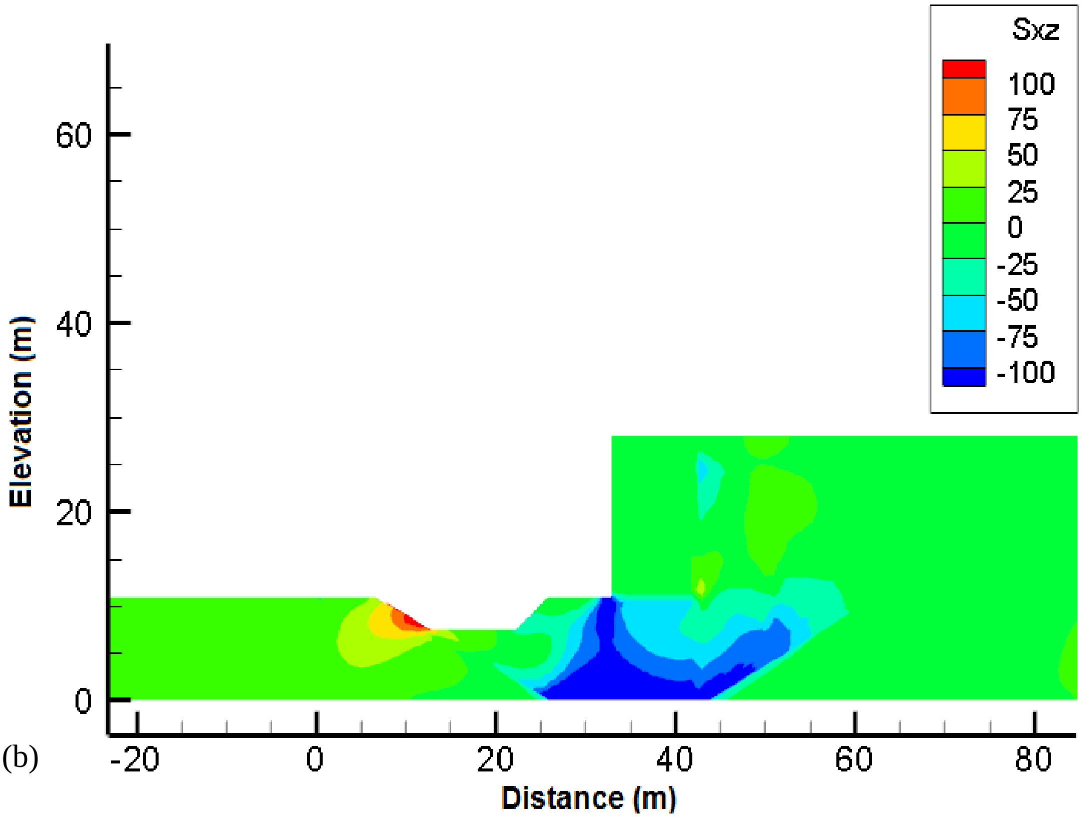

Figure 8.16: σ_{xz} contours for GW, T=10 s, k_s=10E-6 m/s from

a) QS b) PD results, (units kPa)

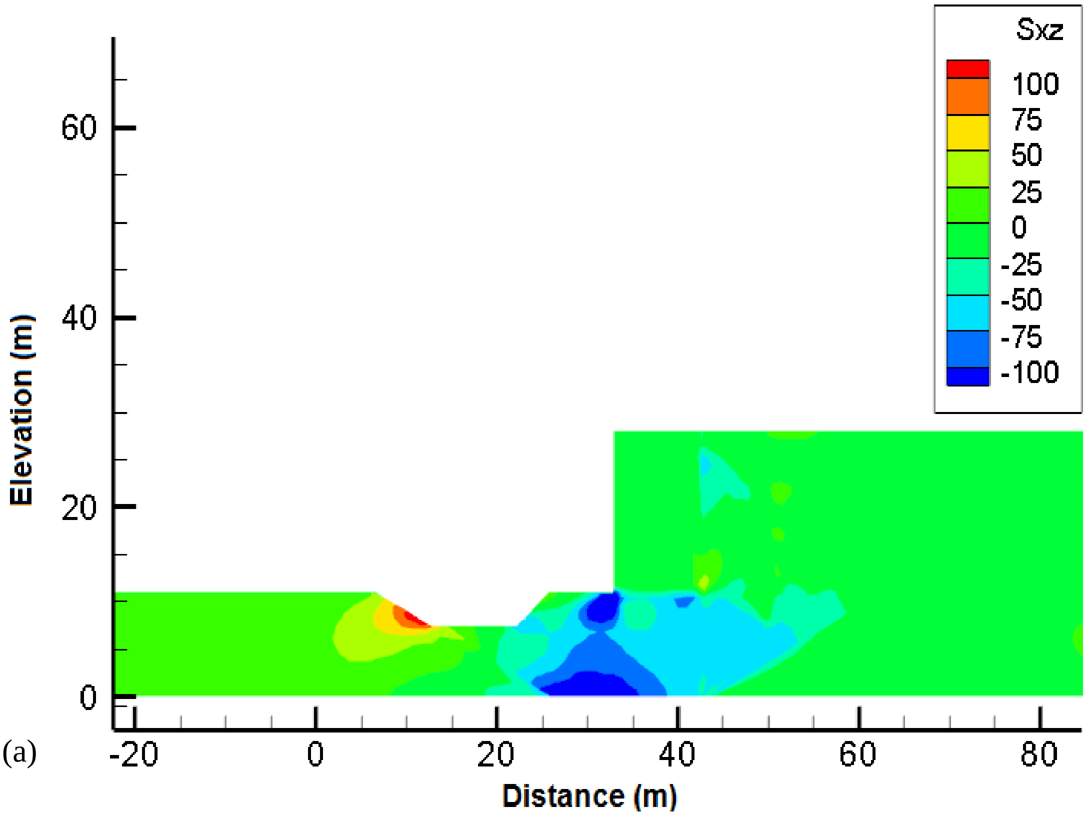

(a)

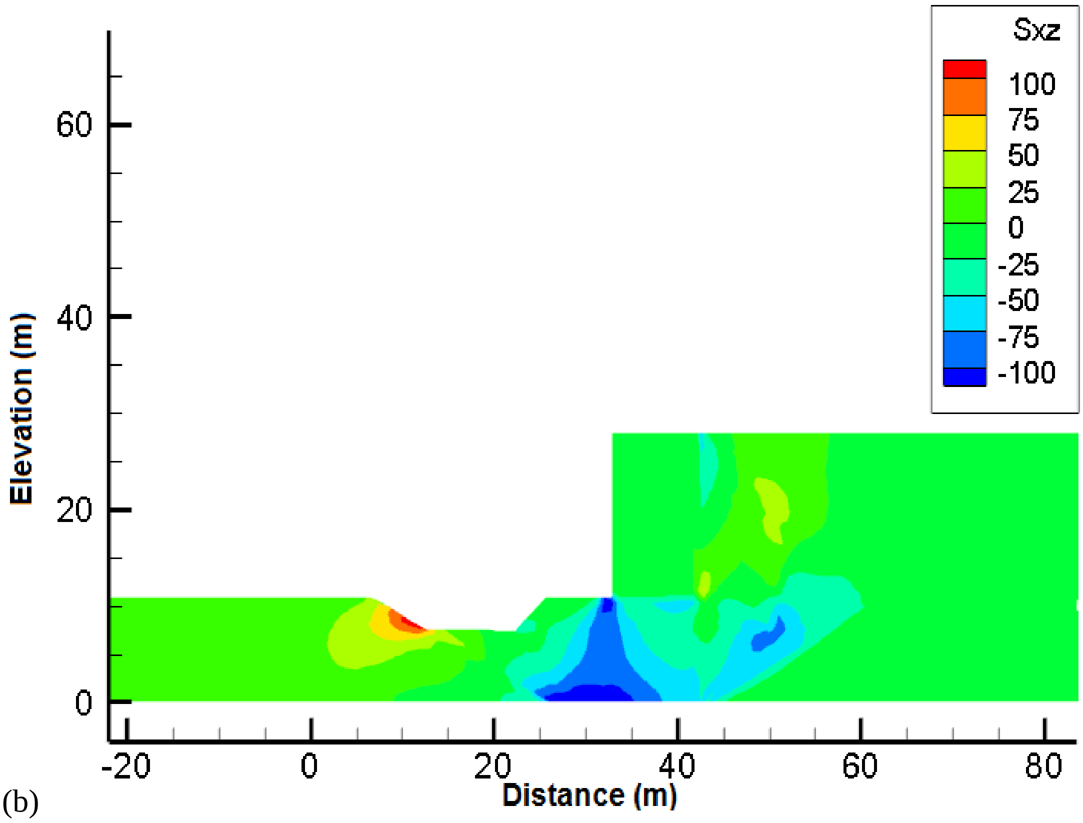

(b)

Figure 8.17: σ_{xz} contours for SP, T=15 s, k_s=10E-6 m/s from

a) QS b) PD results, (units kPa)

9. CONCLUSIONS

In this study, dynamic response and instability of a caisson type quay wall (CTQ)-seabed-backfill system is modeled against standing wave action. The CTQ studied actually exist in reality and the one that experienced some damage at the Kobe Port in Japan was selected as a case study. Although it is not a common practice to evaluate the dynamic response of quay walls under severe wave conditions as more often than not breakwaters are built to protect such structures and the communities behind, sometimes that is not the case as in the case of Ambarli port in Istanbul and hence, it makes conducting such analyses a requirement for researchers. That is why we have carried out a set of parametric studies for understanding the factors contributing to the actual dynamic response of an existing CTQ under standing waves. So we believe that this study has some merit in the state-of-the-art of coastal geotechnical engineering in that regards.

In our model, CTQ is assumed to behave linear elastically and the seabed soil, the backfilland the rubble are all modeled using the poroelastic formulation developed by Biot in terms of the theory of coupled flow and deformation. The mathematical formulation is first written in terms of the governing partial differential equations considering the physical laws behind. Then they are combined to give the final forms in terms of the degrees of freedom of the soil, in this case solid grain displacement and pore water pressure, by neglecting the inertial terms associated with the relative motion of pore water. This leads to the simplified formulations namely the partially dynamic (PD) and the quasi-static forms (QS). These two formulations were used throughout this thesis in the numerical analyses. Classical finite elements are used to discretize the governing equations and dynamic analyses are carried out in time domain until the system has reached steady state response. We, then, focus our attention on the vertical displacements, pore water pressure and shear stress variations in time and 2-D space in the CTQ-seabed-rubble system. Their variations in temporal and spatial domains are evaluated for changing seabed permeability and wave period. These are the key parameters chosen here to study the system behavior. Other important soil and wave parameters such as soil rigidity and the wavelength are of part of an ongoing study.

Based on the results of our study, we find that response parameters mostly increase in magnitude particularly in the rubble as the permeability of the seabed decreases. However, for varying values of wave period, the picture is not that clear and may sometimed yield unexpected behavior as T=10s wave yields as an outlier among others. For example, in some cases it gives the largest vertical displacements. While our work continues in comparing the response with that of the one around the natural period of the combined wall-seabed-rubble system, provided that we know the natural period, it seems that further analyses are required around close proximity of 10s wave. It should also be noted that as the quay wall does its rocking motion under incoming waves, it actually transfers its movement into the stiff rubble backfill behind it which results in significant stress concentrations not just at the toes of the caisson but at the interface between the rubble and the seabed as well. Also, sudden pore pressure dissipations in the seabed, seemingly an interesting result of this study, might be associated with this behavior as there is surely many locations in the seabed where more drained conditions than others exist along the cross sections of interest which are the vertical sections in front of and behind the caisson and a horizontal section underneath it along the interface between the caisson and the rubble.

Instability of the CTQ-seabed system is also studied. For that, standing wave-induced instantaneous liquefaction potential inside the soil around the CTQ is considered. Liquefaction is observed not only at the upper corners of the clay soil and the rubble, but also around the boundaries of the clay layer and the seabed and backfill soil of the CTQ. In general, the liquefaction results are intriguing for k=10E-4 m/s seabed permeabilityin areas close to the seabed surface andbehind the wall. It is also worth mentioning that inertial terms assocaited with the solid motion are not of a major effect on the liquefaction potential of the whole system. Last but not least, the next section summarizes the ongoing study.

10. FUTURE WORKS

Standing wave-induced CTQ-seabed system response is studied in details considering key wave and soil parameters determining the dynamic response of the system. Moreover, instability analyses are made to determine the liquefaction potential. Adding material nonlinearity to FE analyses, further research will be done to draw a complete picture of the actual observed liquefaction behavior of seabed as well as permanent deformations of the soil leading potentially to the failure of the CTQ. Here the liquefaction behavior of seabed is the liquefaction caused by progressive build-up of pore pressure due to cyclic shear stresses under wave loading. Another work to be investigated further is the use of the linear wave theory, to identify exactly what seabed parameter (wavelength of wave period) is causing the real effect on the response in the dynamic analyses. Since the period increment means increasing the wavelength value also and there is a need to do more research on how this affects DOF’s exactly. In addition, the response spectrum can be obtained by analyzing under the effects of variable standing wave period values in subsequent studies.

REFERENCES

Alyami, M., Wilkinson S.M., Rouainia, M. and Cai, F. (2007), "Simulation of Seismic Behaviour of Gravity Quay Wall Using a Generalized Plasticity Model", *Pros. of the 4th Int. Conf. on Earthquake Geotechnical Engineering*, Thessaloniki, Greece.

Biot, M.A. (1941). "General Theory of Three Dimensional Consolidation", *J Applied Physics*, 12, 155-164.

Biot, M.A. (1955). "Theory of Elasticity and Consolidation for a Porous Anisotropic Solid", *J Applied Physics*, 26, 182-185.

Biot, M.A. (1962). "Generalized Theory of Acoustic Propagation in Porous Dissipative Media", *J Acoustical Society of America*, 34(5), 1254-1264.

Cheng, A.H.D. (2016), "Poroelasticity", Vol. 27. Springer.

Cook, R.D., Malkus, D.S., Plesha, M.E. and Witt, R.J. (2001), "SConcepts and applications of finite element analysis", *Fourth Edition, John Wiley and Sons,* New York.

Dakoulas, P. and Gazetas, G. (2005), "Seismic effective-stress analysis of cassion quay walls: Application to Kobe", *Journal of Soils and Foundations,* 45, 133-147.

De Gijt, J. G., and Broeken, M. L. (2005), "Handbook of Quay Walls", *CRC Press*.

De Groot, M.B., Bolton, M.D., Foray, P., Meijers, P., Palmer, A.C., Sandven, R., Sawicki, A. and Teh, T.C. (2006), "Physics of Liquefaction Phenomena under marine structures", Journal of Waterway, Port, Coastal and Ocean Engineering, ASCE Vol.132, No.4, 227-243.

Dean, R. G., and Dalrymple, R. A. (1991). "Water wave mechanics for engineers and scientists", *World Scientific Publishing* Co Inc. Vol.2 p.58

Detournay, E. and Cheng, A. H. D. (1993), "Fundamentals of poroelasticity, comprehensive rock engineering: principles, practice and projects. Analysis and design method".

El-Sharnouby, B., El-Kamhawy, H., and Al-Yami, M. (2004), "Analysis of gravity quay walls", *Alexandria Engineering Journal*, *43*(5), 663-669.

George, N. (2007), “Quays Impacted by Strong Waves and Ways of Strengthening Old Quays Damaged by Waves or from Propeller Induced Scours”, *Doctoral Dissertation, Tei Piraeus – Kingston University,* Athens, Greece.

Guddati, M. N., Savadatti, S., Ulker, M.B.C., Thirunavukkarasu, S., (2009), “FIONA 3D: A General Purpose Object – Oriented Nonlinear Finite Element Program in C++”, *North Carolina State University,* Raleigh, NC, USA.

Gumucio, J. L. (2013), “Design of Quay Walls using the Finite Element Method”. *Master Thesis, Technische Universiteit Delft,* Rotterdam, Nederland.

Iai, S. (2011), “Seismic Performance of Port Structures: Assessment and Remediation”, 7th *National Conference on Earthquake Engineering,* Istanbul, Turkey.

Iai, S. (1998), “Seismic analysis and performance of retaining structures”, *Proceedings of the 1998. Conference on Geotechnical Earthquake Engineering and Soil Dynamics III,* Part 2 (of 2), ASCE, 1020-1044, 1998.

Inagaki, H., Iai, S., Sugano, T., Yamazaki, H. and Inatomi, T. (1996), “Performance of cassion type quay walls at Kope Port”, *Special issue of soils and foundations,* 119-136.

Karakus, H. (2007), “New seismic design approaches for block type quay walls”, *Master Thesis, Middle East Technical University,* Ankara, Turkey.

Khan-Mozahedy, A. B. M. (2015), “Subsidence phenomena of the coastal structures into offshore sandy seabed: a review”. *Int. J. Sci. Eng. Res.*, *6*(7), 1600-1611.

Kirca, V. S. O., Sumer, B. M. and Fredsøe, J. (2013), “Residual liquefaction of seabed under standing waves”. *Journal of Waterway, Port, Coastal, and Ocean Engineering, 139*(6), 489-501.

Kudella, M., Oumeraci, H., De Groot., M.B. and Meijers, P. (2006), “Large-Scale Experiments on Pore Pressure Generation Underneath a Caisson Breakwater”, *J Waterway, Port, Coast. Ocean Engineering*, ASCE 132(4), 310-324.

***Liquefaction and Ports: Kobe*.** (2017), *Retrieved April 22, 2017, from https://research.engineering.ucdavis.edu/gpa/earthquakehazards/liquefaction-ports* “Civil and Environmental Engineering”, University of California.

Liu, X. (2008), “Numerical models for scour and liquefaction around object under currents and waves”, *Doctoral Dissertation, University of Illinois,* Urbana-Champaign, USA.

Lundgren, H., Lindhardt Jacobsen, H.C., Romhild, C.J., (1989), "Stability of breakwaters on porous foundations". In: *Proceedings of the 12th International Conference on Soil Mechanics and Foundation Engineering*, pp. 451–454.

Maeno, S., and Nago, H. (1988), "Settlement of a concrete block into a sand bed under water pressure variation". *In Proceedings of the International Symposium on Modelling Soil-Water-Structure Interactions* (pp.67-76).

Mase, H., Sakai, T. and Sakamoto, M., (1994), "Wave-induced pore water pressures and effective stresses around breakwater". *Ocean Engineering* 21 (4), 361–379.

Okusa, S. (1985), "Wave induced stresses in unsaturated submarine sediments", *Geotechnique* 35 (4), 517–532.

Ozaydin, K. (2005). "Soil Mechanics",. *Birsen Publishing, İstanbul*. p 203 (in Turkish).

Port of Kobe. *(2010), Retrieved April 22, 2017, from http://www.city.kobe.lg.jp/life/access/harbor/english/shisetsu_e.html "City of Kobe",* United Nations Educational, Scientific and Cultural Organization, Kobe City, Japan.

Rendulic, L. (1936), "Relation between void ratio and effective principal stresses for a remoulded silty clay". In *Proc. of 1st International Conference on Soil Mechanics and Foundation Engineering* (Vol. 3, pp. 48-51).

Sakai, T., Gotoh, H., and Yamamoto, T. (1995), "Block subsidence under pressure and flow". In *Coastal Engineering 1994* (pp. 1541-1552).

Sassa, S. and Sekiguchi, H. (1999), "Wave-induced liquefaction of beds of sand in a centrifuge" *Geotechnique,* 49 (5), pp. 621–638

Seed H. B. and Idriss, I. M. (1971), "Simplified Procedure for Evaluating Soil Liquefaction Potential" Journal of the Soil Mechanics and Foundations Division, ASCE, Vol.97(9), pp. 1249-1273.

Sekiguchi, H., Kita, K. and Okamoto, O. (1995), "Response of Poro-Elastoplastic Beds to Standing Waves", *Soils and Foundations, Vol.35, No. 3, 31-42*. Japanese Technical Society.

Shiraishi, N., Palmer, R. Q. and Okamoto, H. (1976), "Quay Wall with Wave Absorber 'Igloo' ", *Proc. Of the 15th Coastal Engineering Conf.*, Honolulu, Hawaii, 2677-2696.

Silvester, R. and Hsu, J. R. C. (1989), "Sines revisited. Journal of Waterway, Port, Coast", *Ocean Engineering,* ASCE 115, 327–344.

Soltanpour, M., Samsami, F., and Sorourian, S. (2010). "Wave-flume experiments of dissipating waves on soft mud." Proc., *32nd Int. Conf. on Coastal Engineering*, Coastal Engineering Research Council of the COPRI (Coasts, Oceans, Ports, Rivers Institute) of the ASCE, Reston, VA.

Sugano, T., Morita, T., Mito, M., Sasaki, T. and Inagaki, H. (1996), "Case Studies of Caisson Type Quay Wall Damage by 1995 Hyogoken-Nanbu Earthquake", *11th World Conference on Earthquake Engineering,* Acapulco, Mexico.

Sumer, B. M., Fredsøe, S., Christensen, S. and Lind, M.T. (1999), "Sinking/Floatation of Pipelines and Other Objects in Liquefied Soil under Waves". *Coastal Engineering* 38, 53-90.

Sumer, B. M. and Fredsøe, J. (2002), "The Mechanics of Scour in the Marine Environment", *Advanced series on Ocean Engineering*, Vol.17, World Scientific Press, Singapore

Sumer, B. M. (2014), "Liquefaction around Marine Structures: (With CD-ROM)", *World Scientific*, Vol.39. New Jersey, Singapore, London, Hong Kong.

Suzuki, K., Takahashi, S. and Kang, Y. (1998), "Experimental Analysis of Wave – Induced Liquefaction in a Fine Sandbed". *Coastal Engineering* 3643-3654.

Tasiopoulou, P., Gerolymos, N. and Gazetas, G. (2014), "Seismic Effective Stress Analysis of Gravity Block Type Quay Walls: Application to Piraeus Port" *2nd European Conference on Earthquake Engineering and Seismology*, Istanbul, Turkey.

Terzaghi, K. (1923), "Die Berechnung der Durchlassigkeitsziffer des Tones aus dem Verlauf der hydrodynamische Spannungserscheinungen", *Sitzber. Akad. Wiss.* Wien, Abt. IIa, 132, 125-138 (in German).

Terzaghi, K. (1925), "Erdbaumechanik auf bodenphysikalischer Grundlage", *Deuticke*, Wien (in German).

Tsai, C. P. and Lee, T. L. (1995), "Standing Wave-Induced Pore Pressure in a Porous Seabed", *Ocean Engineering*, 22(6), 505-517.

Ulker, M. B. C. (2009), "Dynamic Response of Saturated Porous Media: Wave Induced Response and Instability of Seabed", *Doctoral Dissertation, North Carolina State University*, Raleigh, NC, USA.

Ulker, M. B. C. and Rahman, M. S. (2009), "Response of Saturated Porous Media: Different Formulations and Their Validity", *Int J Numer. Anal. Meth. Geomechanics.*, 33(5), 633-664.

Ulker, M. B. C., Rahman, M. S. and Guddati M. N. (2010), "Wave-Induced Dynamic Response and Instability of Seabed around Caisson Breakwater", Ocean Engineering, 37(17-18), 1522-1545.

Ulker, M. B. C. (2012), "Pore Pressure, stress distributions, and instantaneous liquefaction of two-layer soil under waves", *Journal of Waterway, Port, Coastal, and Ocean Engineering*, Vol. 138, No. 6, 435-450.

Ulker, M. B. C. Rahman, M. S. and Guddati, M. N. (2012), "Breaking wave-induced impact response of rubble mound and seabed around a caisson breakwater", *Int. J. Anal. Numer. Mthds in Geomech*. Vol. 36, No. 3, pp. 362-390.

Ulker, M. B. C. and Massah Fard, M. (2016), "Instantaneous Liquefaction of Seabed around Rubble Mound Breakwater under Waves" *Proc 26th International Society Offshore and Polar Engineering Conf,* Rhodes, Greece, ISOPE, 3, 1479-1486.

Verruijt, A. (2013), "Theory and Problems of Poroelasticity", Delft University of Technology.

Yeh, H. and Li, W. (2008), "Tsunami Scour and Sedimentation",*4th International Conference on Scour and Erosion,* Tokyo, Japan, ISCE.

Zen, K., Yamaguchi, H. and Watanabe, A. (1987), "Wave-Induced Liquefaction and Densification in Seabed", *Rept Port Harbour Res. Inst., Nagase, Yokohama, Japan* 26, 125-180 (in Japanese).

Zienkiewicz, O. C., Chan A. H. C., Pastor M., Schrefler B. A. and Shiomi T. (1999), "Computational Geomechanics with Special Reference to Earthquake Engineering", John Wiley and Sons, England.

Zienkiewicz, O. C., Chang, C. T., and Bettess, P. (1980). "Drained, undrained, consolidating and dynamic behavior assumptions in soils." *Geotechnique*, 30(4), 385-395, John Wiley and Sons, England.

APPENDICES

APPENDIX A: The liquefaction hazards at Kobe Port.

Figure A.1: Aerial photograph of collapsed crene.

Figure A.2: Aerial photograph of Port Island in Kobe.

Figure A.3: Ferry ramp collapse.

Figure A.4: Graben behind quay wall.

Figure A.5: Quay wall along channel.

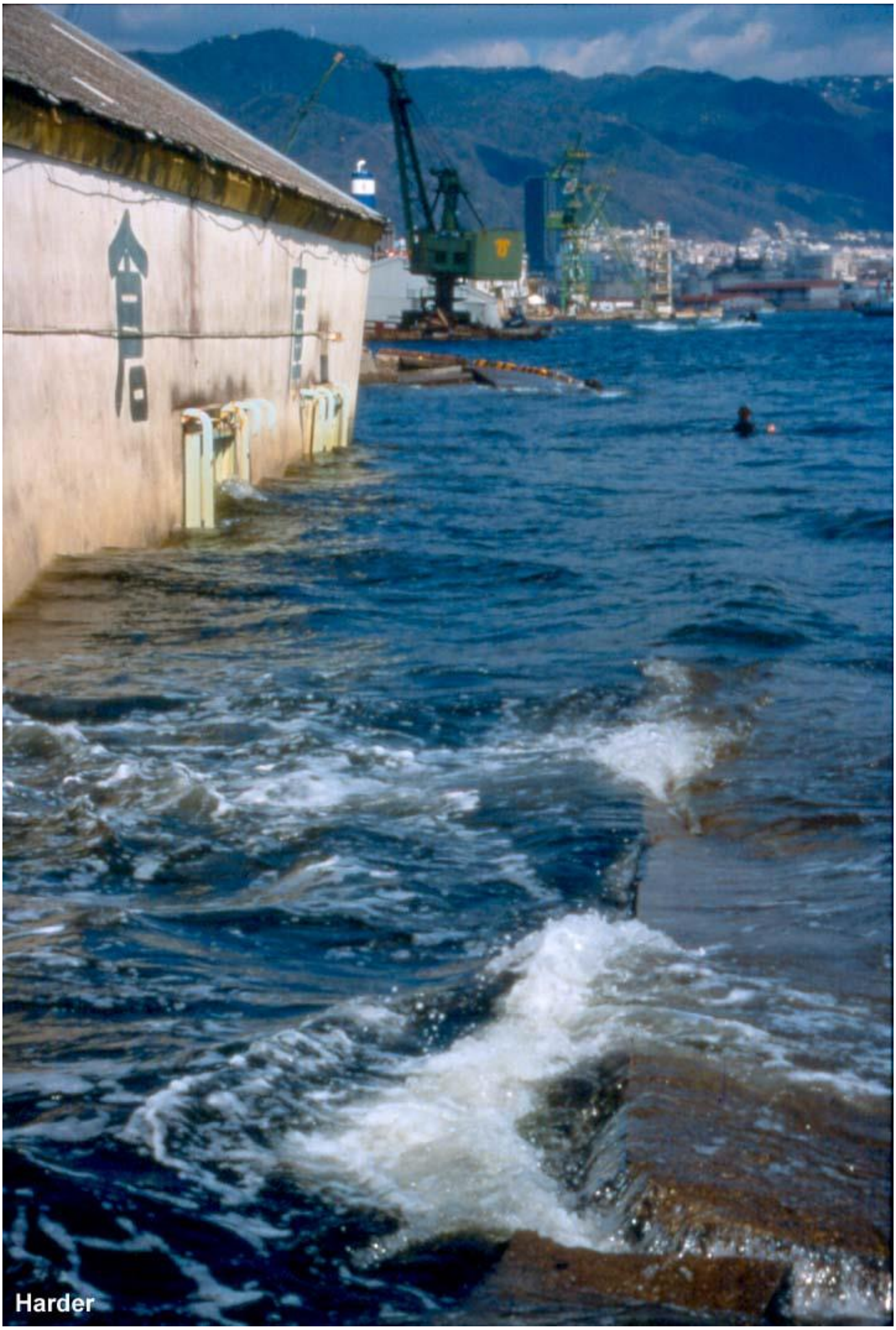

Figure A.6: Submerged pier.

APPENDIX B: Views and maps.

Figure B.1: Satellite View of Port Island, Kobe Port.

Figure B.2: Map of Port Island, Kobe Port.

Figure B.3: Aerial view of Ambarli Port, Istanbul.

CURRICULUM VITAE

Name Surname **: Hasan Giray BAKSI**

Place and Date of Birth **: ISTANBUL / 11.12.1982**

E-Mail **: hasangiraybaksi@hotmail.com**

EDUCATION :

- **2001:** Haydarpaşa Lisesi (High School)
- **2008:** Istanbul Technical University / Civil Engineering Program (Licence)

COMPUTER SKILLS :

- **SAP2000:** Integrated Structural Analysis and Design, CSI, USA.
- **ETABS:** Integrated Analysis, Design and Drafting of Building Systems, CSI, USA.
- **SAFE:** Slab Analysis using Finite Elements, CSI, USA.
- **PERFORM 3D:** Nonlinear Analysis and Performance Assessment of 3-D Structures, CSI America, USA.
- **AutoCAD:** Computer-Aided Design Software, Autodesk, USA.
- **IdeCAD:** Structural Analysis Software, IdeYapı, Turkey.
- **FIONA 3D:** A General Purpose Object – Oriented Nonlinear FiniteElement Program in C++", *North Carolina State University*, Raleigh, NC, USA.

LANGUAGE :

- **English:** Upper Intermediate.
- **Italian:** Elementary.

PROFESSIONAL EXPERIENCE:

- **2009:** BUYAKA Shopping Mall and Towers (Reinforced Concrete). *Static Project Drawing*, Ümraniye, Istanbul, Turkey.
- **2010:** Piri Reis University Campus (Reinforced Concrete). *Static Project, Modelling, Computing and Design*, Tuzla, İstanbul, Turkey.
- **2011:** Lasagrada Hotel (Reinforced Concrete), *Retrofitting Static Project, Modelling, Computing and Design,* Şişli, İstanbul, Turkey.
- **2012:** ETİ Management Center (Reinforced Concrete). *Static Project Modelling, Computing and Design*, Eskişehir, Turkey.
- **2013:** Dumankaya Ritim 44-Story Towers (Reinforced Concrete). *Modelling and Computing of Nonlinear Time History Analysis*, Maltepe, Istanbul, Turkey.
- **2014:** Eren Holding Factory Building (Steel and Reinforced Concrete), *Modelling, Computing and Design*, Eskişehir, Turkey.
- **2014:** Park34 Residences and Penthouses Tower (Reinforced Concrete), *Static Project, Modelling, Computing and Design,* Pendik, İstanbul, Turkey.
- **2015:** Batı-Göz, Hospital (Reinforced Concrete). *Retrofitting Project*, Üsküdar, İstanbul, Turkey.
- **2015:** Cavit Paşa Kiosk (Timber). *Restitution*, Üsküdar, İstanbul.
- **2016:** 3-Story Underground Car Park (Reinforced Concrete). *Modelling, Computing and Design*, Kütahya, Turkey.
- **2016:** Celalettin Bey Kiosk (Timber). *Restitution*, Üsküdar, İstanbul.
- **2016:** Eryaman Stadium (Steel and Reinforced Concrete). *Modelling, Computing and Design*, Ankara, Turkey.
- **2016:** Sıraevler Project (Masonry). *Retrofitting Project.* Şişli, İstanbul, Turkey.
- **2017:** Model School. Vehbi KOC Foundation (Reinforced Concrete). *Static Project*, Beykoz, İstanbul, Turkey.
- **2017:** Büyükyalı Shopping Mall and Residences (Timber, Masonry, Steel and Reinforced Concrete). *Retrofitting Historical Buildings, Static Project and Computing of Nonlinear Time History Analysis*. Zeytinburnu, İstanbul, Turkey.

PUBLICATIONS, PRESENTATIONS AND PATENTS ON THE THESIS:

- **Baksı H. G. and Ülker M. B. C.** (2017), "Analysis of Dynamic Response of a Caisson Type Gravity Quay Wall – Seabed Soil System" *Proc 27th International Society Offshore and Polar Engineering Conf*erence, San Francisco, USA ISOPE (accepted).